PEROXIDES STABILIZED BY PHOSPHINE OXIDES: SYNTHESIS, CHARACTERIZATION, AND APPLICATIONS

A Dissertation

by

FABIAN FELIX ARP

Submitted to the Office of Graduate and Professional Studies of
Texas A&M University
in partial fulfillment of the requirements for the degree of

DOCTOR OF PHILOSOPHY

Chair of Committee,	Janet Bluemel
Committee Members,	Matthew Sheldon
	Hongcai Zhou
	Hans Achim Schuessler
Head of Department,	Simon North

December 2020

Major Subject: Chemistry

ABSTRACT

A large variety of Hilliard adducts with the general motif $(R_3PO{\cdot}H_2O_2)_2$ and Ahn adducts with the composition $R_3PO{\cdot}(HOO)_2CR'R''$ have been synthesized and fully characterized. Their single crystal X-ray structures have been determined and analyzed. The IR and ^{31}P NMR data are in accordance with strong hydrogen bonding of hydrogen peroxide and di(hydroperoxy)alkanes, respectively. The bonding nature of the adduct assemblies has been investigated by DOSY NMR experiments. Raman spectroscopy of the symmetric Hilliard adducts and the ν(O−O) stretching bands confirm the presence of hydrogen-bonded hydrogen peroxide in the solid materials. The solubilities in organic solvents have been quantified to be very high for Hilliard adducts and high for Ahn adducts. Due to these high solubilities in organic solvents their ^{17}O NMR spectra could be recorded in natural abundance, providing well-resolved signals for the P=O and O−O groups. In the case of Ahn adducts, the ^{17}O NMR spectra allow for the full resolution of both signals for the C−O−O−H group.

Reaction of bis(dicyclohexylphosphino)ethane dioxide with hydrogen peroxide leads to an extended crystalline network based on the formation of hydrogen bonds with the P=O groups of the diphosphine dioxide. The structural motif of the network is characterized by X-ray diffraction. A new selective synthesis for an industrially important MEKPO (methyl ethyl ketone peroxide) dimer is described. The dimer is created by reaction of dppe (bis(diphenylphosphino)ethane) dioxide with butanone and hydrogen peroxide. This peroxide is stabilized by forming strong hydrogen bonds to the phosphine oxide groups within an extended network.

Competition experiments between Ahn adducts and their respective phosphine oxides allowed to rank the affinities of the di(hydroperoxy)cycloalkanes for the different phosphine oxide carriers. Based on variable temperature ^{31}P NMR investigations the Gibbs energies of activation $\Delta G^{\ddagger}$ for the adduct dissociation processes at different temperatures, as well as the enthalpy $\Delta H^{\ddagger}$ and entropy $\Delta S^{\ddagger}$ of activation have been determined.

DEDICATION

I thank my husband, Christopher James Arp, and my parents, Sibylle Koehler-Eberle and Markus Eberle, who always supported me in this endeavor.

ACKNOWLEDGEMENTS

I would like to thank my committee chair, Dr. Janet Bluemel for her guidance, support and patience throughout my time at Texas A&M University.

I would like to thank my committee members, Dr. Matthew Sheldon, Dr. Hongcai Zhou, and Dr. Hans Achim Schuessler, for their guidance and support throughout the course of this research.

I would also like to thank our collaborator, Dr. Kit Cummins for his guidance and advice throughout his time as Hagler fellow at Texas A&M University.

I thank Dr. Nattamai Bhuvanesh, Dr. Douglas Elliott and Dr. Vladimir Bakhmoutov for their support and helpful discussions.

I also want to thank my undergraduate researchers Destiny Lindhardt, Kyle Angle, William Dow, Alejandra Rivera, and Aubrey Sergeant, as well as all my collegues in the Bluemel Group.

Thanks also go to my friends and colleagues and the department faculty and staff for making my time at Texas A&M University a great experience.

CONTRIBUTORS AND FUNDING SOURCES

Contributors

The research described in this thesis was supervised by the committee chair, Dr. Janet Bluemel, and supported by the committee members, Dr. Matthew Sheldon and Dr. Hongcai Zhou of the Department of Chemistry, and Dr. Hans Achim Schuessler of the Department of Physics and Astronomy.

Dr. Kit Cummins of the Department of Chemistry at MIT co-supervised part of the work and gave valuable advice. Dr. Nattamai Bhuvanesh performed single crystal X-ray analyses. Part of the work reported in chapter III was performed in collaboration with Dr. Shin Hye Ahn. I thank Dr. Douglas Elliott for help with the DOSY measurements, Dr. Diane Sellers for calibrating the Raman microscope, and Kyle J. Angle (REU) for measuring some solubilities.

All other work conducted for this dissertation was completed by the student independently.

Funding Sources

This work was supported by the National Science Foundation (CHE-1300208 and CHE-1900100). The graduate study was supported by a HEEP fellowship from the Hagler Institute for advanced study at Texas A&M University.

TABLE OF CONTENTS

Page

LIST OF FIGURES

Page

LIST OF SCHEMES

Page

LIST OF TABLES

Page

CHAPTER I

INTRODUCTION*

Hydrogen Peroxide

Peroxides are ubiquitous in daily life.[1] They are active ingredients for disinfecting and bleaching in the production of goods[2] and cosmetics, the household, and wastewater treatment. They also play important roles in medicine, such as the treatment of skin infections, and wound cleaning. Recently, H_2O_2 has been shown to function efficiently for polymer breakdown.[3] Artemisinin and related organic peroxides play special roles as antiparasitic and anti-malarial agents, as underscored by the 2015 Nobel Prize in Medicine awarded to Youyou Tu.[4] Peroxides are also employed in industry, for example, as radical initiators of polymerizations.[1b] Oxidation reactions are crucial for synthetic chemistry, too, and inorganic and organic peroxides, either solo or in the presence of catalysts, play central roles.[1] Recent applications include the oxidation of amines to amides[5] and sulfides to sulfoxides,[6] alkane activation,[7] and epoxidation reactions.[8] Our group[9-18] and many others[19-23] study the practical and theoretical aspects of catalyst-free oxidation of phosphines to their oxides. Furthermore, in academia as well as industry, Baeyer-Villiger oxidations are indispensable for synthesizing esters from ketones.[15,24]

Regarding preparative chemistry, the ideal peroxide would be inexpensive, easily accessible, reproducible in its composition, and soluble in organic solvents. It should be

---

* Reproduced (adapted) from F. F. Arp, N. Bhuvanesh, J. Blümel, *Dalton Trans*. **2019**, *48*, 14312-14325 with permission from the Royal Society of Chemistry.

safe at higher temperatures and with respect to mechanical impact. Furthermore it should be stable at ambient temperatures on the shelf and retain its oxidizing power over prolonged time periods. Finally, a solid oxidizing agent would be desirable that can easily be purified by crystallization and administered in well-defined weight aliquots.

Presently, aqueous H_2O_2 is probably the most ubiquitous oxidizing agent in academic settings, although it is not ideal. The main drawback is the abundance of water in the reaction mixture which might lead to unwanted secondary reactions. Even when side-reactions are not an issue, in case the reagents are not water-soluble the oxidation reactions have to be performed in a biphasic system, slowing rates and requiring phase separations later. Furthermore, commercial aqueous H_2O_2 contains a large amount of nitric acid as a stabilizer to adjust the pH to values between 1 and 2. Nevertheless, commercially available H_2O_2 degrades at unpredictable rates,[25] and has to be titrated[25a,b] prior to each application when exact stoichiometry is crucial. Aqueous H_2O_2 also decomposes quickly in the presence of metal ions, which has recently been shown for traces of Fe^{3+}.[25c]

Water-free formulations of H_2O_2, for example, urea hydrogen peroxide (UHP)[26] and peroxocarbonates[27] are in use. The main disadvantage is that the stoichiometry of these materials is not well defined. Furthermore, they are insoluble in organic solvents and might be hard to remove from the reaction mixtures. Other approaches include encapsulated[28] and immobilized versions of H_2O_2.[29] H_2O_2 adducts of metal complexes with demanding syntheses have been characterized.[30,31] Peroxides like $(Me_3SiO)_2$ and $(CH_3)_2C(OO)$ (DMDO) are applied, but their synthesis and storage are problematic.[31,32]

Phosphine Oxides

Phosphine oxides are important for many different reasons. For example, they are unwanted byproducts of phosphine chemistry, in particular in the field of immobilized catalysts.[33-36] They can be found when monodentate or chelating alkylphosphine ligands[33] or Rh catalysts thereof are bound to a support.[34] Phosphine oxides might also occur when Rh complexes are immobilized via triarylphosphines incorporating rigid tetraphenylelement scaffolds.[35] Furthermore, phosphine oxides are encountered when Pd/Cu Sonogashira[36] and Ni catalysts are immobilized with bi- and tridentate phosphine linkers.[37]

Phosphine oxides are famous as co-products of Wittig and Appel reactions. They can be used to probe the surface acidities of oxide materials[38] and currently receive attention regarding the analysis and decomposition of warfare agents.[39] Flame retardants incorporate P=O groups,[40] and phosphine oxides are also important synthetic intermediates and targets.[16,41]

Phosphine oxides readily form stable hydrogen bonds with diverse types of donors. Examples include hydrogen-bonding with phenols to create extended assemblies for materials science,[42,43] with naphthol,[44] sulfonic acids,[45] and water.[11,13,46] Phosphine oxides with hydrogen bonds to silanols, phenols, and even chloroform have recently been characterized with X-ray diffraction.[17] The potential of phosphine oxides as hydrogen bond acceptors has been studied theoretically,[47] also in combination with hydrogen-bonded H_2O_2.[48]

Furthermore, the influence of hydrogen bonding on the ^{31}P solid-state NMR spectra of phosphine oxides has been analyzed in detail by our group[11-13,17,18] and Shenderovich.[49] When solid phosphine oxides are combined with porous materials, such as silica,[50] they adsorb on the surface by hydrogen-bonding with surface silanol groups, even in the absence of a solvent. This phenomenon and the dynamic properties have also been studied by multinuclear solid-state NMR.[13,18]

Phosphine Oxide Stabilized Peroxides

Recently, we discovered that phosphine oxides have the unique ability to stabilize hydrogen peroxide[11,12] and di(hydroperoxy)alkanes by forming strong hydrogen bonds.[12,14,15] The materials obtained so far exhibit general structural motifs for both adduct forms, the Hilliard adducts $(R_3PO{\cdot}H_2O_2)_2$,[11,12] and the Ahn adducts $R_3PO{\cdot}(HOO)_2CR'R''$ (R, R', R'' = alkyl and aryl).[12,14,15] Preliminary results show that the peroxides are stabilized via well-defined hydrogen bonding by the phosphine oxides without compromising their oxidative efficiency. Both Hilliard and Ahn adducts selectively and instantaneously oxidize phosphines to phosphine oxides, without insertion of oxygen into any P–C bond.[11,12,14,15] The merit of water-free oxidation in particular has been demonstrated by the clean synthesis of the water-sensitive diphosphine dioxide $Ph_2P(O)P(O)Ph_2$.[14] Sulfides are transformed into sulfoxides in organic phases at room temperature without overoxidation to the sulfones.[12,14] Baeyer-Villiger oxidations of ketones are selective and efficient with both Hilliard and Ahn adducts, requiring only traces of acid as catalyst.[15] Lactones have also been synthesized directly from the corresponding Ahn adduct.[15]

Both adduct types are safe and robust towards high temperatures and mechanical stress inflicted by hammering and grinding, with shelf lives of months at ambient temperatures.[11,12,14,15] The peroxides do not contain acids or other impurities.[51] Most importantly, the high solubility of all adducts in organic solvents allows for homogeneous oxidation reactions in one organic phase. The Hilliard and Ahn adducts are solid and stoichiometric and can easily be administered to reaction mixtures.

DOSY NMR

Solid-state structures of Hilliard and Ahn adducts have been investigated previously by single crystal X-ray analysis.[11,12,14,15] This gives comprehensive information on bond lengths and angles with high accuracy. It does not, however, provide reliable information on the bulk material, since the selected crystal might not be representative of the entire sample. This deficiency is mitigated by ^{1}H, ^{31}P, IR, and Raman spectroscopy. However, none of these methods is very reliable in predicting the structures of the adducts in solution. Due to the labile nature of hydrogen bonds, the assumption that the accurate solid-state information acquired by X-ray analysis applies to the dissolved compounds as well needed further investigation.

Diffusion ordered spectroscopy is a technique, in which an array of spectra is recorded and subsequently a 2D plot of NMR resonance versus diffusion constant D is obtained. It is not a 2D NMR technique, since the data is only convoluted in one direction.

Figure 1 shows the pulsed field gradient echo (PGSE) pulse sequence as a simple example of a DOSY pulse sequence. Initially, a 90° pulse applies a uniform

magnetization. Then a gradient pulse is applied. A 180° pulse flips all spins in the opposite direction, the gradient is applied again and the FID is collected.

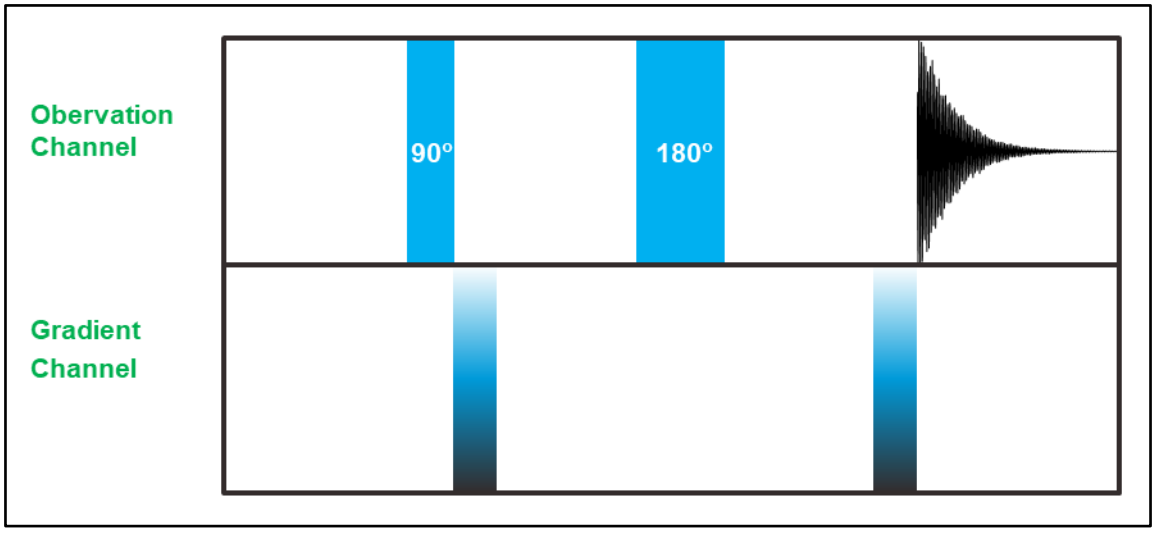

Figure 1 Schematic representation of the pulsed field gradient echo (PGSE) pulse sequence, an example of a simple DOSY pulse sequence.

A simplified representation of how PGSE acts on a sample in an NMR tube is shown in figure 2. Three representative nuclei are shown with a uniform spin pointing in one direct just after being magnetized by a 90° pulse. The dephasing pulse applies a gradient to the direction of the spins. This introduces spatial information into the sample. In the theoretical case without diffusion shown in figure 2, the combination of 180° pulse and application of a gradient pulse, represented as a single refocusing pulse, all spins are directed back into their original direction. The lack of diffusion translates into an overall signal that is equal to the initial magnetization. This residual magnetization

can be related to the magnitude of diffusion in the sample, with perfect retention of the initial magnetization signifying the absence of diffusion.

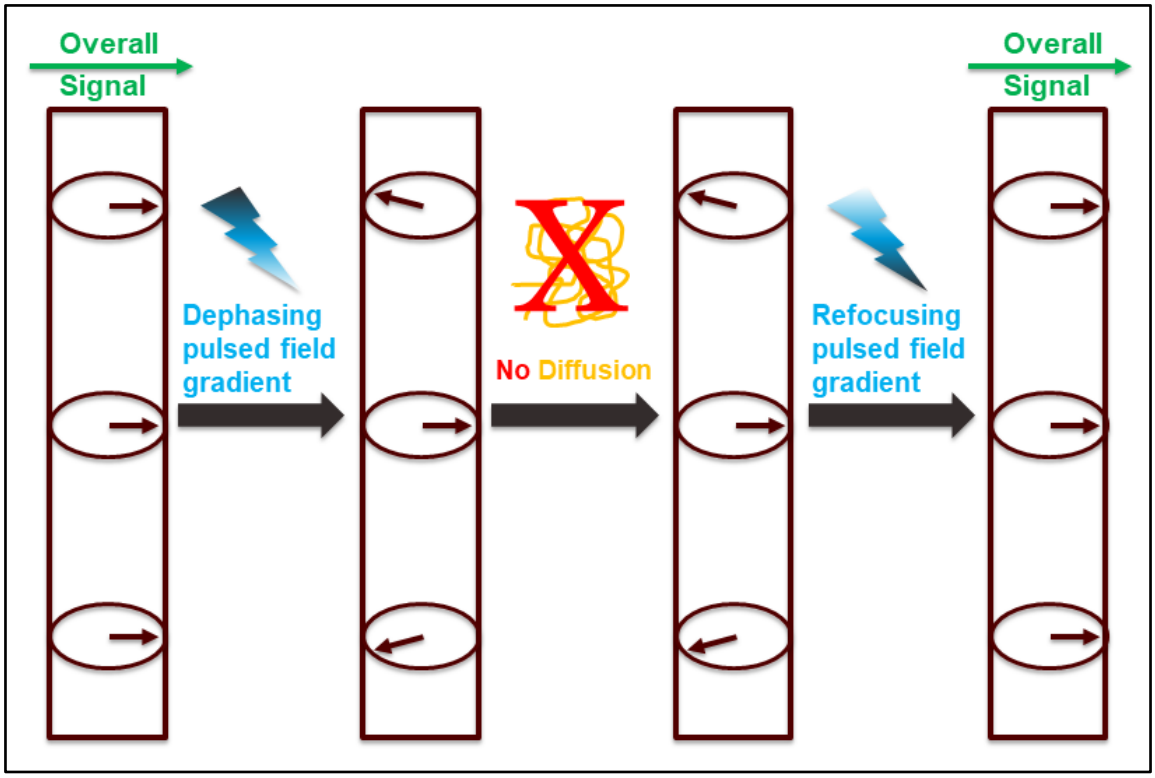

Figure 2 Simplified schematic representation of PGSE acting on an NMR tube with three representative nuclei and no diffusion.

Another representation of how PGSE acts on an NMR sample in an NMR tube is shown in figure 3. In this case, diffusion of the nuclei in solution is not omitted. As in the previous case, three representative nuclei are shown with a uniform spin pointing in one direction just after being magnetized by a 90° pulse. And as in the previous case, the dephasing pulse applies a gradient to the direction of the spins, which introduces spatial

information into the sample. However, if diffusion is taken into account, as represented by the orange arrows, carrying magnetized particles up and down in the NMR tube, the magnetization of the shown six representative nuclei does not correspond perfectly to that after the initial dephasing pulse. Is a refocusing pulse applied, then the original overall signal strength is not reached. This weakening of the residual magnetization can be related to the magnitude of diffusion present in the sample.

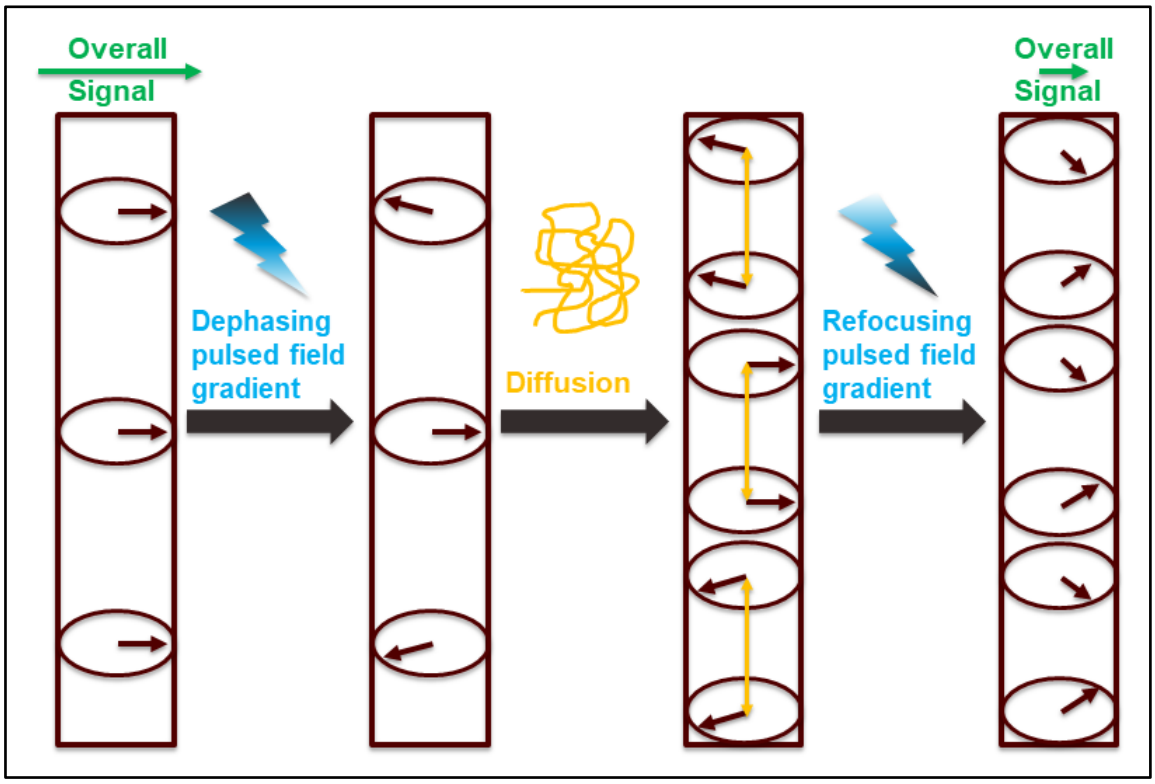

Figure 3 Simplified schematic representation of PGSE acting on an NMR tube with three representative nuclei and some diffusion.

The diffusion constant is then plotted against the chemical shift. This 2D plot shows compounds resolved by their di size and shape. Assuming the shape to be close to spherical, the size can be easily calculated, and compared to the solid-state size of the respective phosphine oxides and adducts. Luckily, the sizes of adduct assemblies and the respective phosphine differ enough, that despite possible inaccuracies stemming, among other causes, from the assumption of spherical shape, meaningful assumptions can be derived.

Dynamic NMR

Qualitative and quantitative assays of chemical kinetics do not only help with the optimization of synthesis conditions, but they can also help elucidate reaction mechanisms.[52] Dynamic NMR experiments are furthermore used to determine the energy of activation and also to separately obtain the enthalpy of activation $\Delta H^{\ddagger}$ and entropy of activation $\Delta S^{\ddagger}$.[53] If two compounds are in equilibrium with each other with an exchange rate (k_r), then their respective NMR signals can be observed separately at the low temperature limit. The latter is reached when k_r is much smaller than the difference in chemical shift of both signals, $\Delta\nu$. If the temperature rises, and k_r approaches $\Delta\nu$, then the two signals start to coalesce, and they form a broad single signal. If the temperature and thus k_r rises further, so that k_r is much larger than $\Delta\nu$, then only a single signal is observed.[54]

In order to quantify k_r at each temperature assayed, spectra can be simulated to fit experimental ones. This leads to accurate k_r values related to temperature, which can

then be used in Eyring plots to give precise values of the Gibbs energy of activation $\Delta G^{\ddagger}$, the enthalpy of activation $\Delta H^{\ddagger}$, and the entropy of activation $\Delta S^{\ddagger}$.

Conclusion

In conclusion, the work presented in this dissertation has confirmed and expanded the knowledge about Hilliard and Ahn adducts in the solid state. Furthermore, it uncovered a several additional structural motifs for peroxide-phosphine oxide binding. The previously unknown behavior of these peroxide adducts in solution has been thoroughly investigated using ^{17}O, dynamic, and DOSY NMR.[1]

References

1 (*a*) "Handbook of Advanced Methods and Processes in Oxidation Catalysis", D. Duprey and F. Cavani, Imperial College Press, 2014; (*b*) F. Cavani, J. H. Teles, *ChemSusChem*, 2009, **2**, 508-534; (*c*) "Peroxides and Peroxide Compounds", A. E. Comyns in *Van Nostrand's Encyclopedia of Chemistry,* John Wiley & Sons, Inc., 2005.

2 Y. Lu, X. Zhao and S. Fang, *Foods*, 2019, **8**, 31, 1-12.

3 H. Ying, Y. Yang, K. Cai and J. Cheng, *Eur. J. Org. Chem.,* 2019, **2019**, 728-731.

4 Nobel Foundation, The Nobel Prize in Physiology or Medicine 2015, 2015.

5 (*a*) C. J. Legacy, A. Wang, B. J. O'Day and M. H. Emmert, *Angew. Chem. Int. Ed*. 2015, **54**, 14907–14910; (*b*) C. J. Legacy and M. H. Emmert, *Synlett* 2016, **27**, 1893–1897.

6 (*a*) P. C. B. Page, B. R. Buckley, C. Elliott, Y. Chan, N. Dreyfus and F. Marken, *Synlett*, 2016, **27**, 80-82; (*b*) D. Habibi, M. A. Zolfigol, M. Safaiee, A. Shamsian and A. Ghorbani-Choghamarani, *Catal. Commun.*, 2009, **10**, 1257–1260; (*c*) H. Golchoubian and F. Hosseinpoor, *Molecules*, 2007, **12***,* 304-311; (*d*) M. Amini, M. Bagherzadeh, Z. Moradi-Shoeili, D. M. Boghaei, A. Ellern and L. K. Woo, *J. Coord. Chem*., 2013, **66**, 464-472; (*e*) T. Okada, H. Matsumuro, S. Kitagawa, T. Iwai, K. Yamazaki, Y. Kinoshita, Y. Kimura and M. Kirihara, *Synlett*, 2015, **26**, 2547-2552; (*f*) J.-W. Chu and B. L. Trout, *J. Am. Chem. Soc.*, 2004, **126**, 900-908; (*g*) E. Wojaczynska and J. Wojaczynski, *Chem. Rev*., 2010, **110**, 4303-4356; (*g*) B. Zhang, S. Li, M. Cokoja, E. Herdtweck, J. Mink, S.-L. Zang, W. A. Herrmann and F. E. Kühn, *Z. Naturforsch B*., 2014, **69b**, 1149-1163; (*h*) Y. Xie, Y. Li, S. Zhou, Y. Zhang, M. Chen and Z. Li, *Synlett*, 2018, **29**, 340-343.

7 (*a*) D. J. Covell and M. C. White, *Tetrahedron*, 2013, **69**, 7771-7778; (*b*) P. E. Gormisky and M. C. White, *J. Am. Chem. Soc.*, 2013, **135**, 14052−14055; (*c*) T. J. Osberger, D. C. Rogness, J. T. Kohrt, A. F. Stepan and M. C. White, *Nature*, 2016, **537**, 214–219; (*d*) J. M. Howell, K. Feng, J. R. Clark, L. J. Trzepkowski and M. C. White, *J. Am. Chem. Soc.*, 2015, **137**, 14590−14593; (*e*) B. H. Brodsky and J. Du Bois, *J. Amer. Chem. Soc.*, 2005, **127**, 15391-15393.

8 (*a*) J. Hou, Y. Chen, B. Cordes, D. Ma, J. Wang, X. Wang, F. E. Kühn, H. Guo and M. D. Zhou, *Chem. Commun*., 2015, **51**, 7439-7442; (*b*) M. D. Zhou, M. Liu, J. Huang, J. Zhang, J. Wang, X. Li, F. E. Kühn and S. L. Zang, *Green Chem*., 2015, **17**, 1186-1193; (*c*) M. Drees, S. A. Hauser, M. Cokoja and F. E. Kühn, *J. Organomet. Chem*., 2013, **748**, 36-45; (*d*) M. A. Goodman and M. R. Detty, *Synlett*, 2006, 1100-1104; (*e*) I. I. E. Markovits, W. A. Eger, S. Yue, M. Cokoja,

C. J. Münchmeyer, B. Zhang, M.-D. Zhou, A. Genest, J. Mink, S.-L. Zang, N. Rösch and F. E. Kühn, *Chem. Eur. J.*, 2013, **19**, 5972-5979; (*f*) H. Yao and D. E. Richardson, *J. Am. Chem. Soc*., 2000, **122**, 3220-3221; (*g*) G. S. Owens and M. M. Abu-Omar, *Chem. Commun.*, 2000, 1165-1166.

9 (*a*) J. Blümel, *Inorg. Chem*., 1994, **33**, 5050-5056; (*b*) J. Sommer, Y. Yang, D. Rambow and J. Blümel, *Inorg. Chem*., 2004, **43**, 7561-7563.

10 T. Posset, F. Rominger and J. Blümel, *Chem. Mater*., 2005, **17**, 586-595.

11 C. R. Hilliard, N. Bhuvanesh, J. A. Gladysz and J. Blümel, *Dalton Trans.,* 2012, **41**, 1742-1754.

12 S. H. Ahn, K. J. Cluff, N. Bhuvanesh and J. Blümel, *Angew. Chem. Int. Ed.*, 2015, **54**, 13341-13345; *Angew. Chem*., 2015, **127**, 13539-13543.

13 C. R. Hilliard, S. Kharel, K. J. Cluff, N. Bhuvanesh, J. A. Gladysz and J. Blümel, *Chem. Eur. J*., 2014, **20**, 17292-17295.

14 S. H. Ahn, N. Bhuvanesh and J. Blümel, *Chem. Eur. J*., 2017, **23**, 16998-17009.

15 S. H. Ahn, D. Lindhardt, N. Bhuvanesh and J. Blümel, *ACS Sustainable Chem. Eng*., 2018, **6**, 6829-6840.

16 S. Kharel, T. Jia, N. Bhuvanesh, J. H. Reibenspies, J. Blümel and J. A. Gladysz, *Chem. Asian J*., 2018, **13**, 2632-2640.

17 S. Kharel, N. Bhuvanesh, J. A. Gladysz and J. Blümel, *Inorg. Chim. Acta*, 2019, **490**, 215-219.

18 S. Kharel, K. J. Cluff, N. Bhuvanesh, J. A. Gladysz and J. Blümel, *Chem. Asian J*., 2019, **14**, DOI: 10.1002/asia.201900632.

19 (*a*) D. W. Stephan, *Science*, 2016, **354**, 1248; (*b*) J. M. Bayne and D. W. Stephan, *Chem. Soc. Rev.*, 2016, **45**, 765-774.

20 M. Mehta, I. G. De la Arada, M. Perez, D. Porwal, M. Oestreich and D. W. Stephan, *Organometallics*, 2016, **35**, 1030−1035.

21 Z. S. Han, N. Goyal, M. A. Herbage, J. D. Sieber, B. Qu, Y. Xu, Z. Li, J. T. Reeves, J.-N. Desrosiers, S. Ma, N. Grinberg, H. Lee, H. P. R. Mangunuru, Y. Zhang, D. Krishnamurthy, B. Z. Lu, J. J. Song, G. Wang and C. H. Senanayake, *J. Am. Chem. Soc*., 2013, **135**, 2474-2477.

22 (*a*) T. E. Barder and S. L. Buchwald, *J. Am. Chem. Soc*., 2007, **129**, 5096-5101; (*b*) D. B. Copley, F. Fairbrother, J. R. Miller and A. Thompson, *Proc. Chem. Soc., London*, 1964, 300–301.

23 (*a*) X. Cai, S. Majumdar, G. C. Fortman, L. M. Frutos, M. Temprado, C. R. Clough, C. C. Cummins, M. E. Germain, T. Palluccio, E. V. Rybak-Akimova, B. Captain and C. D. Hoff, *Inorg. Chem*., 2011, **50**, 9620-9630; (*b*) A. Blake, G. McQuillan, I. Oxton and D. Troy, *J. Mol. Struct*., 1982, **78**, 265-271; (*c*) J. E. Nycz and R. Musiol, *Heteroatom Chem.*, 2006, **17**, 310-316.

24 (*a*) M. Uyanik and K. Ishihara, *ACS Catal*., 2013, **3**, 513-520; (*b*) L. Zhou, X. Liu, J. Ji, Y. Zhang, X. Hu, L. Lin and X. Feng, *J. Am. Chem. Soc*., 2012, **134**, 17023-17026; (*c*) L. Zhou, X. Liu, J. Ji, Y. Zhang, W. Wu, Y. Liu, L. Lin and X. Feng, *Org. Lett*., 2014, **16**, 2938-3941.

25 (a) N. V. Klassen, D. Marchington and H. C. E. McGowan, *Anal. Chem*., 1994, **66**, 2921-2925; (*b*) Y. Cui, B. Zhang, B. Liu, H. Chen, G. Chen and D. Tang, *Microchim. Acta*, 2011, **174**, 137-144; (*c*) T. Tsuneda and T. Taketsugu, *Phys. Chem. Chem. Phys.*, 2018, **20**, 24992-24999.

26 (*a*) L. Ji, Y.-N. Wang, C. Qian and X.-Z. Chen, *Synthesis Commun.*, 2013, **43**, 2256-2264; (*b*) D. Kaur and B. R. Chhabra, *J. Chem., Biol., Phys. Sci. A*, 2013, **3**, 980-987; (*c*) M. C. Ball and S. Massey, *Thermochim. Acta*, 1995, **261**, 95-106; (*d*) J. A. Dobado, J. Molina and D. Portal, *J. Phys. Chem. A*, 1998, **102**, 778-784; (*e*) S. Taliansky, *Synlett*, 2005, 1962–1963; (*f*) M. S. Cooper, H. Heaney, A. J. Newbold and W. R. Sanderson, *Synlett*, 1990, 533-535.

27 (*a*) N. Koukabi, *Synlett*, 2010, 2969-2970; (*b*) A. McKillop and W. R. Sanderson, *J. Chem. Soc., Perkin Trans. 1*, 2000, 471–476; (*c*) D. P. Jones and W. P. Griffith, *J. Chem. Soc., Dalton Trans.*, 1980, 2526-2532.

28 S. Bednarz, B. Ryś and D. Bogdał, *Molecules*, 2012, **17**, 8068-8078.

29 (*a*) T. Jiang, W. Wang and B. Han, *New J. Chem.*, 2013, **37**, 1654-1664; (*b*) G. K. S. Prakash, A. Shakhmin, K. E. Glinton, S. Rao, T. Mathew and G. A. Olah, *Green Chem.*, 2014, **16**, 3616-3622.

30 (*a*) C. Mühle, E.-M. Peters and M. Jansen, *Z. Naturforsch. B*, 2009, **64**, 111-115; (*b*) J. Cho, S. Jeon, S. A. Wilson, L. V. Liu, E. A. Kang, J. J. Braymer, M. H. Lim, B. Hedman, K. O. Hodgson, J. S. Valentine, E. I. Solomon and W. Nam, *Nature*, 2011, **478**, 502-505; (*c*) T. Schölkopf, N.-D. Van and T. Schleid, *Inorg. Chim. Acta*, 2011, **374**, 181-186; (*d*) A. Kunishita, J. D. Scanlon, H. Ishimaru, K. Honda, T. Ogura, M. Suzuki, C. J. Cramer and S. Itoh, *Inorg. Chem*., 2008, **47**, 8222-8232; (*e*) M. Schulz, J. H. Teles, J. Sundermeyer and G. Wahl, US Patent 6,054,407, 2000.

31 K. Korth, A. Schorm, J. Sundermeyer, H. Hermann and G. Boche, *Peroxo Complexes of Molybdenum, Tungsten and Rhenium with Phase Transfer Active Ligands: Catalysts for the Oxidation of Olefins and Aromatics by Hydrogen Peroxide and Bistrimethylsilyl Peroxide* in: *Organosilicon Chemistry IV*, Wiley-VCH, Weinheim, 2000, 238-244.

32 A. V. Arzumanyan, R. A. Novikov, A. O. Terent'ev, M. M. Platonov, V. G. Lakhtin, D. E. Arkhipov, A. A. Korlyukov, V. V. Chernyshev, A. N. Fitch, A. T. Zdvizhkov, I. B. Krylov, Y. V. Tomilov and G. I. Nikishin, *Organometallics*, 2014, **33**, 2230-2246, and refs. cited.

33 (*a*) M. Bogza, T. Oeser and J. Blümel, *J. Organomet. Chem.*, 2005, **690**, 3383-3389; (*b*) R. Fetouaki, A. Seifert, M. Bogza, T. Oeser and J. Blümel, *Inorg. Chim. Acta*, 2006, **359**, 4865-4873.

34 (*a*) J. Blümel, *Coord. Chem. Rev.*, 2008, **252**, 2410-2423; (*b*) J. Guenther, J. Reibenspies and J. Blümel, *Adv. Synth. Catal*., 2011, **353**, 443-460; (*c*) R. Silbernagel, A. Diaz, E. Steffensmeier, A. Clearfield and J. Blümel, *J. Mol. Catal. A*, 2014, **394**, 217-223; (*d*) C. Merckle and J. Blümel, *Adv. Synth. Catal.*, 2003, **345**, 584-588; (*e*) C. Merckle and J. Blümel, *Top. Catal.*, 2005, **34**, 5-15.

35 (*a*) J. H. Baker, N. Bhuvanesh and J. Blümel, *J. Organomet. Chem*., 2017, **847**, 193-203; (*b*) Y. Yang, B. Beele and J. Blümel, *J. Am. Chem. Soc*., **2008**, **130**, 3771-3773; (c) B. Beele, J. Guenther, M. Perera, M. Stach, T. Oeser and J. Blümel, *New J. Chem*., **2010**, **34**, 2729-2731.

36 (*a*) J. C. Pope, T. Posset, N. Bhuvanesh and J. Blümel, *Organometallics*, 2014, **33**, 6750-6753; (*b*) T. Posset and J. Blümel, *J. Am. Chem. Soc.*, 2006, **128**, 8394-8395; (*c*) T. Posset, J. Guenther, J. Pope, T. Oeser and J. Blümel, *Chem. Commun.*, 2011, **47**, 2059-2061.

37 (*a*) S. Reinhard, P. Soba, F. Rominger and J. Blümel, *Adv. Synth. Catal*., **2003**, **345**, 589-602; (b) F. Piestert, R. Fetouaki, M. Bogza, T. Oeser and J. Blümel, *Chem. Commun*., 2005, 1481-1483; (*c*) K. J. Cluff, N. Bhuvanesh and J. Blümel, *Chem. Eur. J*., 2015, **21**, 10138-10148; (*d*) S. Reinhard, K. D. Behringer and J. Blümel, *New J. Chem.*, 2003, **27**, 776-778.

38 (*a*) A. Zheng, S.-B. Liu and F. Deng, *Chem. Rev.*, 2017, **117**, 12475−12531; (*b*) R. Yerushalmi, J. C. Ho, Z. Fan and A. Javey, *Angew. Chem. Int. Ed.*, 2008, **47**, 4440-4442; (*c*) J. P. Osegovic and R. S. Drago, *J. Phys. Chem. B*, 2000, **104**, 147-154; (*d*) S. Hayashi, K. Jimura and N. Kojima, *Bull. Chem. Soc. Jpn.*, 2014, **87**, 69-75; (*e*) S. Machida, M. Sohmiya, Y. Ide and Y. Sugahara, *Langmuir*, 2018*,* **34***,* 12694−12701.

39 (*a*) A. R. Wilmsmeyer, W. O. Gordon, E. D. Davis, B. A. Mantooth, T. A. Lalain and J. R. Morris, *Rev. Sci. Instrum*., 2014, **85**, 014101; (*b*) J. Kemsley, *Chem. Eng. News*, 2014, **92**, 29.

40 (*a*) H. Ren, J. Sun, B. Wu and Y. Zhou, *Polym. Degrad. Stab*., 2007, **92**, 956-961; (*b*) M. A. Espinosa, M. Galia and V. Cadiz, *J. Polym. Sci., Part A: Polym. Chem.*, 2004, **42**, 3516-3526.

41 (*a*) J. Chrzanowski, D. Krasowska and J. Drabowicz, *Heteroatom Chem*., 2018, **29**, DOI:10.1002/hc.21476; (*b*) T. Kovacs and G. Keglevich, *Curr. Org. Chem*., 2017, **21**, 569-585; (*c*) D. Herault, D. H. Nguyen, D. Nuel and G. Buono, *Chem. Soc. Rev*., 2015, **44**, 2508-2528; (*d*) M. D. Fletcher, *Organophosphorus Reagents*, 2004, 171-214; (*e*) H. R. Hays and D. J. Peterson, *Org. Phosphorus Compounds*, 1972, **3**, 341-500; (*f*) H. Adams, R. C. Collins, S. Jones and C. J. A. Warner, *Org. Lett*., 2011, **13**, 6576-6579.

42 (*a*) D. Nunez-Villanueva, C. A. Hunter, *Chem. Sci*., 2017, **8**, 206--213; (*b*) A. E. Stross, G. Iadevaia and C. A. Hunter, *Chem. Sci.*, 2016, **7**, 94-101; (*c*) G. Iadevaia, A. E. Stross, A. Neumann and C. A. Hunter, *Chem. Sci.*, 2016, **7**, 1760-1767; (*d*) R. Cuypers, E. J. R. Sudhölter and H. Zuilhof, *ChemPhysChem*., 2010, **11**, 2230-2240.

43 N. A. Bewick, A. Arendt, Y. Li, S. Szafert, T. Lis, K. A. Wheeler, J. Young and R. Dembinski, *Curr. Org. Chem*., 2015, **19**, 469-474.

44 S. J. Pike and C. A. Hunter, *Org. Biomol. Chem*., 2017, **15**, 9603-9610.

45 N. J. Burke, A. D. Burrows, M. F. Mahon and J. E. Warren, *Inorg. Chim. Acta*, 2006, **359**, 3497-3506.

46 R. Joshi and S. P. Pasilis, *J. Mol. Liquids*, 2015, **209**, 381-386.

47 I. Alkorta and J. Elguero, *J. Phys. Chem. A*, 1999, **103**, 272-279.

48 (*a*) D. V. Ilyin, W. A. Goddard III, J. J. Oppenheim and T. Cheng, *Proceedings of the National Academy of Sciences*, 2018, 201701383, 1; (*b*) T. Tsuneda, J. Miyake and K. Miyatake, *ACS Omega*, 2018, **3**, 259-265.

49 (*a*) E. Y. Tupikina, M. Bodensteiner, P. M. Tolstoy, G. S. Denisov and I. G. Shenderovich, *J. Phys. Chem. C*, 2018, **122**, 1711-1720; (*b*) G. Begimova, E. Y. Tupikina,V. K. Yu, G. S. Denisov, M. Bodensteiner and I. G. Shenderovich, *J. Phys. Chem. C*, 2016, **120**, 8717-8729.

50 K. R. Iler, *The Chemistry of Silica*, John Wiley, New York, 1979.

51 Q. Lin, Y. Jiang, J. Geng, and Y. Qian, *Chem. Eng. J*., 2008, **139**, 264-271.

52 S. Ašperger, *Chemical Kinetics and Inorganic Reaction Mechanisms*, 2003.

53 D. K. Zimmer, R. Shoemaker and R. R. Ruminski, *Inorganica Chim. Acta*, 2006, **359**, 1478-1484.

54 I. R. Kleckner and M. P. Foster, *Biochim. Biophys. Acta*, 2011, **1814**, 942-968.

CHAPTER II

HYDROGEN PEROXIDE ADDUCTS OF TRIARYLPHOSPHINE OXIDES*

Introduction

Hydrogen peroxide and other peroxides are commonly used as disinfectants, drugs, and for many other household and industrial purposes.[1-4] There is also a wide variety of uses in organic[5-8] and inorganic[9-24] chemistry. In order to circumvent the unpredictable degradation of aqueous hydrogen peroxide[25] solid formulations of hydrogen peroxide were developed[26-31]. Other peroxides like $(Me_3SiO)_2$ and $(CH_3)_2C(OO)$ (DMDO) show a very favorable reactivity, but they are not shelf stable.[31,32]

Phosphine oxides are rather inert, well-studied, and benign binding partners for peroxides.[33-50] Thus the formed adducts between peroxides and phosphine oxides profess a desirable stability while being free of typically used stabilizers.[11,12,14,15,51]

Because of the favorable characteristics of these useful and intrinsically interesting Hilliard and Ahn oxidizers we sought to further explore the scope of these phosphine oxide adducts. Regarding later applications on a larger scale, it is desirable to minimize the weight and cost of the solid oxidizers. In this respect the Hilliard adducts are more favorable than the Ahn adducts. Therefore, we focused on the former, also because the only structurally characterized Hilliard adducts reported so far are $(Cy_3PO{\cdot}H_2O_2)_2$,[11] $(^tBu_3PO{\cdot}H_2O_2)_2$,[12] $(Ph_3PO)_2{\cdot}H_2O_2$,[52] and $(Ph_3PO{\cdot}H_2O_2)_2{\cdot}H_2O_2$.[12] The

* Reproduced (adapted) from F. F. Arp, N. Bhuvanesh, J. Blümel, *Dalton Trans*. **2019**, *48*, 14312-14325 with permission from the Royal Society of Chemistry.

Ph_3PO adducts have been the most elusive regarding a well-defined stoichiometry, although they are most desirable because the parent phosphine oxide is inexpensive and a large scale waste product of the synthetic Wittig and Appel processes. In our quest to obtain stoichiometric and highly soluble H_2O_2 adducts, we turned to triarylphosphine oxides, incorporating methyl substituents in the *ortho* and *para* positions of the phenyl rings, as carriers for H_2O_2.

In this contribution we report five new H_2O_2 adducts of triarylphosphine oxides, **1**-**5**, and one H_2O adduct, **6** (Scheme 1). It is demonstrated that the adducts can be synthesized easily, reproducibly, and in a stoichiometric manner. The adducts are fully characterized by single crystal X-ray diffraction, and two general structural motifs are identified. The ^{31}P, ^{13}C, and ^{1}H NMR data are analyzed and compared to the parent phosphine oxides. Due to the high solubility of all adducts, natural abundance ^{17}O NMR spectra are obtainable. The presence of the hydrogen-bonded H_2O_2 molecules is further confirmed by IR and Raman spectroscopy. The solubilities of the adducts in diverse organic solvents is quantified and the association of the adducts in solution is studied by DOSY spectroscopy. The lifetimes of the adducts are monitored in solutions, and key steps of the decomposition mechanism are described.

Results and Discussion

Synthesis and Purification

In order to broaden the range of available hydrogen peroxide adducts and analytical methods for their characterization, the triarylphosphine oxide dimers **1**-**5** and the water adduct **6** have been synthesized (Scheme 1). The syntheses were

straightforward by combining dichloromethane solutions of the corresponding phosphines with 35% aqueous hydrogen peroxide. After phase separation the stoichiometric adducts **1**-**3**, containing two H_2O_2 molecules per assembly, result. Additionally, **4**, incorporating only one H_2O_2 bridge per adduct, is obtained by heating a solution of **1** in toluene to 105 °C for 10 hours. Adduct **5** is obtained as the only product when the synthetic route used for **1**-**3** is applied. Interestingly, no mixed H_2O_2/H_2O adduct has been found so far. Nevertheless, the existence of **4** and **5** suggests that the loss of active oxygen atoms in the adducts occurs in a stepwise manner, as described earlier for the di(hydroperoxy)alkane adducts of phosphine oxides.[15] The H_2O adduct **6** was obtained from **3** by decomposing the bound H_2O_2 with molecular sieves[11] and recrystallizing the product while exposed to the atmosphere.

For the comparison of spectroscopic data, the phosphine oxides corresponding to the adducts **1**-**6**, *p*-Tol_3PO (**7**), *o*-Tol_3PO (**8**), *o*-Tol_2PhPO (**9**), and *o*-$TolPh_2PO$ (**10**) have been synthesized.

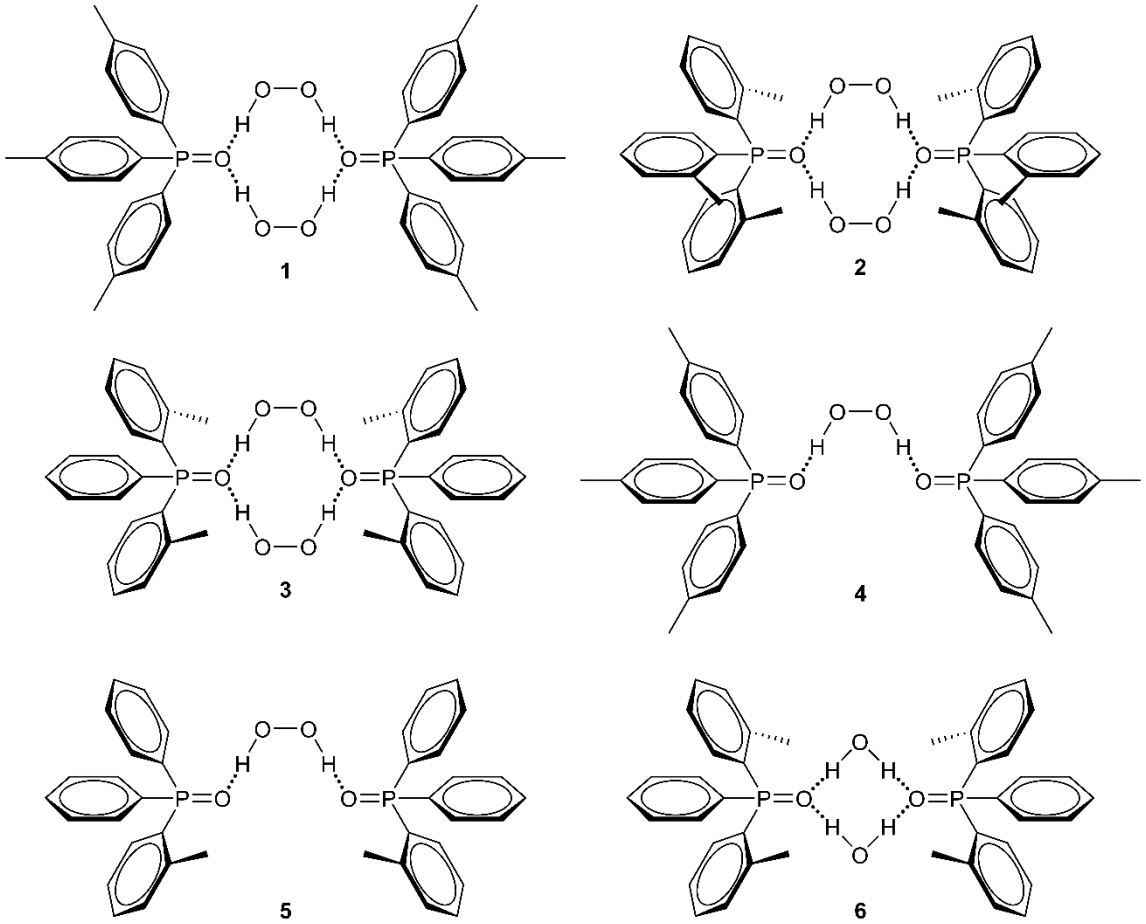

Scheme 1 The H_2O_2 adducts of triarylphosphine oxides **1**-**5** and the H_2O adduct **6**.

The adducts **1**-**5** are stable mechanically and thermally and their melting points and ranges could be determined. The characterization of the adducts was furthermore facilitated by their readiness to crystallize in large habits with dimensions in the cm range (Figure 4). Besides the single crystal X-ray structures, the IR and Raman spectroscopic data are reported. The ^{31}P NMR results are in agreement with earlier findings, and the DOSY experiments elucidate the mono- versus dimeric nature of selected adducts not only in the solid state, but also in solution. Due to the high

solubility of the adducts in organic solvents, the natural abundance ^{17}O NMR spectra could be obtained with well-resolved signals for the P=O and H_2O_2 oxygen nuclei.

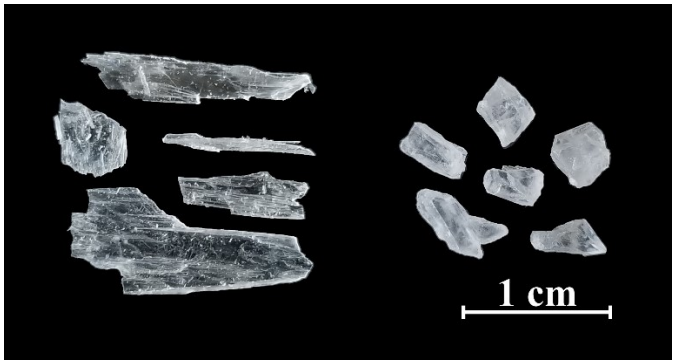

Figure 4 Single crystals of **1** (left) and **2** (right).

X-Ray Crystallography

All adducts **1**-**6** crystallize readily in large colorless specimens of high quality (Figure 4). As earlier research on Ph_3PO as a crystallization aid for amines has shown,[53] the triarylphosphine oxide moieties are most probably responsible for the ease of crystallization. All adducts **1**-**6** have been investigated by single crystal X-ray diffraction. The structures are displayed in Figures 5-11[54] and the P=O bond lengths, O···H and oxygen-oxygen distances O···H−O are summarized in Table 1.

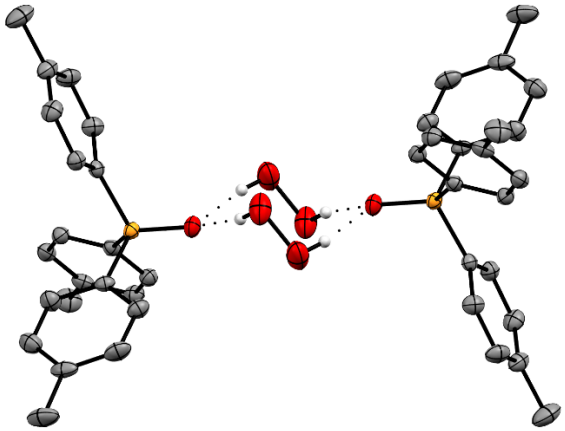

Figure 5 Single crystal X-ray structure of (p-$Tol_3PO{\cdot}H_2O_2)_2$ (**1**).[54]

The adducts **1**-**3** incorporate the H_2O_2 molecules sandwiched between the two P=O groups. The center piece of the assemblies contains the two H_2O_2 molecules in the characteristic chair conformation. The latter has been found earlier for the only other structurally characterized adducts with $(H_2O_2)_2$ cores, $(Cy_3PO{\cdot}H_2O_2)_2$,[11] $(^tBu_3PO{\cdot}H_2O_2)_2$,[12] and $(Ph_3PO{\cdot}H_2O_2)_2{\cdot}H_2O_2$.[12] The H_2O_2 molecules hydrogen-bonded in **1**-**3** feature dihedral angles defined by the H−O−O−H [=O···O−O···O=] angles of 99.042(12)° [89.060(11)°] (**1**), 100.003(18)° [100.069(18)°] (**2**), and 99.277(4)° [98.969(4)°] (**3**), which are considerably larger than the value of 90.2(6)° found in solid H_2O_2. The dihedral angles in the mono-H_2O_2 adducts **4** and **5** are even larger with 131.868(4)° [93.062(5)°] (**4**) and 111.642(6)° [109.300(6)°] (**5**), most probably due to the steric demands of packing in the unit cell.

Although in **1** there appears to be additional space between the two phosphine oxide carrier molecules (Figure 5), it is not used to incorporate a third H_2O_2 molecule, as

found earlier for the triphenylphosphine oxide adduct $(Ph_3PO{\cdot}H_2O_2)_2{\cdot}H_2O_2$.[12] Due to the hydrogen bond formation, the P=O bond order is reduced and the bond is weakened. The P=O bond longer in **1** (1.4988(3) Å)[54] than in the parent phosphine oxide *p*-Tol_3PO (**7**) (1.4885(17) Å).[54]

Regarding the X-ray structure of **2** (Figure 6), it is obvious that the three methyl groups in the *ortho* positions of the phenyl substituents at phosphorus fill more of the space in the immediate surroundings of the two H_2O_2 molecules than the unsubstituted phenyl groups in **1** or in $(Ph_3PO{\cdot}H_2O_2)_2{\cdot}H_2O_2$.[12] However, contemplating only one dimeric assembly, there would still be room for a third H_2O_2 molecule. The unit cell of **2** (Figure 7) displays the arrangement of the dimeric adducts in the crystal lattice. The dense packing of the assemblies and the particular arrangement of the adducts clearly does not facilitate the accommodation of a third H_2O_2 molecule.

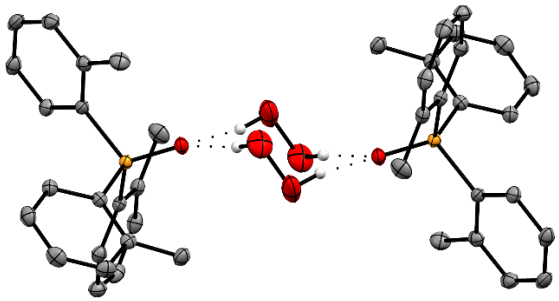

Figure 6 Single crystal X-ray structure of $(o\text{-}Tol_3PO{\cdot}H_2O_2)_2$ (**2**).[54]

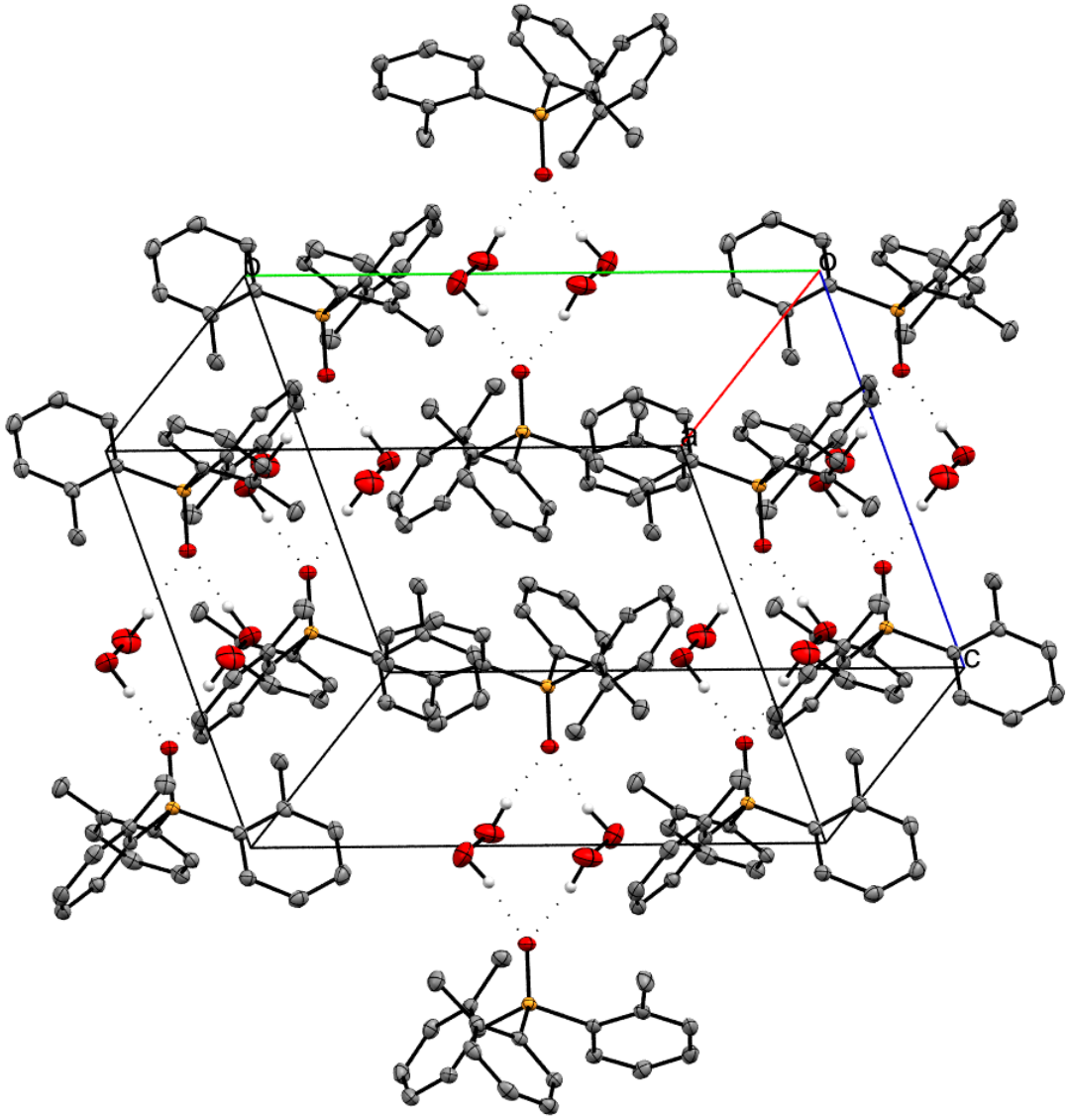

Figure 7 Unit cell of the adduct (o-$Tol_3PO{\cdot}H_2O_2)_2$ (**2**).[54]

The P=O bond in **2** is again elongated (1.5010(3) Å, Table 1) as compared with the neat phosphine oxide o-Tol_3PO (**8**) (1.478(2)/1.481(2) Å).[55] The lengthening of the P=O bond is more substantial (0.020/0.023 Å) than for **1**, so the *ortho* methyl substituents at the phenyl groups clearly have an impact.

Table 1 P=O bond lengths (Å), as well as O···H and oxygen-oxygen distances O···H–O (Å) of the adducts **1**-**6**.[54]

Adduct	P=O bond length (Å)	O···H distance (Å)	O···H–O distance (Å)
1	1.4988(3)	1.9365(3) / 1.9258(4)[a]	2.7734(4) / 2.7651(5)[a]
2	1.5010(3)	1.8228(3) / 1.8815(3)	2.7287(4) / 2.8186(4)
3	1.50455(7)	1.91259(6) / 1.84216(6)[a]	2.76245(8) / 2.69200(9)[a]
4	1.49474(8)	1.92746(9)	2.72339(12)
5	1.4975(3) / 1.4980(3)	1.8478(5) / 1.8706(6)[a]	2.6844(8) / 2.7202(8)[a]
6	1.488(16)	2.0032(16) / 2.0504(16)	2.861(3) / 2.915(3)

[a] Metrics from the major component of the disordered H_2O_2 are reported.

In the X-ray structure of **3** (Figure 8) the two methyl groups in the *ortho* positions of the phenyl substituents at phosphorus fill some of the space around the $(H_2O_2)_2$ core of the assembly. The center of the adducts again assumes the preferred chair conformation, which emerges as the general structural characteristic of all Hilliard H_2O_2 adducts of phosphine oxides with the dimeric motif $(R_3PO{\cdot}H_2O_2)_2$.

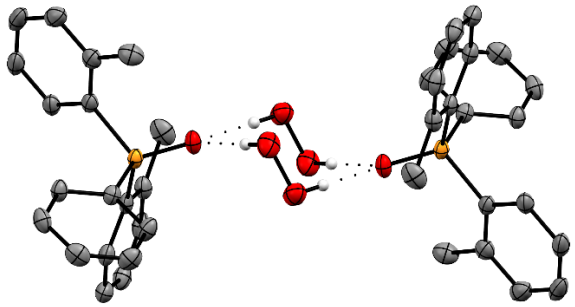

Figure 8 Single crystal X-ray structure of (*o*-$Tol_2PhPO{\cdot}H_2O_2)_2$ (**3**).[54]

Adduct **4** has only half the number of active oxygen atoms as compared to **1**-**3**. It could be isolated as an intermediate in the stepwise release of oxygen when **1** was exposed to elevated temperatures in solution. Therefore, it might become useful as a more robust and mild oxidizer.

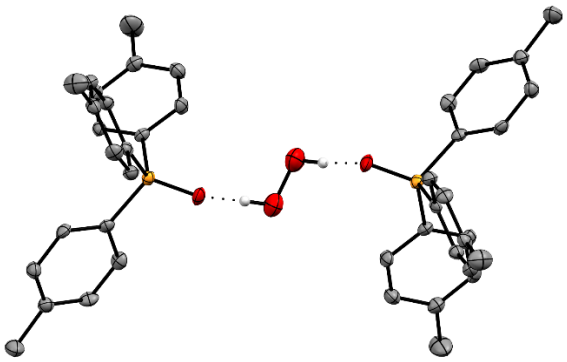

Figure 9 Single crystal X-ray structure of (p-$Tol_3PO)_2 \cdot H_2O_2$ (**4**).[54]

Curiously, the water molecule that is created when **1** loses one active oxygen atom has never been found retained in the structures, i.e., no mixed adduct $(R_3PO)_2 \cdot H_2O \cdot H_2O_2$ has been characterized yet. This corroborates the finding that H_2O_2 is more firmly bound than a water molecule and replaces hydrogen-bonded water from phosphine oxides.[14] In this case, there would be space left for one water molecule, but the packing in the unit cell might prevent its incorporation in the structure. The P=O bond in **4** is lengthened from 1.4885(17) Å for p-Tol_3PO (**7**) to 1.49474(8) Å (Table 1). The difference in the bond lengths is only about 0.006 Å, illustrating the diminished effect of only one hydrogen-bonded H_2O_2 in the adduct on the P=O groups of **4**.

The single crystal X-ray structure of **5** resembles that of **4**, exhibiting the same structural motif $(R_3PO)_2{\cdot}H_2O_2$. The P=O bond lengths (Table 1) is slightly larger in **5**, while the O···H distance is correspondingly shorter.

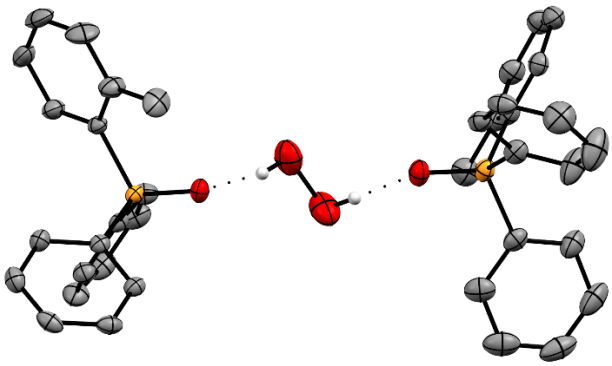

Figure 10 Single crystal X-ray structure of $(o\text{-TolPh}_2PO)_2{\cdot}H_2O_2$ (**5**).[54]

The phosphine oxide hydrate **6** shows the high affinity of phosphine oxides for water[11,13] and is the first triarylphosphine oxide water adduct with the structural motif $(R_3PO{\cdot}H_2O)_2$ described so far (Figure 11). Only the hemihydrate $(p\text{-Tol}_3PO)_2{\cdot}H_2O$ has been reported previously.[56] The other structurally characterized hydrate, $(Cy_3PO{\cdot}H_2O)_2$, incorporates a trialkylphosphine oxide.[13]

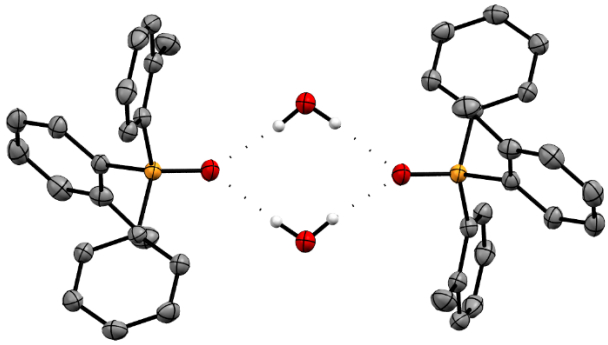

Figure 11 Single crystal X-ray structure of (*o*-$Tol_2PhPO_2 \cdot H_2O)_2$ (**6**).[54]

The four oxygen atoms per assembly of **6** lie in a plane (Figure 11). The P=O bond of **6** is the shortest among the adducts **1-6**, and it can be concluded that the hydrogen bonding of the P=O groups to H_2O is weaker than the bonding to H_2O_2. The H−O−H angle amounts to 104.6°.

All O···H distances in **1-5** confirm the presence of hydrogen bonding, as they are within the range of 1.8228(3)-1.9365(3) Å (Table 1).[58] Hydrogen bonds typically exhibit O···H distances of 1.85 to 1.95 Å.[58] The H_2O adduct **6** shows slightly longer O···H distances, but the structure nevertheless suggests the presence of hydrogen bonds (Figure 11). Furthermore, the O···H−O distances of **1-5**, which are another indicator for the formation of hydrogen bonds,[58] all lie within the range of 2.6844(8)-2.8186(4) Å (Table 1). This confirms strong hydrogen bonding, as the values are between 2.75 and 2.85 Å.[58] Only for the H_2O adduct **6**, the O···H−O distances of 2.861(3)/2.915(3) Å are slightly larger, but the visual impression of the presence of hydrogen bonds again dominates.

^{31}P NMR Spectroscopy

Due to the high solubiliy of the H_2O_2 adducts of the phosphine oxides in organic solvents (see below), ^{31}P NMR spectra can be recorded in short periods of time. For precise referencing, a capillary with liquid $ClPPh_2$ as the standard was centered in the NMR tubes. The changes of the ^{31}P chemical shifts of the adducts **1-6**, as compared with the corresponding phosphine oxides **7-10** are noticeable (Table 2). The observable trend is that the formation of the hydrogen bond leads to deshielding of the ^{31}P nuclei due to electron density being relocated towards the oxygen in the P=O group. Therefore, the chemical shift values are generally higher for the adducts than for the phosphine oxides.

Table 2 ^{31}P NMR chemical shifts of the adducts **1-6** and their corresponding phosphine oxides **7-10** in $CDCl_3$ and the differences of the chemical shift values.

Adduct	$\delta(^{31}P)$ of adducts [ppm]	**R_3PO**	$\delta(^{31}P)$ of R_3PO [ppm]	$\Delta\delta(^{31}P)$ [ppm]
1	30.44	**7**	29.28	1.16
2	37.90	**8**	37.51	0.39
3	36.47	**9**	34.66	1.81
4	30.47	**7**	29.28	1.19
5	33.50	**10**	31.42	2.08
6	34.96	**9**	34.66	0.30

In contrast to the ^{31}P chemical shifts, there are only minimal changes in the ^{1}H and ^{13}C NMR data when creating the H_2O_2 adduct from a phosphine oxide. This can, for example, be seen when comparing the $\delta(^{13}C)$ and $J(^{31}P\text{-}^{13}C)$ values of **2** with those of **8**.[59]

^{17}O NMR Spectroscopy

While ^{31}P NMR spectroscopy is a routine method, ^{17}O NMR poses some challenges. The Larmor frequency of ^{17}O is in a favorable range, but its natural abundance is only 0.037%, which is about half of the value for ^{2}H. ^{17}O is a quadrupolar nucleus with a nuclear spin of I = 5/2. The quadrupole moment Q = $-2.6 \cdot 10^{-26}$ is of moderate size,[60] and therefore ^{17}O NMR signals can be expected to be broader than 100 Hz for species with unsymmetric electronic surroundings of the ^{17}O nucleus. Most ^{17}O NMR studies have been performed using isotopically enriched samples to facilitate the measurements. Examples include investigations of organic peroxides[61-63] and alkyl hydrotrioxides.[64] Furthermore, the peroxide binding to the active center of an enzyme[65] and polymer degradation mechanisms have been studied using ^{17}O NMR.[66] Enriched samples were also used for ^{17}O solid-state NMR investigations of hydrogen bonding in carboxylic acids,[67] and for studying polymorphs of triphenylphosphine oxide.[68]

However, due to the fast quadrupolar relaxation, transients can be collected in rapid succession and compounds with sufficient solubility in non viscous solvents are accessible to ^{17}O NMR in natural abundance, without isotopic enrichment. Fortunately, the adducts **1**-**6** are very soluble in organic solvents (see below). Especially their high solubility in CD_2Cl_2 is favorable because it allows the measurement of very concentrated samples in a non viscous solvent. The low viscosity of CD_2Cl_2 reduces the correlation time of the adducts and therefore diminishes the halfwidths of the quadupolar ^{17}O NMR signals.[60]

A representative ^{17}O NMR spectrum is shown in Figure 12 and all ^{17}O NMR data of the H_2O_2 adducts **1**-**5**, the H_2O adduct **6**, and the corresponding phosphine oxides **7**-**10** are summarized in Table 3. The spectrum in Figure 12 shows the clearly resolved signals of **2** due to the large chemical shift dispersion of ^{17}O. The hydrogen-bonded H_2O_2 resonates at 184.32 ppm, the P=O oxygen nucleus at 60.04 ppm. The signal at −5.05 ppm corresponds to H_2O hydrogen-bonded to the P=O group. It came into existence in the course of the measurement due to slow decomposition of the H_2O_2 at the elevated temperature of 35 °C, which was applied in order to reduce the viscosity of the solution and therewith the correlation time and linewidth.[60]

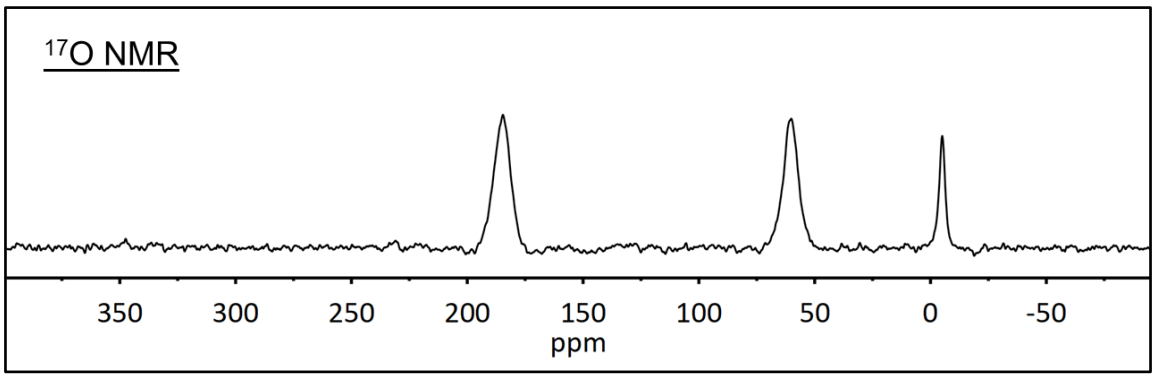

Figure 12 ^{17}O NMR spectrum of (*o*-$Tol_3PO{\cdot}H_2O_2)_2$ (**2**) in CD_2Cl_2, recorded at 35 °C.

Table 3 ^{17}O NMR chemical shifts $\delta(^{17}O)$ (signal halfwidths $\Delta\nu_{1/2}$ [Hz]) of the adducts **1-6** and their corresponding phosphine oxides **7-10** in CH_2Cl_2.

Adduct	$\delta(^{17}O)$ [ppm] of bound H_2O_2/H_2O ($\Delta\nu_{1/2}$ [Hz])	$\delta(^{17}O)$ [ppm] of P=O group ($\Delta\nu_{1/2}$ [Hz])	$\delta(^{17}O)$ [ppm] of R_3PO ($\Delta\nu_{1/2}$ [Hz])	
1	183.96 (494)	46.60 (365)	**7**	48.10 (434)
2	184.32 (548)	60.04 (429)	**8**	61.84 (517)
3	184.97 (253)	53.05 (302)	**9**	59.96 (125)*
4	(not obs.)	47.78 (359)	**7**	48.10 (434)
5	184.23 (462)	46.22 (407)	**10**	48.99 (231)[#]
6	-6.69 (81.8)*	59.74 (284.4)*	**9**	59.96 (125)*

*The species **6** and **9** were not sufficiently soluble in CH_2Cl_2 and were therefore measured in acetonitrile at 75 °C. The signal of **9** is split into a doublet with $^1J(^{31}P\text{-}^{17}O)$ = 159.6 Hz. [#] $^1J(^{31}P\text{-}^{17}O)$ = 163.5 Hz.

The $\delta(^{17}O)$ of the P=O groups are found within the range of 46.60 to 60.04 ppm, in accordance with other compounds incorporating phosphorus-oxygen double bonds.[69] As compared to the $\delta(^{17}O)$ of the P=O group of **1** (46.60 ppm) (Table 3) the chemical shift for the oxygen nucleus of $Ph_3P=O$ in $CDCl_3$ has been reported as 43.3 ppm.[70] The deviation from this value and in general the variation of the $\delta(^{17}O)$ for the P=O groups in **1-6** and **7-10** reflects the presence of substituents at the aromatic rings. Furthermore, the solvent dependence of ^{17}O NMR chemical shifts can be substantial.[63] The solvent dependence of the halfwidths $\Delta\nu_{1/2}$ of the ^{17}O NMR signals is illustrated by the measurements of **6** and **9** in acetonitrile. The $\Delta\nu_{1/2}$ values are smaller when the measurements were performed in acetonitrile at 75 °C (Table 3). Under these conditions the halfwidth $\Delta\nu_{1/2}$ of the ^{17}O phosphine oxide resonance of **9** is small enough to reveal its splitting into a doublet with $^1J(^{31}P\text{-}^{17}O)$ = 159.6 Hz. This value is in accordance with

the literature (160 Hz).[70] Acetonitrile and the elevated temperature of 75 °C were not used as a solvent for **1**-**5** due to concerns that it could decompose the H_2O_2 adducts (see below) in the course of the measurements or compete with the P=O groups as a hydrogen acceptor for H_2O_2.[63]

Regarding the $\delta(^{17}O)$ of the P=O groups in the adducts **1**-**6** with those of the corresponding phosphine oxides **7**-**10** measured in the same solvents (excluding the pair **3**/**9**) shows that hydrogen bonding leads to a slight, but consistent upfield shift of the signals ranging from 0.22 (**6**/**9**) over 0.32 (**4**/**7**), 1.5 (**1**/**7**) and 1.8 (**2**/**8**) to 2.77 (**5**/**10**) ppm (Table 3). Obviously, the electron density around the oxygen nucleus is increased by the pull of electrons from the aromatic rings and phosphorus towards oxygen and the hydrogen bond. This leads to a shielding of ^{17}O and the observed upfield shift.

The ^{17}O NMR resonances of the hydrogen-bonded H_2O_2 moieties of **1**-**3** and **5** are in the narrow range between 183.62 and 184.97 ppm (Table 3). Compared with the literature value of 180 ppm in different solvents,[62,65] all hydrogen-bonded H_2O_2 in the adducts experience a downfield shift between 3.62 and 4.97 ppm. Obviously, the hydrogen bonding reduces the electron density around the ^{17}O nuclei, leading to a deshielding and higher $\delta(^{17}O)$ values. For the H_2O adduct **6** (Table 3) and the H_2O liberated by the decomposition of H_2O_2 in **2** (Figure 12), upfield shifts of -6.69 and −5.05 ppm as compared to pure water with $\delta(^{17}O) = 0$ ppm, are observed. The reason for this is most probably that hydrogen bonding among water molecules reduces the electron density at the ^{17}O nucleus in H_2O more than the hydrogen bonding with a P=O group.

DOSY NMR Spectroscopy

In the solid state the adducts **1-3** consist of dimers that are held together by strong hydrogen bonds. However, no information about the dissociation in different solvents is available at this time. Since Hilliard adducts can be transformed into Ahn adducts by exchange of H_2O_2 with $(HOO)_2CR_2$,[14] it is assumed that a certain degree of dissociation of the dimers $(R_3PO{\cdot}H_2O_2)_2$ takes place in solution. To clarify this issue, we sought to employ Diffusion-Ordered NMR Spectroscopy (DOSY) to probe the hydrogen bond association in **1-3**.[71] The phosphine oxide carriers of the adducts provide access to the straightforward ^{31}P DOSY experiments.[72-73] The resulting values should be within a ±1 Å error margin. The obtained Stokes diameters of the adducts and their corresponding phosphine oxides were compared with the maximal sizes of the species, as defined by the largest H···H distance within one molecule or assembly in the X-ray structure (Table 4). The reliability of the measurements is corroborated by the fact that the Stokes diameters of the adduct-free phosphine oxides correspond very well to the sizes calculated from their structures. This also confirms that there is no association between the phosphine oxides.[73] Next, we sought to apply the method to the most stable Hilliard adduct[11] with a trialkylphosphine oxide carrier. For $(Cy_3PO{\cdot}H_2O_2)_2$[11] in THF, a Stokes diameter of 18 Å was obtained. This corresponds well to the maximal H···H distance of 16.9 Å within the error margin of the DOSY measurement. Therefore, one can conclude that this adduct undergoes only minimal dissociation in THF and remains mainly dimeric.

Table 4 Stokes diameters obtained from DOSY measurements in the given solvents, and maximal H···H distances of the adducts and their corresponding phosphine oxides, derived from the single crystal X-ray structures.

Adduct	**Stokes Diameter [Å]**		**Maximal H···H distance [Å]**	
	R_3PO	**Adduct**	**R_3PO**	**Adduct**
$(Cy_3PO{\cdot}H_2O_2)_2$[11]	11	18 (THF-d_8)	10.066	16.911[11]
1	10	9 (THF-d_8) 11 (C_6D_6) 12 (Tol-d_8)	11.277	17.938
2	10	11 (C_6D_6)	9.503	16.355
3	-	11 (C_6D_6)	9.610	16.932

For the adducts with triarylphosphine oxide carriers **1-3**, however, the Stokes diameters are more in the range of the phosphine oxides (Table 4). In order to exclude that the polar solvent THF led to the dissociation of the dimeric adducts, the DOSY experiments were also performed using benzene and toluene. Nevertheless, only a marginal increase of the Stokes diameters of the adducts, as compared to their corresponding phosphine oxides, was found. Therefore, it is concluded that the adducts **1-3** incorporating triarylphosphine oxide carriers undergo dissociation in solution. Since the Stokes diameters of the adducts are still 1 to 2 Å larger than the values for the phosphine oxides, it is assumed that the dissociation leads to the monomeric adducts of the type $R_3PO{\cdot}H_2O_2$. In a monomeric adduct the H_2O_2 molecule is "dangling" at the P=O oxygen atom and has a high degree of freedom regarding its motions without compromising the strength of the hydrogen bond. It can, for example, fold towards the substituents at phosphorus and in this way the size of the assembly can be minimized.

Therefore, the Stokes diameter of a monomeric adduct is only slightly larger than that of the phosphine oxide. The assumption that the adducts do not completely dissociate into R_3PO and H_2O_2 is also corroborated by the fact that the adducts show much higher solubility in most organic solvents than the parent phosphine oxides.

IR and Raman Spectroscopy

The IR spectra[74] of the H_2O_2 adducts **1**-**5** and the parent phosphine oxides **7**-**10** corroborate the results from ^{31}P NMR spectroscopy (Table 5, Figure 13). The stretching frequencies and therewith wavenumbers for the P=O groups are lower for **1**-**5** as compared to **7**-**10** because the hydrogen bonding with H_2O_2 weakens the double bond. The lower bond order means that less energy is required to excite the stretching mode of the bond in the adducts and therefore lower wavenumbers are observed. The differences $\Delta\nu$(P=O) are in the range of 8-27 cm^{-1}, in accordance with an earlier limited study of mostly non-stoichiometric H_2O_2 adducts.[11]

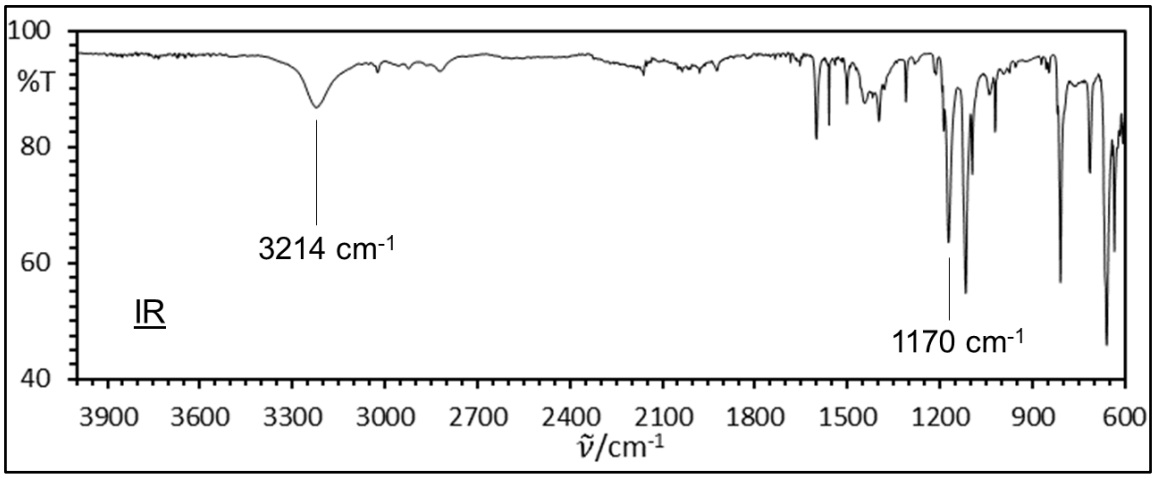

Figure 13 IR spectrum of the neat H_2O_2 adduct (p-$Tol_3PO{\cdot}H_2O_2)_2$ (**1**).

The ν(O−H) stretching bands of the hydrogen-bonded H_2O_2 in **1-5** display wavenumbers of 3214 to 3271 cm^{-1} which can be clearly distinguished from potential water bands around 3400 cm^{-1}.[11,74] The hydrogen bonding of the H_2O_2 to the P=O group weakens the O−H bonds which leads to lower ν(O−H) wavenumbers. In comparison, the water adduct **6** displays an O−H stretching band at 3450 cm^{-1}.

Table 5 IR stretching frequencies ν(P=O) [cm^{-1}] of the P=O groups of the H_2O_2 adducts **1-5** and comparison with their corresponding neat phosphine oxides **7-10** Δν(P=O) [cm^{-1}], ν(O−H) of hydrogen-bonded H_2O_2, and the Raman ν(O−O) stretching frequencies of the hydro-bonded H_2O_2.

Adduct / phosphine oxide	ν(P=O) [cm^{-1}] of adduct / phosphine oxide	Δν(P=O) [cm^{-1}]	ν(O-H) of adducts [cm^{-1}]	ν(O−O) [cm^{-1}]
1 / 7	1170 / 1185	15	3214	868
2 / 8	1150 / 1158	8	3271	869
3 / 9	1149 / 1176	27	3286	877
4 / 7	1172 / 1185	13	3225	871
5 / 10	1168 / 1190	22	3261	871
6 / 9	1159 / 1176	17	3450	-

Due to the favorable symmetry of the adducts **1-5**, the Raman spectra showed the O−O stretching bands (Table 5). One representative Raman spectrum is displayed in Figure 14. The ν(O−O) values are found within the narrow range from 868 to 877 cm^{-1}. They are in agreement with the theoretically predicted values for $(Ph_3PO{\cdot}H_2O_2)_2$.[48b] As expected, due to the bond order of one, the wavenumers are much lower than those found for O_2 gas (1556 cm^{-1})[75] and O_2^- (1139 cm^{-1}).[76] Basically, the ν(O−O) for hydrogen-bonded H_2O_2 in **1-5** lies in between the values for aqueous (99.5%) H_2O_2 (880

cm^{-1})[77] and H_2O_2 vapor (864 cm^{-1}).[78] However, the O−O bonds in **1**-**5** are still stronger than those in alkali peroxides (736-790 cm^{-1})[79] or the popular oxidizing agent ^{t}BuOOH (847 cm^{-1}).[80]

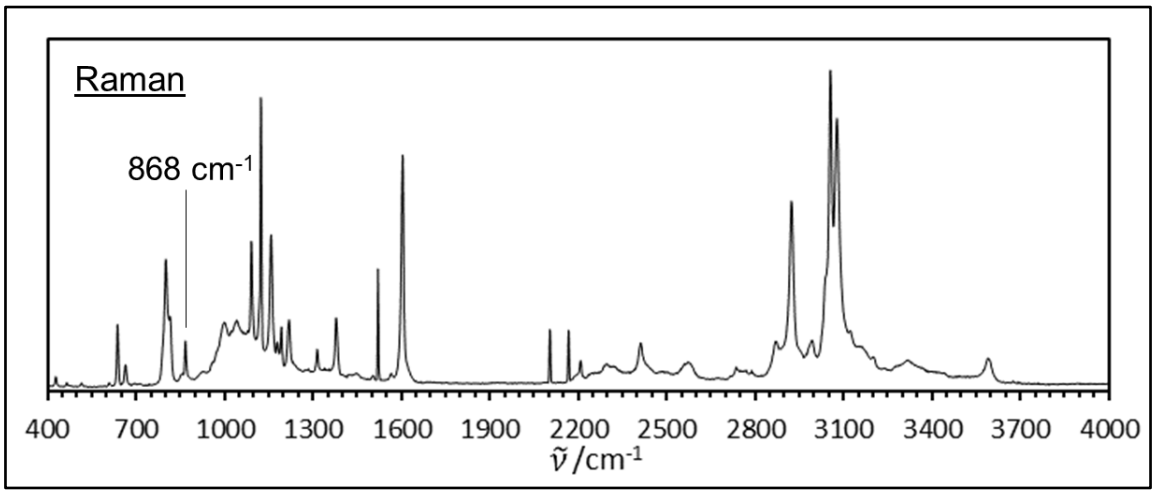

Figure 14 Raman spectrum of the neat H_2O_2 adduct (p-$Tol_3PO{\cdot}H_2O_2)_2$ (**1**).

Solubilities

The H_2O_2 adducts **1**-**5** are highly soluble in the most common organic solvents (Figure 15). The quantified solubilities of **1**-**5** are highest in the protic solvents MeOH and EtOH. For example, more than 750 mg of **2** can be dissolved in one mL of MeOH. But even in $CHCl_3$ the solubilities are substantial. Overall, the solubilities in non protic solvents like THF or CH_2Cl_2 are highest for adducts containing *o*-Tol substituents at phosphorus, while they are in general lowest for those with only *p*-Tol groups. This is most probably due to the shielding of the polar H_2O_2 moieties by the methyl groups in the *ortho* positions, rendering the $R_3PO{\cdot}H_2O_2$ assemblies more hydrophobic. Curiously,

all adducts are only sparingly soluble in water and hexane. This is, however, favorable with respect to isolating and purifying the adducts. After the biphasic synthesis the adducts are found in the organic phase. Large crystals can then be grown by overlaying this phase with hexane or pentane.

The high solubility of **1**-**5** in organic solvents can be exploited for many oxidation reactions. They can be performed in one organic phase, rendering a biphasic reaction mixture obsolete. Especially in cases where a large amount of water in the aqueous phase might lead to unwanted secondary products this is advantageous. Having all educts dissolved in one phase also allows the reactions to proceed faster as compared to processes that only take place at phase boundaries. Naturally, no phase separation or cumbersome drying of the products is required when performing the reactions with **1**-**5** in organic solvents. The one water molecule formed per P=O group for **1**-**3** (per two P=O groups for **4** and **5**) when all peroxy groups have reacted remains firmly bound to the phosphine oxide carriers and will not interfere with the product or the progress of the reaction. The water adducts reported earlier[11,13] and adduct **6** (Scheme 1, Figure 11). After oxidation reactions, for example Baeyer Villiger, phosphine, or sulfide oxidations,[12,14,15] the phosphine oxides can easily be removed by precipitating them from the reaction mixtures with water or hexanes. Alternatively, the phosphine oxides can be bound to insoluble inorganic supports like silica[9a,34a] and separated from the supernatant reaction mixtures by decanting. After recharging with H_2O_2 the tethered phosphine oxides can be reused.

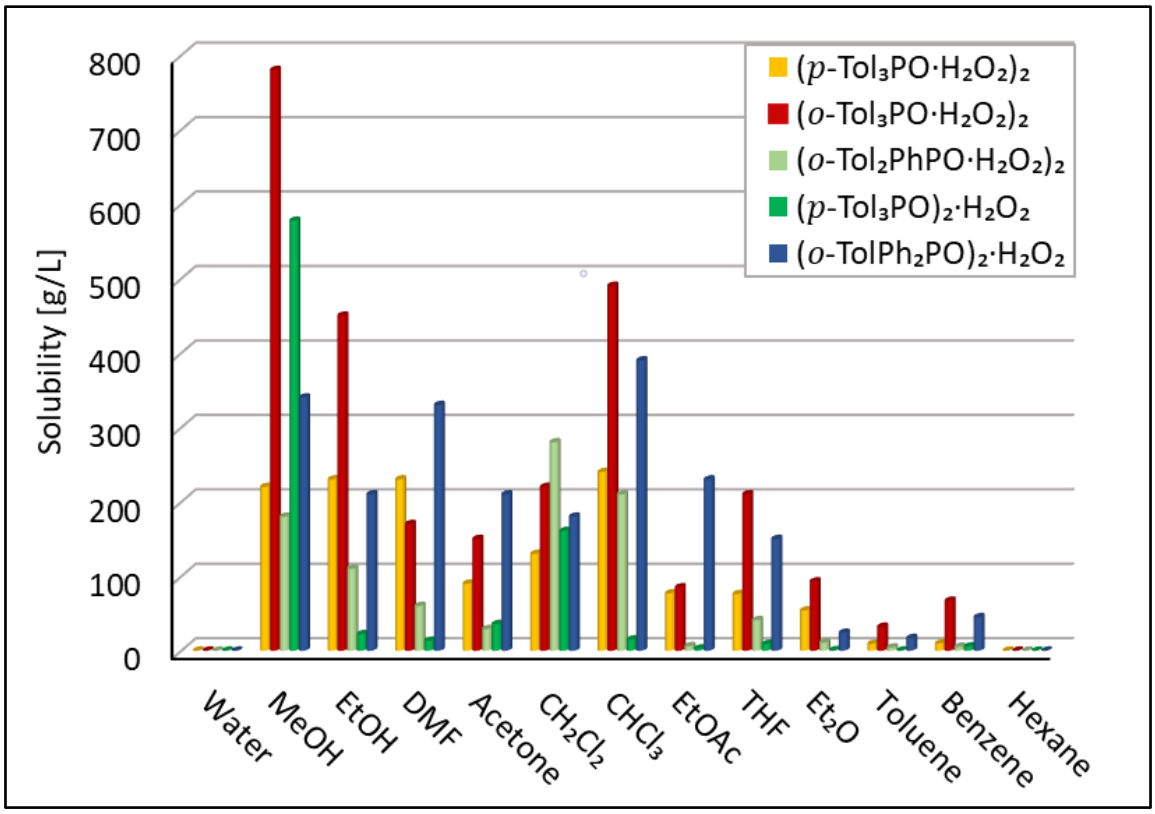

Figure 15 Solubilities of the adducts **1**-**5** in representative solvents.

Shelf Lives

The H_2O_2 adducts **1**-**5** are remarkably stable with respect to dry grinding and hammering. They do not react to sudden impact or release gas in a violent manner. Only when the powders are brought directly into a flame oxygen is released at slow speed without any pronounced audible or visual effect. Most of the adducts can even be molten without initial decomposition, while the oxygen effervesces in tiny bubbles at a higher temperature. It should be noted, however, that prolonged application of vacuum will eventually remove H_2O_2 from the phosphine oxide carrier. Lower yields of adducts are

obtained as a consequence, when prolonged vacuum is applied during the synthesis. On the other hand, combining the phosphine oxides with aqueous H_2O_2 at 0 °C instead of ambient temperature, more than one H_2O_2 molecule per P=O group will be incorporated in the adduct, as also reported previously for $(Ph_3PO{\cdot}H_2O_2)_2{\cdot}H_2O_2$.[12]

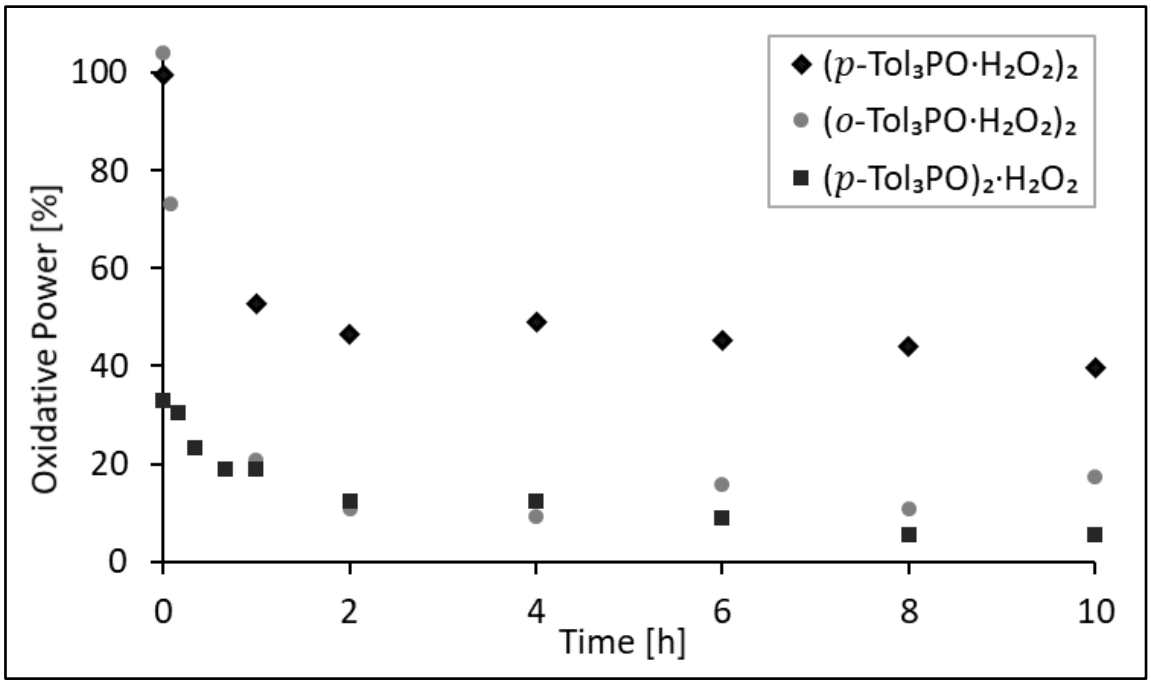

Figure 16 Oxidative power of compounds **1**, **2** and **4** while being heated to 105 °C in toluene (top trace) or chlorobenzene (bottom two curves).

As solids, the adducts **1-5** remain oxidatively active over weeks at ambient temperature. The oxidative power can be monitored by a standardized *in situ* ^{31}P NMR test.[12,13,22b] For **1**, for example, 100% oxidative power corresponds to one active oxygen atom per P=O group. Due to the stability of the adducts, solutions of **1**, **2**, and **4** were

heated to 105 °C in toluene and chlorobenzene, and aliquots were tested in the course of time for oxidative power (Figure 16). First, **1** was dissolved and heated in toluene (Figure 16, top curve). After 10 hours at 105 °C, adduct **1** lost about half its oxidative power and was converted into **4**. Clearly, the loss of active oxygen occurs in a stepwise manner, with the second H_2O_2 being retained much longer than the first one. The mono-H_2O_2 adduct **4** was isolated, dissolved in chlorobenzene, and heated to 105 °C (Figure 16, square symbols). Within 10 hours in this solvent the oxidative power was nearly entirely lost. The same scenario was found when **2** was dissolved in chlorobenzene and heated to 105 °C for 10 hours (Figure 16, round symbols). The fact that the oxygen loss was faster in chlorobenzene than in toluene speaks for the assumption that the decomposition of H_2O_2 in the adducts proceeds by a radical mechanism.

Conclusions

In order to investigate whether H_2O_2 adducts of triarylphosphine oxides can be obtained with a common structural motif and a stoichiometric composition, five new hydrogen peroxide adducts of phosphine oxides have been synthesized and fully characterized, (*p*-$Tol_3PO{\cdot}H_2O_2)_2$ (**1**), (*o*-$Tol_3PO{\cdot}H_2O_2)_2$ (**2**), (*o*-$Tol_2PhPO{\cdot}H_2O_2)_2$ (**3**), (*p*-$Tol_3PO)_2{\cdot}H_2O_2$ (**4**), and (*o*-$TolPh_2PO)_2{\cdot}H_2O_2$ (**5**). For comparison of the analytical data, the water adduct (*o*-$Tol_2PhPO{\cdot}H_2O)_2$ (**6**) was obtained. The single crystal X-ray diffraction studies of **1**-**3** show that there is a common structural motif with two H_2O_2 moieties hydrogen-bound and bridging two phosphine oxide molecules. The same basic principle is observed for adduct **6**, with two H_2O molecules and two P=O groups constituting the core of the assembly, held together by hydrogen bonding. The adducts **4**

and **5** each contain one H_2O_2 molecule sandwiched between two P=O groups and held in its place by hydrogen bonding.

^{31}P NMR spectroscopy of the adducts **1**-**6**, in comparison with the corresponding parent phosphine oxides **7**-**10** shows a downfield shift of the signals as the common trend. The hydrogen bonding of the P=O groups reduces the electron density around the ^{31}P nuclei, thus deshielding them. The solubilities of all adducts and phosphine oxides are very high in representative organic solvents and allow natural abundance ^{17}O NMR spectroscopy. The hydrogen bonding in the adducts leads to lower $\delta(^{17}O)$ values due to the shielding of the ^{17}O nuclei of the P=O groups as compared to the parent phosphine oxides. The ^{17}O NMR chemical shifts of the hydrogen-bonded H_2O_2 molecules, on the other hand, are higher than the value for H_2O_2 in aqueous solution. This result confirms that the hydrogen bonding of H_2O_2 to P=O groups is stronger than to H_2O molecules. DOSY spectroscopy revealed that the H_2O_2 adduct of a trialkylphosphine oxide, $(Cy_3PO{\cdot}H_2O_2)_2$, remains predominantly dimeric in solution, while the triarylphosphine oxide adducts **1**-**3** show a higher tendency to dissociate.

IR spectroscopy corroborates the NMR results, as the P=O bonds are weakened in the adducts and therefore the stretching frequencies ν(P=O) are lowered as compared to those of the corresponding phosphine oxides. The ν(O−H) stretching frequencies of the bridging H_2O_2 moieties in **1**-**5** also display lower values than the water adduct **6**. Raman spectroscopy has allowed to determine the stretching frequencies of the O−O bonds of the hydrogen-bonded H_2O_2 molecules in **1**-**5**.

The decomposition of **1**, **2**, and **4** has been monitored in toluene and chlorobenzene at elevated temperature. The adduct **1** is transformed into **4** within ten hours, indicating that the active oxygen of an adduct assembly is lost in a stepwise manner and that the mono-H_2O_2 adduct **4** is thermally more robust than **1**. However, in chlorobenzene all oxidative power is lost within ten hours at 105 °C.

In the context of previous studies from our group and others, this work highlights the immense structural diversity and interesting reactivity of the P=O···H arrangement. The stepwise loss of the active oxygen from the two H_2O_2 bridges of the phosphine oxide adducts and retention of the H_2O molecules, in combination with the high solubility of the adducts, guarantee that the adducts will find applications, for example, as oxidizers in academic synthesis or as polymerization starters.

Experimental Section

General Considerations

All reactions were carried out using standard Schlenk line techniques and a purified N_2 atmosphere, if not stated otherwise. Reagents purchased from Sigma Aldrich or VWR were used without further purification. Aqueous H_2O_2 solution (35% w/w) was obtained from Acros Organics and used as received. Solvents were dried by boiling them over sodium, then they were distilled and stored under purified nitrogen. Acetone, dichloromethane (Aldrich, ACS reagent grade) and ethanol (200 proof) were dried over 3 Å molecular sieves (EMD Chemical Inc.) prior to use.

*Solubility Measurements of **1-5***

The adducts (5 to 12 mg amounts) were placed into tared 20 mL vials. The desired solvent was added in dropsized portions while shaking the vial vigorously at 20 °C. Once all solid was dissolved, the overall weight gain was recorded, and the solvent volume was calculated.

NMR Spectroscopy

The ^{1}H, ^{13}C, and ^{31}P NMR spectra were recorded at 499.70, 125.66, and 202.28 MHz on a 500 MHz Varian spectrometer. The ^{13}C and ^{31}P NMR spectra were recorded with ^{1}H decoupling if not stated otherwise. Neat Ph_2PCl ($\delta(^{31}P)$ = +81.92 ppm) in a capillary centered in the 5 mm NMR tubes was used for referencing the ^{31}P chemical shifts of dissolved compounds. For referencing the ^{1}H and ^{13}C chemical shifts the residual proton and the carbon signals of the solvents were used (C_6D_6: $\delta(^{1}H)$ = 7.16 ppm, $\delta(^{13}C)$ = 128.00 ppm; $CDCl_3$: $\delta(^{1}H)$ = 7.26 ppm, $\delta(^{13}C)$ = 77.00 ppm). The signal assignments are based on comparisons with analogous phosphine oxides[11-15,17] and $^{1}H,^{1}H$-COSY, $^{1}H,^{13}C$-HSQC, $^{1}H,^{13}C$-HMBC, and ^{31}P-decoupled NMR spectra. The assignments of all *o*-Tol substituent signals follows the numbering in the scheme provided under the Experimental description of **2**.

^{17}O NMR Spectroscopy

The natural abundance ^{17}O NMR spectra were recorded using 0.3 to 0.5 molar CH_2Cl_2 solutions of the compounds at 35 °C. A Varian 500 NMR spectrometer equipped with a 5 mm broadband probe operating at 67.79 MHz was employed. The following measurement parameters have been optimized to yield spectra of good quality with

$0.8 \cdot 10^6$ to $1.4 \cdot 10^6$ scans: spectral window (73.5 kHz), number of data points (7353), measurement pulse length (20 µs), pulse angle (90°), relaxation delay (30 ms), and acquisition time (100 ms). The chemical shifts were referenced externally using pure D_2O ($\delta(^{17}O) = 0$ ppm).

^{31}P DOSY

The ^{31}P DOSY NMR measurements were performed using a Varian 500 NMR spectrometer equipped with a 5 mm broad band probe operating at 202.33 MHz. 0.01 to 0.02 molar solutions of the compounds in THF-d_8 were investigated at 25 °C. Hereby, 20 gradient increments were measured after optimizing the following parameters: diffusion gradient length (2.7 ms), diffusion delay (100 ms), spectral window (6.1 kHz), complex points (4096), measurement pulse length (12.65 µs), pulse angle (90°), relaxation delay (30 s), acquisition time (675 ms), number of scans (16), and number of steady state pulses (32).

IR Spectroscopy

The IR spectra of the neat powders of all adducts and compounds were recorded with a Shimadzu IRAffinity-1 FTIR spectrometer equipped with a Pike Technologies MIRacle ATR plate.

Raman Spectroscopy

The Raman spectra were acquired using a Jobin-Yvon Horiba Labram HR instrument coupled to an Olympus BX41 microscope with 514.51 nm laser excitation from an Ar-ion laser. A 600 lines/mm grating and an acquisition time of 2 s were applied. 60 scans gave spectra of good quality.

X-Ray Diffraction

See appendix A.

Synthesis and Characterization of Adducts

Tri-*p*-tolylphosphine oxide H_2O_2 adduct (*p*-$Tol_3PO{\cdot}H_2O_2)_2$ (1). *p*-Tol_3P (457 mg, 1.5 mmol) was placed in a Schlenk flask under a nitrogen atmosphere and dissolved in dichloromethane (5 mL). Under stirring 2.15 mL of aqueous hydrogen peroxide (35%, 25 mmol) were added to the solution. The mixture was stirred vigorously for 30 min, then the phases were separated, and the solvent was allowed to slowly evaporate from the organic phase at ambient temperature and pressure. A colorless powder was obtained. Recrystallization from dichloromethane (4 mL) and pentane (2 mL) by slow evaporation gave **1** in the form of a crystalline colorless solid (475 mg, 0.671 mmol, 89% yield). Melting range 142-146 °C.

NMR (δ, $CDCl_3$), $^{31}P\{^1H\}$ 30.44 (s); ^1H 8.09-7.79 (br s, O*H*), 7.53 (dd, $^3J(^{31}P\text{-}^1H)$ = 11.9 Hz, $^3J(^1H\text{-}^1H)$ = 8.0 Hz, 6H, H_o), 7.25 (dd, $^3J(^1H\text{-}^1H)$ = 8.0 Hz, $^4J(^{31}P\text{-}^1H)$ = 2.1 Hz, 6H, H_m), 2.39 (s, 9H, CH_3); ^{13}C 142.41 (d, $^4J(^{31}P\text{-}^{13}C)$ = 2.6 Hz, C_p), 132.16 (d, $^2J(^{31}P\text{-}^{13}C)$ = 10.3 Hz, C_o), 129.31 (d, $^1J(^{31}P\text{-}^{13}C)$ = 106.8 Hz, C_i), 129.28 (d, $^3J(^{31}P\text{-}^{13}C)$ = 12.5 Hz, C_m), 21.71 (d, $^5J(^{31}P\text{-}^{13}C)$ = 1.3 Hz, *C*H_3).

Tri-*o*-tolylphosphine oxide H_2O_2 adduct (*o*-$Tol_3PO{\cdot}H_2O_2)_2$ (2). *o*-Tol_3P (1.20 g, 3.94 mmol) was dissolved in dichloromethane (14 mL) in a Schlenk flask under ambient atmosphere and the solution was cooled to 0 °C. While stirring, 6.07 mL of aqueous hydrogen peroxide (35%, 71.0 mmol) were added. The reaction mixture was

stirred vigorously for 1.5 h, while it slowly warmed up to 23 °C. The phases were separated, and the solvent was allowed to evaporate from the organic phase at ambient temperature and pressure. A colorless solid was obtained (1.363 g, 1.923 mmol, 98% yield). Melting range 134-137 °C.

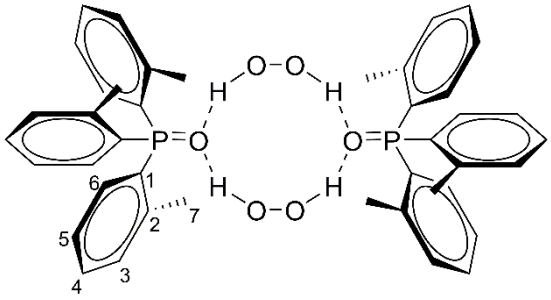

NMR (δ, $CDCl_3$), $^{31}P\{^1H\}$ 37.90 (s); ^1H 7.44 (tt, $^3J(^1H\text{-}^1H)$ = 7.5 Hz, $^5J(^{31}P\text{-}^1H)$ = $^4J(^1H\text{-}^1H)$ = 1.6 Hz, 3H, H4), 7.31 (ddquint, $^3J(^1H\text{-}^1H)$ = 7.5 Hz, $^4J(^{31}P\text{-}^1H)$ = 4.1 Hz, $^4J(^1H\text{-}^1H)$ = 0.8 Hz, 3H, H3), 7.15 (dt, $^3J(^1H\text{-}^1H)$ = 7.8 Hz, $^4J(^{31}P\text{-}^1H)$ = 2.7 Hz, 3H, H5), 7.09 (ddd, $^3J(^{31}P\text{-}^1H)$ = 14.0 Hz, $^3J(^1H\text{-}^1H)$ = 7.7 Hz, $^4J(^1H\text{-}^1H)$ = 1.5 Hz, 3H, H6), 6.86-6.59 (br s, OH), 2.48 (s, 9H, H7); ^{13}C 143.49 (d, $^2J(^{31}P\text{-}^{13}C)$ = 7.6 Hz, C2), 132.92 (d, $^2J(^{31}P\text{-}^{13}C)$ = 12.9 Hz, C6), 132.05 (d, $^3J(^{31}P\text{-}^{13}C)$ = 10.4 Hz, C3), 131.93 (d, $^4J(^{31}P\text{-}^{13}C)$ = 2.6 Hz, C4), 130.46 (d, $^1J(^{31}P\text{-}^{13}C)$ = 101.5 Hz, C1), 125.55 (d, $^3J(^{31}P\text{-}^{13}C)$ = 12.8 Hz, C5), 22.03 (d, $^3J(^{31}P\text{-}^{13}C)$ = 3.9 Hz, C7).

Di-*o*-tolylphenylphosphine oxide H_2O_2 adduct (*o*-$Tol_2PhPO{\cdot}H_2O_2)_2$ (3). *o*-Tol_2PhP (232 mg, 0.8 mmol) was placed in a Schlenk flask and dissolved in

dichloromethane (2.7 mL) under a nitrogen atmosphere. While stirring, 1.2 mL of aqueous hydrogen peroxide (35%, 14 mmol) were added. The mixture was stirred vigorously for more 30 min, then the phases were separated, and the solvent was allowed to slowly evaporate from the organic phase at ambient temperature and pressure. Adduct **3** was obtained as a crystalline, slightly yellow solid (280 mg, 0.4 mmol, 100% yield). mp 145 °C.

NMR (δ, $CDCl_3$), $^{31}P\{^1H\}$ 36.47 (s); ^1H 7.65 – 7.55 (m, 3H, H_o, H_p, Ph), 7.48 (dt, $^3J(^1H\text{-}^1H)$ = 7.6 Hz, $^4J(^{31}P\text{-}^1H)$ = 2.8 Hz, 2H, H_m, Ph), 7.44 (dt, $^3J(^1H\text{-}^1H)$ = 7.6 Hz, $^4J(^1H\text{-}^1H)$ = 0.9 Hz, 2H, H4), 7.31 (dd, $^3J(^1H\text{-}^1H)$ = 7.4 Hz, $^4J(^{31}P\text{-}^1H)$ = 4.1 Hz, 2H, H3), 7.15 (dt, $^3J(^1H\text{-}^1H)$ = 7.4 Hz, $^4J(^{31}P\text{-}^1H)$ = 2.5 Hz, 2H, H5), 7.02 (ddd, $^3J(^{31}P\text{-}^1H)$ = 13.9 Hz, $^3J(^1H\text{-}^1H)$ = 7.3 Hz, $^4J(^1H\text{-}^1H)$ = 0.9 Hz, 2H, H6), 5.98 – 5.60 (br s, 2H, OH), 2.50 (s, 6H, CH_3); ^{13}C 143.55 (d, $^2J(^{31}P\text{-}^{13}C)$ = 7.8 Hz, C2), 133.13 (d, $^2J(^{31}P\text{-}^{13}C)$ = 13.2 Hz, C6), 132.38 (d, $^2J(^{31}P\text{-}^{13}C)$ = 9.8 Hz, C_o, Ph), 132.25 (d, $^4J(^{31}P\text{-}^{13}C)$ = 2.6 Hz, C4), 132.17 (d, $^3J(^{31}P\text{-}^{13}C)$ = 10.4 Hz, C3), 132.08 (d, $^1J(^{31}P\text{-}^{13}C)$ = 103.3 Hz, C_i, Ph), 132.06 (d, $^4J(^{31}P\text{-}^{13}C)$ = 2.8 Hz, C_p, Ph), 130.27 (d, $^1J(^{31}P\text{-}^{13}C)$ = 103.1 Hz, C1), 128.73 (d, $^3J(^{31}P\text{-}^{13}C)$ = 12.1 Hz, C_m, Ph), 125.54 (d, $^3J(^{31}P\text{-}^{13}C)$ = 13.0 Hz, C5), 21.97 (d, $^3J(^{31}P\text{-}^{13}C)$ = 4.4 Hz, C7).

Tri-*p*-tolylphosphine oxide H_2O_2 adduct (*p*-$Tol_3PO)_2{\cdot}H_2O_2$ (4). (*p*-$Tol_3PO{\cdot}H_2O_2)_2$ (**1**) (514 mg, 0.725 mmol) was dissolved in toluene (30 mL). The solution was stirred and heated to 105 °C for 10 h. During this time, 12 aliquots of 1.5 mL were collected, and the oxidative power was monitored by ^{31}P NMR using

triphenylphosphine and the method described earlier.[12] The oxidative power was diminished to 55% over 10 h of heating. The residual liquid was slowly cooled to -35 °C. Hereby, a colorless solid was obtained, which was redissolved in a mixture of dichloromethane and pentane (2:1, 10 mL). Slow evaporation of the solvents led to the formation of large colorless crystals of **4** (370.6 mg, 0.549 mmol, 76% yield). Melting range 116-137 °C.

NMR (δ, $CDCl_3$), $^{31}P\{^1H\}$ 30.47 (s); ^1H 7.54 (dd, $^3J(^{31}P\text{-}^1H)$ = 11.9 Hz, $^3J(^1H\text{-}^1H)$ = 8.1 Hz, 6H, H_o), 7.26 (dd, $^3J(^1H\text{-}^1H)$ = 7.8 Hz, $^4J(^{31}P\text{-}^1H)$ = 2.1 Hz, 6H, H_m), 6.84-6.46 (br s, O*H*), 2.40 (s, 9H, CH_3); ^{13}C 142.48 (d, $^4J(^{31}P\text{-}^{13}C)$ = 2.6 Hz, C_p), 132.22 (d, $^2J(^{31}P\text{-}^{13}C)$ = 10.4 Hz, C_o), 129.40 (d, $^1J(^{31}P\text{-}^{13}C)$ = 107.4 Hz, C_i), 129.33 (d, $^3J(^{31}P\text{-}^{13}C)$ = 12.6 Hz, C_m), 21.73 (d, $^5J(^{31}P\text{-}^{13}C)$ = 1.3 Hz, *C*H_3).

Diphenyl-*o*-tolylphosphine oxide H_2O_2 adduct (*o*-TolPh$_2$PO)$_2$·H_2O_2 (5). *o*-TolPh$_2$P (221 mg, 0.8 mmol) was placed in a Schlenk flask and dissolved in dichloromethane (2.7 mL) under a nitrogen atmosphere. Under stirring 1.2 mL of aqueous hydrogen peroxide (35%, 14 mmol) were added to the solution. The mixture was stirred vigorously for 30 min. before the phases were separated. Then the solvent was allowed to slowly evaporate from the organic phase at ambient temperature and pressure. Adduct **5** was obtained as a crystalline, slightly yellow solid (285 mg, 0.4 mmol, 100% yield). Melting range 129-132 °C.

NMR (δ, $CDCl_3$), $^{31}P\{^1H\}$ 33.50 (s); ^1H 7.64 (dd, $^3J(^{31}P\text{-}^1H)$ = 12.1 Hz, $^3J(^1H\text{-}^1H)$ = 6.9 Hz, 4H, H_o, Ph), 7.56 (tq, $^3J(^1H\text{-}^1H)$ = 7.3 Hz, $^5J(^{31}P\text{-}^1H) \approx {}^4J(^1H\text{-}^1H)$ = 1.4 Hz,

2H, H_p, Ph), 7.47 (dt, $^3J(^1H\text{-}^1H)$ = 7.6 Hz, $^4J(^{31}P\text{-}^1H)$ = 2.9 Hz, 4H, H_m, Ph), 7.43 (t, $^3J(^1H\text{-}^1H)$ = 7.5 Hz, 1H, H4, *o*-Tol), 7.29 (dd, $^3J(^1H\text{-}^1H)$ = 7.6 Hz, $^4J(^{31}P\text{-}^1H)$ = 4.2 Hz, 1H, H3, *o*-Tol), 7.14 (dt, $^3J(^1H\text{-}^1H)$ = 7.5 Hz, $^4J(^{31}P\text{-}^1H)$ = 2.2 Hz, 1H, H5, *o*-Tol), 7.01 (ddd, $^3J(^{31}P\text{-}^1H)$ = 14.2 Hz, $^3J(^1H\text{-}^1H)$ = 7.7 Hz, $^4J(^1H\text{-}^1H)$ = 1.4 Hz, 1H, H6, *o*-Tol) 2.44 (s, 6H, CH_3); ^{13}C 143.42 (d, $^2J(^{31}P\text{-}^{13}C)$ = 8.1 Hz, C2), 133.63 (d, $^2J(^{31}P\text{-}^{13}C)$ = 13.1 Hz, C6), 132.39 (d, $^4J(^{31}P\text{-}^{13}C)$ = 2.6 Hz, C4), 132.15 (d, $^1J(^{31}P\text{-}^{13}C)$ = 104.2 Hz, C_i, Ph), 132.06 (d, $^4J(^{31}P\text{-}^{13}C)$ = 2.8 Hz, C_p, Ph), 132.05 (d, $^3J(^{31}P\text{-}^{13}C)$ = 10.5 Hz, C3), 131.99 (d, $^2J(^{31}P\text{-}^{13}C)$ = 9.9 Hz, C_o, Ph), 130.24 (d, $^1J(^{31}P\text{-}^{13}C)$ = 104.0 Hz, C1), 128.72 (d, $^3J(^{31}P\text{-}^{13}C)$ = 12.2 Hz, C_m, Ph), 125.33 (d, $^3J(^{31}P\text{-}^{13}C)$ = 13.0 Hz, C5), 21.76 (d, $^3J(^{31}P\text{-}^{13}C)$ = 4.9 Hz, C7).

Di-*o*-tolylphenylphosphine oxide H_2O adduct (*o*-$Tol_2PhPO{\cdot}H_2O)_2$ (6). (*o*-$Tol_2PhPO{\cdot}H_2O_2)_2$ (**3**) (434 mg, 0.637 mmol) was placed in a Schlenk flask and dissolved in dichloromethane (30 mL). Dry molecular sieves (350 mg) were added and the mixture was stirred for 18 h at 20 °C. The molecular sieves were allowed to settle and the supernatant was collected with a syringe. The solvent was removed *in vacuo*. The colorless residue was recrystallized from toluene while being exposed to the atmosphere. The water adduct **6** was obtained as a crystalline colorless solid (340 mg, 0.524 mmol, 82% yield). Melting range 109-120 °C.

NMR (δ, $CDCl_3$), $^{31}P\{^1H\}$ 34.96 (s); ^{1}H 7.56-7.45 (m, 3H, H_o, H_p, Ph), 7.42 – 7.37 (m, 2H, H_m, Ph), 7.35 (t, $^3J(^1H\text{-}^1H)$ = 7.5 Hz, 2H, H4, *o*-Tol), 7.22 (dd, $^3J(^1H\text{-}^1H)$ = 7.7 Hz, $^4J(^{31}P\text{-}^1H)$ = 4.0 Hz, 2H, H3, *o*-Tol), 7.06 (dt, $^3J(^1H\text{-}^1H)$ = 7.5 Hz, $^4J(^{31}P\text{-}^1H)$ =

2.2 Hz, 2H, H5, *o*-Tol), 6.95 (ddd, $^{3}J(^{31}P\text{-}^{1}H)$ = 14.0 Hz, $^{3}J(^{1}H\text{-}^{1}H)$ = 7.7 Hz, $^{4}J(^{1}H\text{-}^{1}H)$ = 1.1 Hz, 2H, H6, *o*-Tol), 2.43 (s, 6H, CH_3); ^{13}C 143.54 (d, $^{2}J(^{31}P\text{-}^{13}C)$ = 7.8 Hz, C2), 133.08 (d, $^{2}J(^{31}P\text{-}^{13}C)$ = 12.9 Hz, C6), 132.75 (d, $^{1}J(^{31}P\text{-}^{13}C)$ = 102.9 Hz, C_i, Ph), 132.38 (d, $^{2}J(^{31}P\text{-}^{13}C)$ = 9.6 Hz, C_o, Ph), 132.12 (d, $^{3}J(^{31}P\text{-}^{13}C)$ = 10.3 Hz, C3) 132.05 (d, $^{4}J(^{31}P\text{-}^{13}C)$ = 2.6 Hz, C4), 131.87 (d, $^{4}J(^{31}P\text{-}^{13}C)$ = 2.8 Hz, C_p, Ph), 130.91 (d, $^{1}J(^{31}P\text{-}^{13}C)$ = 102.3 Hz, C1), 128.66 (d, $^{3}J(^{31}P\text{-}^{13}C)$ = 12.0 Hz, C_m, Ph), 125.48 (d, $^{3}J(^{31}P\text{-}^{13}C)$ = 12.9 Hz, C5), 21.99 (d, $^{3}J(^{31}P\text{-}^{13}C)$ = 4.4 Hz, C7).

References

1 (*a*) "Handbook of Advanced Methods and Processes in Oxidation Catalysis", D. Duprey and F. Cavani, Imperial College Press, 2014; (*b*) F. Cavani, J. H. Teles, *ChemSusChem*, 2009, **2**, 508-534; (*c*) "Peroxides and Peroxide Compounds", A. E. Comyns in *Van Nostrand's Encyclopedia of Chemistry,* John Wiley & Sons, Inc., 2005.

2 Y. Lu, X. Zhao and S. Fang, *Foods*, 2019, **8**, 31, 1-12.

3 H. Ying, Y. Yang, K. Cai and J. Cheng, *Eur. J. Org. Chem.,* 2019, **2019**, 728-731.

4 Nobel Foundation, The Nobel Prize in Physiology or Medicine 2015, 2015.

5 (*a*) C. J. Legacy, A. Wang, B. J. O'Day and M. H. Emmert, *Angew. Chem. Int. Ed*. 2015, **54**, 14907–14910; (*b*) C. J. Legacy and M. H. Emmert, *Synlett* 2016, **27**, 1893–1897.

6 (*a*) P. C. B. Page, B. R. Buckley, C. Elliott, Y. Chan, N. Dreyfus and F. Marken, *Synlett*, 2016, **27**, 80-82; (*b*) D. Habibi, M. A. Zolfigol, M. Safaiee, A. Shamsian and A. Ghorbani-Choghamarani, *Catal. Commun.*, 2009, **10**, 1257–1260; (*c*) H. Golchoubian and F. Hosseinpoor, *Molecules*, 2007, **12***,* 304-311; (*d*) M. Amini, M. Bagherzadeh, Z. Moradi-Shoeili, D. M. Boghaei, A. Ellern and L. K. Woo, *J. Coord. Chem*., 2013, **66**, 464-472; (*e*) T. Okada, H. Matsumuro, S. Kitagawa, T. Iwai, K. Yamazaki, Y. Kinoshita, Y. Kimura and M. Kirihara, *Synlett*, 2015, **26**, 2547-2552; (*f*) J.-W. Chu and B. L. Trout, *J. Am. Chem. Soc.*, 2004, **126**, 900-908; (*g*) E. Wojaczynska and J. Wojaczynski, *Chem. Rev*., 2010, **110**, 4303-4356; (*g*) B. Zhang, S. Li, M. Cokoja, E. Herdtweck, J. Mink, S.-L. Zang, W. A. Herrmann and F. E. Kühn, *Z. Naturforsch B*., 2014, **69b**, 1149-1163; (*h*) Y. Xie, Y. Li, S. Zhou, Y. Zhang, M. Chen and Z. Li, *Synlett*, 2018, **29**, 340-343.

7 (*a*) D. J. Covell and M. C. White, *Tetrahedron*, 2013, **69**, 7771-7778; (*b*) P. E. Gormisky and M. C. White, *J. Am. Chem. Soc.*, 2013, **135**, 14052−14055; (*c*) T. J. Osberger, D. C. Rogness, J. T. Kohrt, A. F. Stepan and M. C. White, *Nature*, 2016, **537**, 214–219; (*d*) J. M. Howell, K. Feng, J. R. Clark, L. J. Trzepkowski and M. C. White, *J. Am. Chem. Soc.*, 2015, **137**, 14590−14593; (*e*) B. H. Brodsky and J. Du Bois, *J. Amer. Chem. Soc.*, 2005, **127**, 15391-15393.

8 (*a*) J. Hou, Y. Chen, B. Cordes, D. Ma, J. Wang, X. Wang, F. E. Kühn, H. Guo and M. D. Zhou, *Chem. Commun*., 2015, **51**, 7439-7442; (*b*) M. D. Zhou, M. Liu, J. Huang, J. Zhang, J. Wang, X. Li, F. E. Kühn and S. L. Zang, *Green Chem*., 2015, **17**, 1186-1193; (*c*) M. Drees, S. A. Hauser, M. Cokoja and F. E. Kühn, *J. Organomet. Chem*., 2013, **748**, 36-45; (*d*) M. A. Goodman and M. R. Detty, *Synlett*, 2006, 1100-1104; (*e*) I. I. E. Markovits, W. A. Eger, S. Yue, M. Cokoja,

C. J. Münchmeyer, B. Zhang, M.-D. Zhou, A. Genest, J. Mink, S.-L. Zang, N. Rösch and F. E. Kühn, *Chem. Eur. J.*, 2013, **19**, 5972-5979; (*f*) H. Yao and D. E. Richardson, *J. Am. Chem. Soc*., 2000, **122**, 3220-3221; (*g*) G. S. Owens and M. M. Abu-Omar, *Chem. Commun.*, 2000, 1165-1166.

9 (*a*) J. Blümel, *Inorg. Chem*., 1994, **33**, 5050-5056; (*b*) J. Sommer, Y. Yang, D. Rambow and J. Blümel, *Inorg. Chem*., 2004, **43**, 7561-7563.

10 T. Posset, F. Rominger and J. Blümel, *Chem. Mater*., 2005, **17**, 586-595.

11 C. R. Hilliard, N. Bhuvanesh, J. A. Gladysz and J. Blümel, *Dalton Trans.,* 2012, **41**, 1742-1754.

12 S. H. Ahn, K. J. Cluff, N. Bhuvanesh and J. Blümel, *Angew. Chem. Int. Ed.*, 2015, **54**, 13341-13345; *Angew. Chem*., 2015, **127**, 13539-13543.

13 C. R. Hilliard, S. Kharel, K. J. Cluff, N. Bhuvanesh, J. A. Gladysz and J. Blümel, *Chem. Eur. J*., 2014, **20**, 17292-17295.

14 S. H. Ahn, N. Bhuvanesh and J. Blümel, *Chem. Eur. J*., 2017, **23**, 16998-17009.

15 S. H. Ahn, D. Lindhardt, N. Bhuvanesh and J. Blümel, *ACS Sustainable Chem. Eng*., 2018, **6**, 6829-6840.

16 S. Kharel, T. Jia, N. Bhuvanesh, J. H. Reibenspies, J. Blümel and J. A. Gladysz, *Chem. Asian J*., 2018, **13**, 2632-2640.

17 S. Kharel, N. Bhuvanesh, J. A. Gladysz and J. Blümel, *Inorg. Chim. Acta*, 2019, **490**, 215-219.

18 S. Kharel, K. J. Cluff, N. Bhuvanesh, J. A. Gladysz and J. Blümel, *Chem. Asian J*., 2019, **14**, DOI: 10.1002/asia.201900632.

19 (*a*) D. W. Stephan, *Science*, 2016, **354**, 1248; (*b*) J. M. Bayne and D. W. Stephan, *Chem. Soc. Rev.*, 2016, **45**, 765-774.

20 M. Mehta, I. G. De la Arada, M. Perez, D. Porwal, M. Oestreich and D. W. Stephan, *Organometallics*, 2016, **35**, 1030−1035.

21 Z. S. Han, N. Goyal, M. A. Herbage, J. D. Sieber, B. Qu, Y. Xu, Z. Li, J. T. Reeves, J.-N. Desrosiers, S. Ma, N. Grinberg, H. Lee, H. P. R. Mangunuru, Y. Zhang, D. Krishnamurthy, B. Z. Lu, J. J. Song, G. Wang and C. H. Senanayake, *J. Am. Chem. Soc*., 2013, **135**, 2474-2477.

22 (*a*) T. E. Barder and S. L. Buchwald, *J. Am. Chem. Soc*., 2007, **129**, 5096-5101; (*b*) D. B. Copley, F. Fairbrother, J. R. Miller and A. Thompson, *Proc. Chem. Soc., London*, 1964, 300–301.

23 (*a*) X. Cai, S. Majumdar, G. C. Fortman, L. M. Frutos, M. Temprado, C. R. Clough, C. C. Cummins, M. E. Germain, T. Palluccio, E. V. Rybak-Akimova, B. Captain and C. D. Hoff, *Inorg. Chem*., 2011, **50**, 9620-9630; (*b*) A. Blake, G. McQuillan, I. Oxton and D. Troy, *J. Mol. Struct*., 1982, **78**, 265-271; (*c*) J. E. Nycz and R. Musiol, *Heteroatom Chem.*, 2006, **17**, 310-316.

24 (*a*) M. Uyanik and K. Ishihara, *ACS Catal*., 2013, **3**, 513-520; (*b*) L. Zhou, X. Liu, J. Ji, Y. Zhang, X. Hu, L. Lin and X. Feng, *J. Am. Chem. Soc*., 2012, **134**, 17023-17026; (*c*) L. Zhou, X. Liu, J. Ji, Y. Zhang, W. Wu, Y. Liu, L. Lin and X. Feng, *Org. Lett*., 2014, **16**, 2938-3941.

25 (a) N. V. Klassen, D. Marchington and H. C. E. McGowan, *Anal. Chem*., 1994, **66**, 2921-2925; (*b*) Y. Cui, B. Zhang, B. Liu, H. Chen, G. Chen and D. Tang, *Microchim. Acta*, 2011, **174**, 137-144; (*c*) T. Tsuneda and T. Taketsugu, *Phys. Chem. Chem. Phys.*, 2018, **20**, 24992-24999.

26 (*a*) L. Ji, Y.-N. Wang, C. Qian and X.-Z. Chen, *Synthesis Commun.*, 2013, **43**, 2256-2264; (*b*) D. Kaur and B. R. Chhabra, *J. Chem., Biol., Phys. Sci. A*, 2013, **3**, 980-987; (*c*) M. C. Ball and S. Massey, *Thermochim. Acta*, 1995, **261**, 95-106; (*d*) J. A. Dobado, J. Molina and D. Portal, *J. Phys. Chem. A*, 1998, **102**, 778-784; (*e*) S. Taliansky, *Synlett*, 2005, 1962–1963; (*f*) M. S. Cooper, H. Heaney, A. J. Newbold and W. R. Sanderson, *Synlett*, 1990, 533-535.

27 (*a*) N. Koukabi, *Synlett*, 2010, 2969-2970; (*b*) A. McKillop and W. R. Sanderson, *J. Chem. Soc., Perkin Trans. 1*, 2000, 471–476; (*c*) D. P. Jones and W. P. Griffith, *J. Chem. Soc., Dalton Trans.*, 1980, 2526-2532.

28 S. Bednarz, B. Ryś and D. Bogdał, *Molecules*, 2012, **17**, 8068-8078.

29 (*a*) T. Jiang, W. Wang and B. Han, *New J. Chem.*, 2013, **37**, 1654-1664; (*b*) G. K. S. Prakash, A. Shakhmin, K. E. Glinton, S. Rao, T. Mathew and G. A. Olah, *Green Chem.*, 2014, **16**, 3616-3622.

30 (*a*) C. Mühle, E.-M. Peters and M. Jansen, *Z. Naturforsch. B*, 2009, **64**, 111-115; (*b*) J. Cho, S. Jeon, S. A. Wilson, L. V. Liu, E. A. Kang, J. J. Braymer, M. H. Lim, B. Hedman, K. O. Hodgson, J. S. Valentine, E. I. Solomon and W. Nam, *Nature*, 2011, **478**, 502-505; (*c*) T. Schölkopf, N.-D. Van and T. Schleid, *Inorg. Chim. Acta*, 2011, **374**, 181-186; (*d*) A. Kunishita, J. D. Scanlon, H. Ishimaru, K. Honda, T. Ogura, M. Suzuki, C. J. Cramer and S. Itoh, *Inorg. Chem*., 2008, **47**, 8222-8232; (*e*) M. Schulz, J. H. Teles, J. Sundermeyer and G. Wahl, US Patent 6,054,407, 2000.

31 K. Korth, A. Schorm, J. Sundermeyer, H. Hermann and G. Boche, *Peroxo Complexes of Molybdenum, Tungsten and Rhenium with Phase Transfer Active Ligands: Catalysts for the Oxidation of Olefins and Aromatics by Hydrogen Peroxide and Bistrimethylsilyl Peroxide* in: *Organosilicon Chemistry IV*, Wiley-VCH, Weinheim, 2000, 238-244.

32 A. V. Arzumanyan, R. A. Novikov, A. O. Terent'ev, M. M. Platonov, V. G. Lakhtin, D. E. Arkhipov, A. A. Korlyukov, V. V. Chernyshev, A. N. Fitch, A. T. Zdvizhkov, I. B. Krylov, Y. V. Tomilov and G. I. Nikishin, *Organometallics*, 2014, **33**, 2230-2246, and refs. cited.

33 (*a*) M. Bogza, T. Oeser and J. Blümel, *J. Organomet. Chem.*, 2005, **690**, 3383-3389; (*b*) R. Fetouaki, A. Seifert, M. Bogza, T. Oeser and J. Blümel, *Inorg. Chim. Acta*, 2006, **359**, 4865-4873.

34 (*a*) J. Blümel, *Coord. Chem. Rev.*, 2008, **252**, 2410-2423; (*b*) J. Guenther, J. Reibenspies and J. Blümel, *Adv. Synth. Catal*., 2011, **353**, 443-460; (*c*) R. Silbernagel, A. Diaz, E. Steffensmeier, A. Clearfield and J. Blümel, *J. Mol. Catal. A*, 2014, **394**, 217-223; (*d*) C. Merckle and J. Blümel, *Adv. Synth. Catal.*, 2003, **345**, 584-588; (*e*) C. Merckle and J. Blümel, *Top. Catal.*, 2005, **34**, 5-15.

35 (*a*) J. H. Baker, N. Bhuvanesh and J. Blümel, *J. Organomet. Chem*., 2017, **847**, 193-203; (*b*) Y. Yang, B. Beele and J. Blümel, *J. Am. Chem. Soc*., **2008**, **130**, 3771-3773; (c) B. Beele, J. Guenther, M. Perera, M. Stach, T. Oeser and J. Blümel, *New J. Chem*., **2010**, **34**, 2729-2731.

36 (*a*) J. C. Pope, T. Posset, N. Bhuvanesh and J. Blümel, *Organometallics*, 2014, **33**, 6750-6753; (*b*) T. Posset and J. Blümel, *J. Am. Chem. Soc.*, 2006, **128**, 8394-8395; (*c*) T. Posset, J. Guenther, J. Pope, T. Oeser and J. Blümel, *Chem. Commun.*, 2011, **47**, 2059-2061.

37 (*a*) S. Reinhard, P. Soba, F. Rominger and J. Blümel, *Adv. Synth. Catal*., **2003**, **345**, 589-602; (b) F. Piestert, R. Fetouaki, M. Bogza, T. Oeser and J. Blümel, *Chem. Commun*., 2005, 1481-1483; (*c*) K. J. Cluff, N. Bhuvanesh and J. Blümel, *Chem. Eur. J*., 2015, **21**, 10138-10148; (*d*) S. Reinhard, K. D. Behringer and J. Blümel, *New J. Chem.*, 2003, **27**, 776-778.

38 (*a*) A. Zheng, S.-B. Liu and F. Deng, *Chem. Rev.*, 2017, **117**, 12475−12531; (*b*) R. Yerushalmi, J. C. Ho, Z. Fan and A. Javey, *Angew. Chem. Int. Ed.*, 2008, **47**, 4440-4442; (*c*) J. P. Osegovic and R. S. Drago, *J. Phys. Chem. B*, 2000, **104**, 147-154; (*d*) S. Hayashi, K. Jimura and N. Kojima, *Bull. Chem. Soc. Jpn.*, 2014, **87**, 69-75; (*e*) S. Machida, M. Sohmiya, Y. Ide and Y. Sugahara, *Langmuir*, 2018*,* **34***,* 12694−12701.

39 (*a*) A. R. Wilmsmeyer, W. O. Gordon, E. D. Davis, B. A. Mantooth, T. A. Lalain and J. R. Morris, *Rev. Sci. Instrum*., 2014, **85**, 014101; (*b*) J. Kemsley, *Chem. Eng. News*, 2014, **92**, 29.

40 (*a*) H. Ren, J. Sun, B. Wu and Y. Zhou, *Polym. Degrad. Stab*., 2007, **92**, 956-961; (*b*) M. A. Espinosa, M. Galia and V. Cadiz, *J. Polym. Sci., Part A: Polym. Chem.*, 2004, **42**, 3516-3526.

41 (*a*) J. Chrzanowski, D. Krasowska and J. Drabowicz, *Heteroatom Chem*., 2018, **29**, DOI:10.1002/hc.21476; (*b*) T. Kovacs and G. Keglevich, *Curr. Org. Chem*., 2017, **21**, 569-585; (*c*) D. Herault, D. H. Nguyen, D. Nuel and G. Buono, *Chem. Soc. Rev*., 2015, **44**, 2508-2528; (*d*) M. D. Fletcher, *Organophosphorus Reagents*, 2004, 171-214; (*e*) H. R. Hays and D. J. Peterson, *Org. Phosphorus Compounds*, 1972, **3**, 341-500; (*f*) H. Adams, R. C. Collins, S. Jones and C. J. A. Warner, *Org. Lett*., 2011, **13**, 6576-6579.

42 (*a*) D. Nunez-Villanueva, C. A. Hunter, *Chem. Sci*., 2017, **8**, 206--213; (*b*) A. E. Stross, G. Iadevaia and C. A. Hunter, *Chem. Sci.*, 2016, **7**, 94-101; (*c*) G. Iadevaia, A. E. Stross, A. Neumann and C. A. Hunter, *Chem. Sci.*, 2016, **7**, 1760-1767; (*d*) R. Cuypers, E. J. R. Sudhölter and H. Zuilhof, *ChemPhysChem*., 2010, **11**, 2230-2240.

43 N. A. Bewick, A. Arendt, Y. Li, S. Szafert, T. Lis, K. A. Wheeler, J. Young and R. Dembinski, *Curr. Org. Chem*., 2015, **19**, 469-474.

44 S. J. Pike and C. A. Hunter, *Org. Biomol. Chem*., 2017, **15**, 9603-9610.

45 N. J. Burke, A. D. Burrows, M. F. Mahon and J. E. Warren, *Inorg. Chim. Acta*, 2006, **359**, 3497-3506.

46 R. Joshi and S. P. Pasilis, *J. Mol. Liquids*, 2015, **209**, 381-386.

47 I. Alkorta and J. Elguero, *J. Phys. Chem. A*, 1999, **103**, 272-279.

48 (*a*) D. V. Ilyin, W. A. Goddard III, J. J. Oppenheim and T. Cheng, First-principles–based reaction kinetics from reactive molecular dynamics simulations: Application to hydrogen peroxide decomposition, *Proceedings of the National Academy of Sciences*, 2018, 201701383, 1; (*b*) T. Tsuneda, J. Miyake and K. Miyatake, *ACS Omega*, 2018, **3**, 259-265.

49 (*a*) E. Y. Tupikina, M. Bodensteiner, P. M. Tolstoy, G. S. Denisov and I. G. Shenderovich, *J. Phys. Chem. C*, 2018, **122**, 1711-1720; (*b*) G. Begimova, E. Y. Tupikina,V. K. Yu, G. S. Denisov, M. Bodensteiner and I. G. Shenderovich, *J. Phys. Chem. C*, 2016, **120**, 8717-8729.

50 K. R. Iler, *The Chemistry of Silica*, John Wiley, New York, 1979.

51 Q. Lin, Y. Jiang, J. Geng, and Y. Qian, Removal of Organic Impurities with Activated Carbons for Ultra-Pure Hydrogen Peroxide Preparation. *Chem. Eng. J*., 2008, **139**, 264-271.

52 D. Thierbach, F. Huber and H. Preut, *Acta Crystallogr., Sect. B: Struct. Crystallogr. Cryst. Chem.*, 1980, **36**, 974-977.

53 M. C. Etter, P. W. Baures, Triphenylphosphine Oxide as a Crystallization Aid, *J. Am. Chem. Soc.*, 1988, **110**, 639-640.

54 The following CCDC reference numbers contain the supplementary crystallographic data for the corresponding compounds **1**-**7** for this paper: 1898472 ((*p*-$Tol_3PO{\cdot}H_2O_2)_2$, **1**), 1898473 ((*o*-$Tol_3PO{\cdot}H_2O_2)_2$, **2**), 1898474 ((*o*-$Tol_2PhPO\ H_2O_2)_2$, **3**), 1898475 ((*p*-$Tol_3PO)_2{\cdot}H_2O_2$, **4**), 1898476 ((*o*-$TolPh_2PO)_2{\cdot}H_2O_2$, **5**), 1930449 ((*o*-$Tol_2PhPO\ H_2O)_2$, **6**), and 1937469 (*p*-Tol_3PO, **7**). These data can be obtained free of charge from the Cambridge Crystallographic Data Centre via www.ccdc.cam.ac.uk/data_request/cif.

55 F. R. Fronczek, *CSD Communication*, 2014. DOI: 10.5517/cc138jkg.

56 M. R.Churchill, R. F. See, S. L. Randall and J. D. Atwood, *Acta Cryst. C*, 1993, **49**, 345-347.

58 (*a*) G. A. Jeffrey, *An Introduction to Hydrogen Bonding*; Oxford University Press: Oxford, **1997**; (*b*) E. N. Baker and R. E. Hubbard, Hydrogen Bonding in Globular Proteins, *Prog. Biophys. Mol. Biol.* 1984, **44**, 97-179.

59 R. M. Denton, J. An, B. Adeniran, A. J. Blake, W. Lewis and A. M. Poulton, *J. Org. Chem.*, 2011, **76***,* 6749-6767.

60 H. C. E. McFarlane and W. McFarlane, *Oxygen* in *Multinuclear NMR*, J. Mason Ed., Plenum Press, New York, 1987.

61 R. Curci, G. Fusco, O. Sciacovelli and L. Troisi, *J. Mol. Catal.*, 1985, **32**, 251-257.

62 J. J. Barieux and J. P. Schirmann, *Tetrahedron Lett.*, 1987, **28**, 6443-6446.

63 A. L. Baumstark, P. C. Vasquez and P. Balakrishnan, *Tetrahedron Lett.*, 1985, **26**, 2051-2054.

64 B. Plesničar, J. Cerkovnik, T. Tekavec and J. Koller, *Chem. Eur. J.*, 2000, **6**, 809-819.

65 M. Căsný, D. Rehder, H. Schmidt, H. Vilter and V. Conte, *J. Inorg. Biochem.*, 2000, **80**, 157-160.

66 T. M. Alam, M. Celina, R. A. Assink, R. L. Clough, K. T. Gillen and D. R. Wheeler, *Macromolecules*, 2000, **33**, 1181–1190.

67 A. Wong, K. J. Pike, R. Jenkins, G. J. Clarkson, T. Anupõld, A. P. Howes, D. H. G. Crout, A. Samoson, R. Dupree and M. E. Smith, *J. Phys. Chem. A*, 2006, **110**, 1824-1835.

68 D. L. Bryce, K. Eichele and R. E. Wasylishen, *Inorg. Chem.*, 2003, **42**, 5085-5096.

69 H. Dahn, V. V. Toan and M.-N. Ung-Truong, *Magn. Reson. Chem.* 1992, **30**, 1089-1096.

70 R. D. Sammons, P. A. Frey, K. Bruzik and M.-D. Tsai, *J. Am. Chem. Soc*., 1983, **105**, 5455-5461.

71 E. J. Cabrita and S. Berger, *Magn. Reson. Chem.*, 2001, **39**, S142-S148.

72 J. L. Cook, C. A. Hunter, C. M. R. Low, A. Perez-Velasco and J. G. Vinter, *Angew. Chem. Int. Ed.*, 2007, **46**, 3706-3709.

73 G. Kagan, W. Li, R. Hopson and P. G. Williard, *Org. Lett.*, 2009, **11**, 4818-4821.

74 H. Günzler and H.-U. Gremlich, *IR-Spektroskopie*, 4th ed., Wiley-VCH, **2003**.

75 W. H. Fletcher and J. S. Rayside, *J. Raman Spectrosc.*, 1974, **2**, 3-14.

76 M. Hayyan, M. A. Hashim and I. M. AlNashef, *Chem. Rev.*, 2016, **116**, 3029-3085.

77 R. C. Taylor and P. C. Cross, *J. Chem. Phys.*, 1956, **24**, 41-44.

78 P. A. Giguére and T. K. K. Srinivasan, *J. Raman Spectrosc.*, 1974, **2**, 125-132.

79 H. H. Eysel and S. Thym, *Z. anorg. allg. Chem*., 1975, **411**, 97-102.

80 V. Vacque, B. Sombret, J. P. Huvenne, P. Legrand and S. Suc, *Spectrochim. Acta A: Mol. Biomol. Spectrosc.*, 1997, **53**, 55-66.

CHAPTER III

SELECTIVE SYNTHESIS AND STABILIZATION OF PEROXIDES VIA PHOSPHINE OXIDES*

Introduction

Phosphine oxides are compounds that have been described in inorganic chemistry textbooks for a long time. Recently, they came back into the spotlight in many different areas. They are, for example, unwanted byproducts of phosphine coordination chemistry, especially in the field of immobilized catalysts.[1-4] Many linkers that are used to tether metal complexes to solid oxide supports contain phosphine groups. Once the latter are oxidized to phosphine oxides, the catalyst is no longer retained and leaches from the support.[5] Furthermore, phosphine oxides are co-products of Wittig and Appel reactions. In another field, they are applied to probe surface acidities[6] and recently became the focus of attention regarding the decomposition of warfare agents.[7] In this context, phosphine oxides have been shown to be very mobile on surfaces, which leads to interesting line-narrowing effects in the ^{31}P solid-state NMR spectra due to the averaging out of anisotropic interactions, most importantly the Chemical Shift Anisotropy (CSA).[8,9] Finally, it should be noted that phosphine oxides are important synthetic targets and intermediates.[10,11] For example, they are used for Mitsunobu reactions since a long time,[11g] and recently became the focus of attention as redox-free Mitsunobu organocatalysts.[11h]

---

* Reproduced from F. F. Arp, S. H. Ahn, N. Bhuvanesh, J. Blümel, *New J. Chem.*, 2019, **43**,17174-17181 with permission from the Centre National de la Recherche Scientifique (CNRS) and the Royal Society of Chemistry.

One of the most important features of phosphine oxides is that they form hydrogen bonds with a variety of different donors. For example, phenols have been used in combination with phosphine oxides to create extended hydrogen-bonded networks.[12,13] Furthermore, hydrogen bonding with naphthol,[14] sulfonic acids,[15] and water has been reported.[8,16-18] Even silanols, phenols, and chloroform crystallize as hydrogen-bonded assemblies.[19] Besides single crystal X-ray diffraction, ^{31}P solid-state NMR spectroscopy is a powerful method to analyze the hydrogen bonding characteristics of diverse P(V) species.[8-10,17,20]

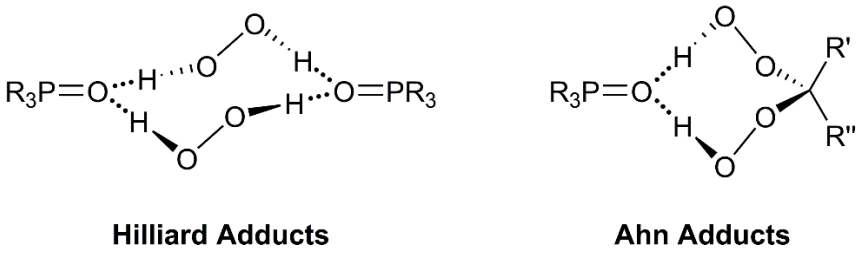

Figure 17 Selected previously reported Hilliard adducts (R = Cy, *t*-Bu, Ph, *o*-Tol, *p*-Tol)[17,18,21] and Ahn adducts (R, = Cy, Ph, Et; R', R" = Me, Et, Pr, $(CH_2)_{5\text{-}7}$).[21-23]

We discovered recently that phosphine oxides are also able to stabilize hydrogen peroxide and di(hydroperoxy)alkanes by forming hydrogen bonds.[17,18,21-23] The Hilliard adducts can be generated by exposing phosphines or phosphine oxides to aqueous H_2O_2. They exhibit most commonly the structural motifs $(R_3PO{\cdot}H_2O_2)_2$ or $(R_3PO)_2{\cdot}H_2O_2$.[21-23] Ahn adducts form assemblies of the type $R_3PO{\cdot}(HOO)_2CR'R''$ (R, R', R" = alkyl and aryl) when phosphines, their oxides, or Hilliard adducts are reacted with ketones in the

presence of aqueous H_2O_2.[21-23] Figure 17 shows the most common structures of Hilliard[17,18,21] and Ahn[21-23] adducts synthesized and characterized so far. Importantly, all adducts are safe and robust with respect to mechanical and thermal impact. Even when bringing the powders directly into a flame, the oxygen escapes without a pronounced audible or visual effect. These stable, solid Hilliard and Ahn adducts are easy to synthesize, they crystallize readily, and are currently investigated regarding their potential as oxidizers.[21-23]

Peroxides are ubiquitous and immensely important in daily life, medicine, academia, and industry.[24-27] Recent applications in synthesis include the oxidation of amines[28] and sulfides,[29] alkane activation,[30] epoxidations,[31] and Baeyer-Villiger oxidations.[23,32]

Unfortunately, the most ubiquitous oxidizing agent, aqueous H_2O_2, is far from ideal. The abundance of water it inevitably delivers to the reaction mixture can lead to unwanted secondary reactions. Additionally, most oxidations have to be performed in a biphasic system, slowing rates and requiring phase separations later. Commercial aqueous H_2O_2 also contains nitric acid as stabilizer. Aqueous H_2O_2 degrades at unpredictable rates,[33] especially in the presence of metal ion traces[33c] and requires titration prior to critical applications.[33a,b] Water-free formulations of H_2O_2, like urea hydrogen peroxide (UHP)[34] and peroxocarbonates[35] do not have well-defined compositions and are insoluble in organic solvents. Encapsulated versions of H_2O_2,[36] and its adducts of metal complexes are known but not readily available commercially or

synthetically.[37,38] The peroxides $(Me_3SiO)_2$ and $(CH_3)_2C(OO)$ (DMDO) are applied, but their synthesis and storage are problematic.[38,39]

In this contribution we describe the creation of a solid, crystalline network with well-defined composition that stabilizes H_2O_2 by hydrogen-bonding to the P=O groups of dcpe dioxide (bis(dicyclohexylphosphino)ethane dioxide). Furthermore, we report a selective synthesis and the stabilization of a MEKPO (methyl ethyl ketone peroxide) dimer by hydrogen-bonding with dppe dioxide. Again, an extended network is obtained that has also been characterized by single crystal X-ray diffraction. Reaction of acetylacetone with aqueous H_2O_2, in the presence or absence of a phosphine oxide resulted in the formation of two cyclic peroxides.

Results and Discussion

Hilliard adducts[17,18,21] (Figure 17) have already proven to be safe, soluble, and solid incarnations of H_2O_2 with known and reproducible stoichiometry. However, to render them more competitive with aqueous H_2O_2, the weight of the carrier phosphine oxide needs to be reduced. One approach towards this goal is to offer a diphosphine dioxide, bis(dicyclophosphino)ethane dioxide, for stabilizing the H_2O_2. The envisioned species included a monomeric adduct with to intramolecular P=O groups, $(CH_2Cy_2PO{\cdot}H_2O_2)_2$, and a cyclic dimer containing four H_2O_2 molecules bridging four P=O functions, $[(CH_2Cy_2PO{\cdot}H_2O_2)_2]_2$. The formation of cyclic structures seemed likely, especially with respect to Shenderovich's work on cyclic trimers of phosphinic acids.[40]

However, when dcpe dioxide was reacted with aqueous H_2O_2, an extended network with a zig-zag chain structure was formed (**1**, Figure 18). The material **1**

crystallized easily and could be investigated by single crystal X-ray diffraction (Figure 19). The P=O groups of each diphosphine dioxide molecule are oriented in opposite directions, with a dihedral angle of 180°. This structural feature has been observed previously for Ahn adducts of dppe (bis(diphenylphosphino)ethane) dioxide.[22] Every H_2O_2 molecule forms hydrogen bonds to two P=O groups of neighboring dcpe dioxide molecules. The short distance of 1.755 Å between the P=O oxygen and the H atoms corroborates the hydrogen bonding, as this distance is even slightly shorter than the values in the characteristic range that spans from 1.85 to 1.95 Å.[42] Additionally, the hydrogen bonding manifests itself in the short distance between the two O−H···O oxygen atoms (2.704 Å), which also lies slightly below the typical range of values from 2.75 to 2.85 Å.[43] The P=O groups are weakened and elongated (1.501 Å) due to the hydrogen bonding, consistent with comparable values of the Hilliard adducts described earlier.[17,18,21]

The ^{31}P NMR resonance of adduct **1** also has a different chemical shift (53.78 ppm) than the signal of dcpe dioxide (54.27 ppm). The hydrogen bonding does, however, not manifest in a different IR wavenumber for ν(P=O) in **1**, as the same value of 1134 cm^{-1} is measured for the neat compound dcpe dioxide. The smaller differences in the IR and NMR chemical shift values, as compared to previously described Hilliard adducts[17,18,21] are most probably due to the fact that in **1** only one hydrogen bond is formed between H_2O_2 and a P=O group, while the majority of the Hilliard adducts have two. However, regarding the longterm stability of material **1**, it compares favorably with dimeric Hilliard adducts. For example, after about three years of storage in the

laboratory atmosphere at room temperature (22 °C), solid **1** retained 58% of its original oxidative power. Under the same conditions, after ca. three years, (*p*-$Tol_3PO{\cdot}H_2O_2)_2$ only retains 33% of its oxidative power.[18]

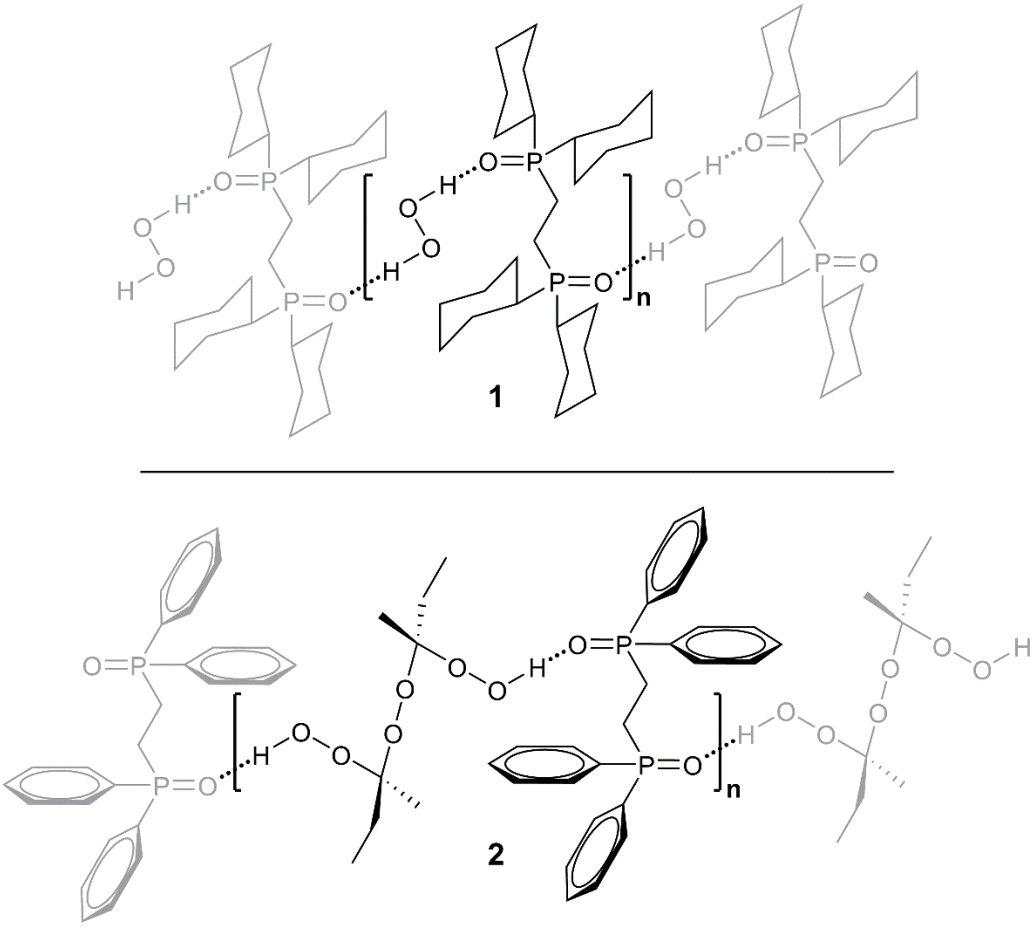

Figure 18 The new materials **1** and **2**.

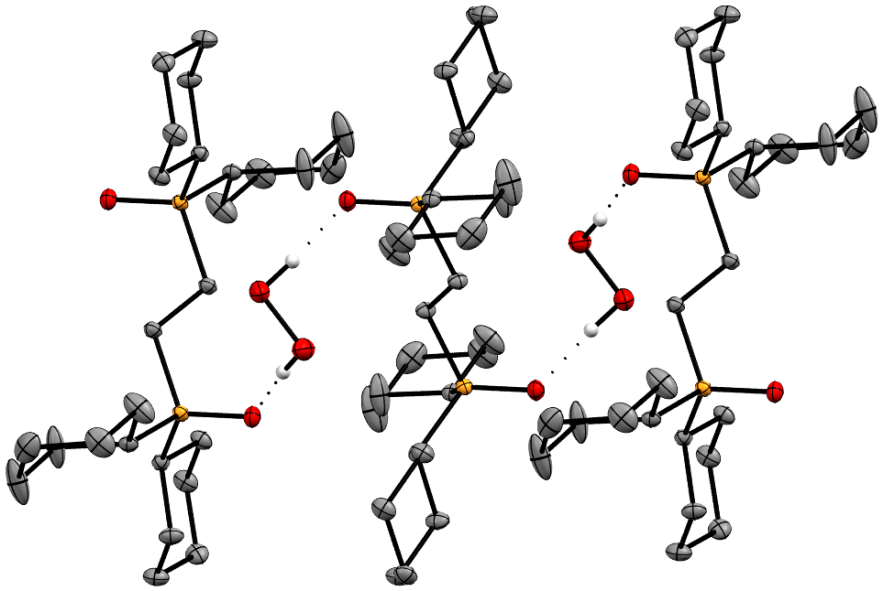

Figure 19 Single crystal X-ray structure of the hydrogen peroxide adduct $[(CH_2Cy_2PO)_2 \cdot H_2O_2]_n$ (**1**).[41]

Based on the experience that phosphine oxides can efficiently stabilize bis(dihydroperoxy)alkanes via hydrogen bonding to form Ahn adducts,[21-23] we sought to create an Ahn adduct with reduced weight of the phosphine oxide carrier. This should render Ahn adducts more competitive with respect to the commercially available aqueous H_2O_2. We approached the new synthesis by using the dioxide of bis(diphenylphosphino)ethane (dppe dioxide) as carrier with lower weight and sought to produce the Ahn adduct $(CH_2Ph_2PO \cdot (HOO)_2CMeEt)_2$, in analogy to $(CH_2Ph_2PO \cdot (HOO)_2CEt_2)_2$ that has been reported previously.[22]

Interestingly, when butanone was reacted with aqueous H_2O_2 in the presence of dppe dioxide, the dimeric peroxide $(HOOCMeEtO)_2$ was obtained. This peroxide dimer is stabilized by forming a hydrogen-bonded extended network with dppe dioxide,

$[(CH_2Ph_2PO)_2 \cdot (HOOCMeEtO)_2]_n$ (**2**) (Figure 18). The material **2** is obtained in an unoptimized yield of 83%.

The selective formation of adduct **2** is remarkable regarding the properties and especially the reactivity of MEKPO (methyl ethyl ketone peroxides). MEKPO represents an indispensable class of reagents in the polymer industry, where it is used as a catalyst for acrylic resins or as curing agent for unsaturated polyester resins.[44,45] However, despite its importance, it is regarded as a very hazardous material. Therefore, great efforts have been undertaken to produce MEKPO under controlled reaction conditions and on small scales, for example, by using a microreactor.[45] At present, MEKPO oligomers are synthesized by reacting butanone (MEK, methyl ethyl ketone) with H_2O_2 in a batchwise manner. The initial product is most probably EtC(OH)(OOH)Me that undergoes secondary reactions to yield a mixture of linear and cyclic oligomers.[44] These oligomers are impossible to separate economically and therefore MEKPO is applied as a mixture based on the wt% of active oxygen.[44,45] Industrial batches of MEKPO still contain residual MEK which increases its explosion hazard. Additionally, for industrial applications MEKPO is diluted with DMP (*o*-dimethylphthalate) to 40-60% solutions. Furthermore, it is a strong oxidizing agent and a corrosive. Acute and chronic toxicity can occur as an occupational hazard. Inhalation of MEKPO can lead to pneumonitis, acidosis, and liver and renal failure.[46] Finally, MEKPO is prone to runaway reactions when coming into contact with a variety of substances, for example, bases, or Fe(II/III) salts.[47]

In contrast, material **2** is a much more benign version of MEKPO. It is solid, has a low vapor pressure, and besides the phosphine oxide carrier it is free of additives. Material **2** exhibits a well-defined composition and is less prone to uncontrolled decomposition. In fact, when mechanical stress like grinding or hammering are applied, no detonation occurs and bringing **2** into a flame only leads to slow release of gas without pronounced visible or audible effects. Nevertheless, the active oxygen content of **2** amounts to 7.5 wt%, which is close to the range of commercially available MEKPO for academic use (32-35 wt% solutions with 8.7-9.0 wt% active oxygen).

In order to determine the longevity of peroxides that are stabilized by hydrogen-bonding in Hilliard[17,18,21] or Ahn adducts,[21-23] we have previously developed a method to quickly determine their oxidative power. The method is based on offering the peroxide a weighed amount of PPh_3 in excess and integrating the ^{31}P NMR signals of residual PPh_3 and produced $OPPh_3$ after the oxidation reaction.[21] Accordingly, for material **2**, an oxidative power of 100% would correspond to three active oxygen atoms per adduct unit (Figure 18). It turns out that the peroxide in **2** is stabilized very well by the dppe dioxide, and after 4.7 years of exposure to the atmosphere in a drawer in the lab at ambient temperature its remaining oxidative power still amounts to 24%.

Material **2** crystallizes readily and in large habits, and therefore the structure could also be characterized by single crystal X-ray diffraction (Figure 20).

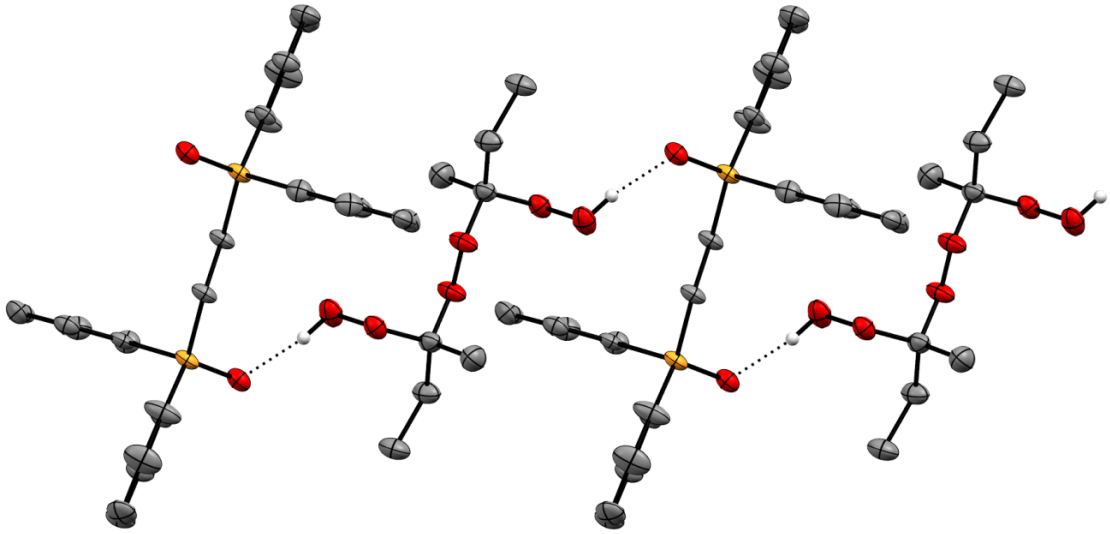

Figure 20 Single crystal X-ray structure of adduct **2**.[41]

The two ketal carbon atoms in the dimeric peroxide component of the network display *R* and *S* configurations, therewith constituting the *meso* compound. The two hydroperoxy groups are hydrogen-bonded to the phosphine oxide groups. The two hydrogen-bonded P=O groups of the dppe dioxide point in opposite directions with a dihedral angle of 180°, in analogy to the extended network of material **1**. The ideal packing with dppe dioxide (Figure 20) may promote the formation of the dimeric peroxide as opposed to the di(hydroperoxy)butane moieties found in the adducts $Ph_3PO{\cdot}(HOO)_2CEtMe$ and $Cy_3PO{\cdot}(HOO)_2CEtMe$.[22] The crucial factor explaining the ease of crystallization of material **2** and favoring the structure of the network might be the similar lengths of the P−C−C−P (4.412 Å) unit of the diphosphine dioxide and the C−O−O−C (3.571 Å) moiety of the dimeric peroxide, which allow for their parallel and

strainless stacking in the crystal. The slight difference in the lengths allows the hydrogen bonds to retain the favorable linear O···H−O arrangement.

Every MEKPO moiety forms hydrogen bonds to two P=O groups of adjacent dppe dioxide molecules. The distance of 1.783 Å between the P=O oxygen and the H atoms indicates the hydrogen bonding, being even slightly shorter than the values in the characteristic range from 1.85 to 1.95 Å.[42] Furthermore, the hydrogen bonding leads to a short distance between the two O−H···O oxygen atoms (2.627 Å), which is slightly outside at the lower end of the typical range of values (2.75 to 2.85 Å).[43] The P=O groups are elongated (1.497 Å) due to the hydrogen bonding, consistent with comparable values of the Ahn adducts described earlier.[21-23] Correspondingly, the ^{31}P NMR resonance of **2** undergoes a downfield shift to 36.91 ppm with respect to 31.5 ppm reported for the adduct-free dppe dioxide.[48] The hydrogen bonding also manifests in the slight lowering of the IR wavenumber ν(P=O) in **2** to 1173 cm^{-1} as compared to 1175 cm^{-1} for dppe dioxide.[48]

Similarly to the Ahn adducts described previously,[21-23] the solubility of **2** is highest in methylene chloride (66.9 mg/mL). It is relatively low in benzene (1.43 mg/mL), methanol (1.72 mg/mL), and dimethylformamide (2.24 mg/mL). Most probably, the nature of **2** with its extended hydrogen-bonded network leads to the comparatively low solubilities in the latter three solvents. Dichloromethane, due to its ability to strongly interact with P=O groups,[19] might be able to split **2** into smaller, more soluble fragments of the network. It has been demonstrated earlier by DOSY experiments that in methylene chloride dimeric Hilliard adducts with triarylphosphine

oxide carriers are dissociating into monomers.[18] Nevertheless, it is noteworthy that even the lower solubilities are more than sufficient for potential applications of **2** as a polymerization starter.[49]

Since dppe dioxide proved to be able to form multiple hydrogen bonds to di(hydroperoxy)alkanes, the next step in our synthesis endeavor involved expanding the scope of offered ketones to diketones. In this way, the weight of the adduct assemblies per active oxygen atom could be reduced. Furthermore, we sought to probe whether both carbonyl groups of a diketone could undergo nucleophilic attack by H_2O_2[21,22] to each form the di(hydroperoxy)alkane moiety. The latter would be stabilized immediately by hydrogen-bonding to the offered phosphine oxide groups.

To test this idea, acetylacetone was selected as the 1,3-diketone because it is very versatile and, depending on the reaction conditions and additives, it can yield a variety of different products.[50-52] Dppp dioxide (bis(diphenylphosphino)propane dioxide) was chosen as the phosphine oxide partner. The P=O groups are in close enough proximity to form strong hydrogen bonds, while the $(CH_2)_3$ tether between them should allow for sufficient flexibility to orient them towards the two di(hydroperoxy)alkane moieties potentially created from acetylacetone.

Interestingly, the presence of dppp dioxide does not prevent the cyclization of the diketone when being treated with aqueous H_2O_2. This result is in contrast to the cases of previously reported adducts, where the phosphine oxides formed hydrogen bonds with the di(hydroperoxy)alkane moieties and thereby prevented the condensation leading to cyclic acetone peroxide or butanone peroxide.[21-23] The cyclic peroxide **3** is formed

according to the pathway diplayed in Scheme 2. Acetylacetone undergoes two consecutive nucleophilic attacks by aqueous H_2O_2 to form selectively the *trans*-cycloperoxides **3** (Scheme 2). The presence of nitric acid as stabilizer in the aqueous H_2O_2 most probably facilitates the nucleophilic attacks. However, it is remarkable that no I_2 was needed as a catalyst to create the dioxolane as reported for similar 1,3-diketone transformations to dioxolanes previously.[53] In contrast to earlier reports of *cis*/*trans* mixtures,[52] only the trans isomer of **3** was obtained. Furthermore, in the sole presence of H_2O_2 and strong acids, bridged tetraoxanes have been reported.[51]

Depending on the amount of H_2O_2, either *trans*-3,5-dimethyl-1,2-dioxolane-3,5-diol (**3**) or *trans*-3,5-dihydroperoxy-3,5-dimethyl-1,2-dioxolane (**4**) is isolated as the sole product (Figure 21). Curiously, the mixed dioxolane **5**,[52] containing one OH and one OOH substituent (Figure 21), was not observed.

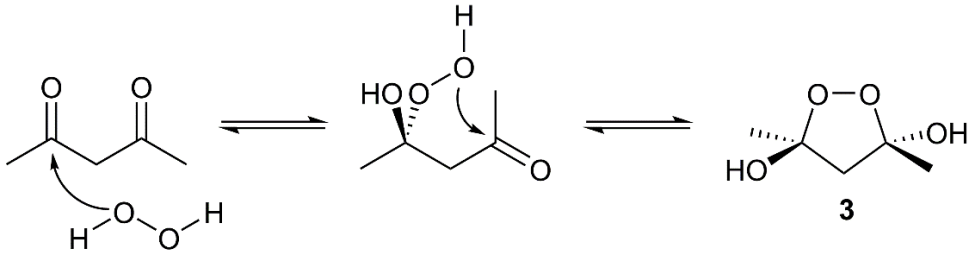

Scheme 2 Synthesis of the cyclic dioxolane derivative **3**.

It is remarkable that only the *trans* isomers are formed in both cases, while in the literature *cis/trans* isomer mixtures of **3** and **4** are obtained by different syntheses.[52,54]

Since both **3** and **4** crystallize readily, the *trans* substitution is also proven by their single crystal X-ray structures.[41,55] Figure 22 displays the structure of **3**,[41] the structure of **4** is in accord with the literature.[41,54,55]

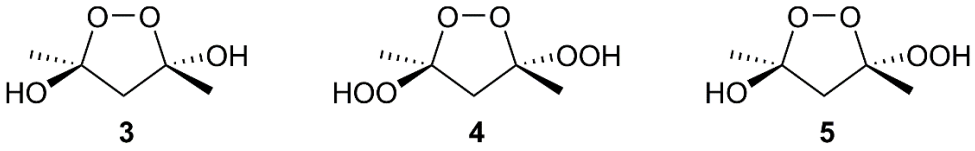

Figure 21 Possible products of the reaction of acetylacetone with aqueous H_2O_2. Only **3** and **4**, but not **5** were observed experimentally.

Both dioxolanes **3** and **4** form an intricate network of hydrogen bonds with neighboring molecules (Figure 22), which may be the reason for their ease of crystallization. Furthermore, these intermolecular hydrogen bonds might compete with the adduct formation via the P=O groups of the phosphine oxides, in this way favoring the cyclic molecular products **3** and **4**.

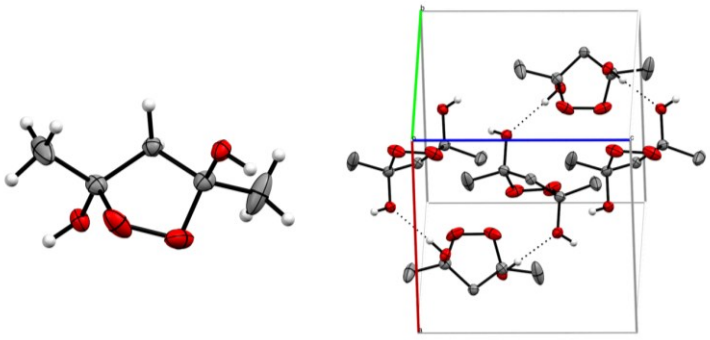

Figure 22 Single crystal X-ray structure of **3** (left) and **3** in the unit cell (right).[41]

It is also noteworthy that compounds **3** and **4** could be obtained selectively and isolated in high yields of 71% and 68%, respectively. No elaborate purification operations like column chromatography, and no catalysts like I_2 and $SnCl_2 \cdot 2H_2O$ were needed.[52,54] Furthermore, the aqueous H_2O_2 used was not as concentrated with 35 wt% (compared to 50 wt%) and no concentrated H_2SO_4 had to be added, in contrast to a previously described procedure.[54]

Conclusion

For preparative chemistry, the ideal peroxide would be inexpensive, easily accessible, reproducible in its composition, and soluble in organic solvents. It should be safe and stable at ambient temperatures on the shelf. Finally, a solid oxidizing agent would be desirable that can easily be administered.

In this contribution we describe the easy synthesis, purification, and characterization of a H_2O_2 adduct of a diphosphine oxide (**1**), and an adduct containing a MEKPO dimer (**2**). Furthermore, the selective syntheses of two dioxolane derivatives (**3** and **4**) are described.

The reaction of bis(dicyclohexylphosphino)ethane dioxide with hydrogen peroxide leads to an extended crystalline network based on the formation of hydrogen bonds with the P=O groups of the diphosphine dioxide. The novel structural motif of the network is characterized by X-ray diffraction. Furthermore, a new selective synthesis for an industrially important MEKPO dimer and its stabilization by a diphosphine dioxide is described. The dimer is created by reaction of dppe dioxide with butanone and aqueous hydrogen peroxide. This dimeric peroxide is stabilized by strong hydrogen bonds to the

phosphine oxide groups within an extended network, which has been characterized by single crystal X-ray diffraction. The dimeric peroxide material can easily be purified by crystallization. It is solid with a low vapor pressure and therefore poses less of a health hazard at the workplace than pure MEKPO. Phosphine oxide-supported MEKPO does not show tendencies to explode and is stable on the shelf at ambient temperatures over years. Furthermore, it is soluble in organic solvents, with the highest solubility in methylene chloride. In summary, material **2** might be an attractive alternative to MEKPO in the future.

The reaction of acetylacetone with aqueous H_2O_2, irrespective of the presence of phosphine oxide, leads to the unprecedented stereoselective formation of two dioxolane derivatives in high isolated yields. Both cyclic peroxides have been obtained in crystalline forms suitable for single crystal X-ray diffractions and their stereochemistry has been determined.

Experimental Section

General Considerations

All reactions were carried out using standard Schlenk line techniques and a purified N_2 atmosphere, if not stated otherwise. Reagents purchased from Sigma Aldrich or VWR were used without further purification. Aqueous H_2O_2 solution (35% w/w) was obtained from Acros Organics and used as received. Solvents were dried by boiling them over sodium, then they were distilled and stored under purified nitrogen. Dichloromethane (Aldrich, ACS reagent grade) was dried over 3 Å molecular sieves (EMD Chemical Inc.) prior to use.

NMR Spectroscopy

The ^{1}H, ^{13}C, and ^{31}P NMR spectra were recorded at 499.70, 125.66, and 202.28 MHz on a 500 MHz Varian spectrometer. The ^{13}C and ^{31}P NMR spectra were recorded with ^{1}H decoupling. Neat Ph_2PCl ($\delta(^{31}P)$ = +81.92 ppm) in a capillary centered in the 5 mm NMR tubes was used for referencing the ^{31}P chemical shifts. For referencing the ^{1}H and ^{13}C chemical shifts the residual proton and the carbon signals of the solvents were used (C_6D_6: $\delta(^{1}H)$ = 7.16 ppm, $\delta(^{13}C)$ = 128.00 ppm; $CDCl_3$: $\delta(^{1}H)$ = 7.26 ppm, $\delta(^{13}C)$ = 77.00 ppm). The signal assignments are based on $^{1}H,^{1}H$-COSY, $^{1}H,^{13}C$-HSQC, and $^{1}H,^{13}C$-HMBC NMR spectra. Virtual couplings are indicated and the frequency distances of the outer lines are reported.[56]

X-Ray Diffraction

See appendix B.

Synthesis and Characterization

Bis(dicyclohexylphosphino)ethane dioxide H_2O_2 adduct $[Cy_2POCH_2CH_2POCy_2 \cdot H_2O_2]_n$ (1). Bis(dicyclohexylphosphino)ethane (169 mg, 0.4 mmol) is placed in a Schlenk flask under nitrogen atmosphere and dissolved in dichloromethane (1.4 mL). While stirring vigorously, aqueous hydrogen peroxide is added (0.6 mL, 35%, 7 mmol) and the biphasic mixture is stirred for 30 min. The phases are separated, and the organic phase is layered with 5 mL of pentane. After slow evaporation of the solvents, adduct **1** is obtained in the form of colorless needles (149 mg, 0.30 mmol, 76%). Melting range (decomp.) 135-145 °C.

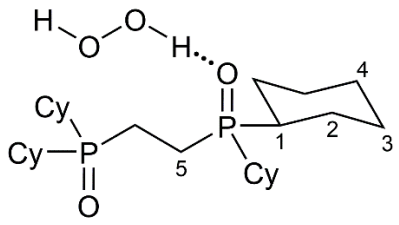

NMR (δ, $CDCl_3$), $^{31}P\{^1H\}$ 53.78 (s); ^1H 7.65 (br. s, 2H, OOH), 1.93 (s, 4H, H5), 1.91 (d, $^2J(^1H\text{-}^1H)$ = 16.4 Hz, 8H, $H2_{eq}$), 1.85-1.72 (m, 12H, H1, $H3_{eq}$), 1.71-1.63 (m, 4H, $H4_{eq}$), 1.34 (q, $^3J(^1H\text{-}^1H)$ = 10.4 Hz, 8H, $H2_{ax}$), 1.27-1.14 (m, 2H, $H3_{ax}$, $H4_{ax}$); $^{13}C\{^1H\}$ 36.26 (virtual triplet, 93.4 Hz, C1), 26.53 (virtual triplet, 12.1 Hz, C3), 25.87 (s, C4), 25.57 (virtual triplet, 28.8 Hz, C2), 15.10 (virtual triplet, 92.9 Hz, C5). IR: ν(O-H) = 3159 cm^{-1}, ν(P=O) = 1134 cm^{-1}.

Bis(diphenylphosphino)ethane dioxide (2,2'-peroxydi(butane-2-peroxol) adduct $[(CH_2Ph_2P(O))_2\cdot(HOOCMeEtO)_2]_n$ (2). Bis(diphenylphosphino)ethane (dppe) dioxide (103 mg, 0.24 mmol) is dissolved in toluene (10 mL) in a round bottom flask. Butanone (10 mL, 112 mmol) and aqueous H_2O_2 (0.1 mL, 35%, 1.2 mmol) of aqueous H_2O_2 is added, and the reaction mixture is stirred overnight. The solution is concentrated to 5 mL in vacuum, then the mixture is left to stand exposed to the atmosphere, so that the product can crystallize. Adduct **2** is obtained in the form of large, colorless, rectangular crystals (126 mg, 0.20 mmol, 83% yield). Mp (decomp.) >176 °C.

NMR (δ, $CDCl_3$), $^{31}P\{^1H\}$ 36.91 (s); ^1H 11.27 (br. s, 2H, OOH), 7.76-7.71 (m, 8H, H_o), 7.56-7.51 (m, 4H, H_p), 7.49-7.45 (m, 8H, H_m), 2.59 (d, $^2J(^{31}P\text{-}^1H)$ = 2.7 Hz, 4H, PCH_2), 1.81 (q, $^3J(^1H\text{-}^1H)$ = 7.6 Hz, 4H, CH_2CH_3), 1.44 (s, 6H, CCH_3), 1.03 (t, $^3J(^1H\text{-}$

^{1}H) = 7.6 Hz, 6H, CH_2CH_3); $^{13}C\{^{1}H\}$ 132.49 (s, C_p), 130.73 (virtual triplet, 102.8 Hz, C_i), 130.70 (virtual triplet, 9.4 Hz, C_o), 129.08 (virtual triplet, 12.2 Hz, C_m), 111.73 (s, CCH_3), 26.15 (s, CH_2CH_3), 21.31 (virtual triplet, 66.0 Hz, PCH_2), 17.49 (s, CCH_3), 8.39 (s, CH_2CH_3). IR: ν(O-H) = 3254 cm^{-1}, ν(P=O) = 1173 cm^{-1}.

***Trans*-3,5-dimethyl-3,5-diol-1,2-dioxolane** (**3**). Dppp (bis(diphenylphosphino)-propane) (1.001 g, 2.43 mmol) is dissolved in dichloromethane (60 mL). Aqueous H_2O_2 (5.0 mL, 35%, 58 mmol) is added, and the solution is stirred for 1 h. The organic layer is collected using a separation funnel, and the solvent is removed *in vacuo*. The resulting white residue is dissolved in acetylacetone (2.5 mL, 24.3 mmol), followed by the addition of excess aqueous H_2O_2 (0.1 mL, 35%, 1.2 mmol). The solution is stirred for 3 d, then the mixture is allowed to stand for crystallization. The product **3** is obtained in the form of white, crystalline needles (94 mg, 0.71 mmol, 71% yield with respect to amount of H_2O_2 added to the acetylacetone).

Alternative procedure: Acetylacetone (100 mg, 1 mmol) is weighed into a vial and aqueous H_2O_2 (0.15 mL, 35%, 1.7 mmol) is added. The solution is stirred overnight, and the most of the water is removed *in vacuo*. Benzene (1.0 mL) is added to precipitate the product, which is filtered and dried *in vacuo* (83 mg, 0.62 mmol, 62% yield). Mp (decomp.) 82 °C.

NMR (δ, $CDCl_3$), ^{1}H 2.74 (s, 2H, CH_2), 1.63 (s, 6H, CH_3); ^{13}C 105.50 (s, O*C*), 55.23 (CH_2), 22.59 (CH_3). ^{1}H and ^{13}C NMR data match literature values.[52]

***Trans*-3,5-dihydroperoxy-3,5-dimethyl-1,2-dioxolane** (**4**). Acetylacetone (100 mg, 1 mmol) is weighed into a vial and combined with 1.0 mL (10 mmol) of aqueous H_2O_2. The solution is stirred overnight, and the excess of water is removed *in vacuo*. The product precipitates when benzene (1.0 mL) is added (113 mg, 0.68 mmol, 68% yield). Mp (decomp.) 98 °C.

NMR (δ, $CDCl_3$), ^{1}H 8.54 (s, 2H, O*H*), 2.74 (s, 2H, CH_2), 1.63 (s, 6H, CH_3); ^{13}C 112.99 (s, O*C*), 51.11 (*C*H_2), 17.52 (*C*H_3). ^{1}H and ^{13}C NMR data match literature values.[52]

References

1 (*a*) J. Blümel, *Coord. Chem. Rev.*, 2008, **252**, 2410-2423; (*b*) J. Guenther, J. Reibenspies and J. Blümel, *Adv. Synth. Catal*., 2011, **353**, 443-460; (*c*) R. Silbernagel, A. Diaz, E. Steffensmeier, A. Clearfield and J. Blümel, *J. Mol. Catal. A*, 2014, **394**, 217-223; (*d*) C. Merckle and J. Blümel, *Adv. Synth. Catal.*, 2003, **345**, 584-588; (*e*) C. Merckle and J. Blümel, *Top. Catal.*, 2005, **34**, 5-15; (*f*) J. Guenther, N. Bhuvanesh and J. Blümel, *Mol. Catal*. 2019, DOI: 10.1016/j.mcat.2019.110629.

2 (*a*) J. H. Baker, N. Bhuvanesh and J. Blümel, *J. Organomet. Chem*., 2017, **847**, 193-203; (*b*) Y. Yang, B. Beele and J. Blümel, *J. Am. Chem. Soc*., **2008**, **130**, 3771-3773; (c) B. Beele, J. Guenther, M. Perera, M. Stach, T. Oeser and J. Blümel, *New J. Chem*., 2010, **34**, 2729-2731.

3 (*a*) J. C. Pope, T. Posset, N. Bhuvanesh and J. Blümel, *Organometallics*, 2014, **33**, 6750-6753; (*b*) T. Posset and J. Blümel, *J. Am. Chem. Soc.*, 2006, **128**, 8394-8395; (*c*) T. Posset, J. Guenther, J. Pope, T. Oeser and J. Blümel, *Chem. Commun.*, 2011, **47**, 2059-2061.

4 (*a*) S. Reinhard, P. Soba, F. Rominger and J. Blümel, *Adv. Synth. Catal*., **2003**, **345**, 589-602; (b) F. Piestert, R. Fetouaki, M. Bogza, T. Oeser and J. Blümel, *Chem. Commun*., 2005, 1481-1483; (*c*) K. J. Cluff, N. Bhuvanesh and J. Blümel, *Chem. Eur. J*., 2015, **21**, 10138-10148; (*d*) S. Reinhard, K. D. Behringer and J. Blümel, *New J. Chem.*, 2003, **27**, 776-778.

5 (*a*) J. Blümel, *Inorg. Chem*., 1994, **33**, 5050-5056; (*b*) J. Sommer, Y. Yang, D. Rambow and J. Blümel, *Inorg. Chem*., 2004, **43**, 7561-7563; (*c*) T. Posset, F. Rominger and J. Blümel, *Chem. Mater*., 2005, **17**, 586-595.

6 (*a*) A. Zheng, S.-B. Liu and F. Deng, *Chem. Rev.*, 2017, **117**, 12475−12531; (*b*) R. Yerushalmi, J. C. Ho, Z. Fan and A. Javey, *Angew. Chem. Int. Ed.*, 2008, **47**, 4440-4442; (*c*) J. P. Osegovic and R. S. Drago, *J. Phys. Chem. B*, 2000, **104**, 147-154; (*d*) S. Hayashi, K. Jimura and N. Kojima, *Bull. Chem. Soc. Jpn.*, 2014, **87**, 69-75; (*e*) S. Machida, M. Sohmiya, Y. Ide and Y. Sugahara, *Langmuir*, 2018*,* **34***,* 12694−12701.

7 (*a*) A. R. Wilmsmeyer, W. O. Gordon, E. D. Davis, B. A. Mantooth, T. A. Lalain and J. R. Morris, *Rev. Sci. Instrum*., 2014, **85**, 014101; (*b*) J. Kemsley, *Chem. Eng. News*, 2014, **92**, 29.

8 C. R. Hilliard, S. Kharel, K. J. Cluff, N. Bhuvanesh, J. A. Gladysz and J. Blümel, *Chem. Eur. J*., 2014, **20**, 17292-17295.

9 S. Kharel, K. J. Cluff, N. Bhuvanesh, J. A. Gladysz and J. Blümel, *Chem. Asian J.*, 2019, **14**, 2704-2711.

10 S. Kharel, T. Jia, N. Bhuvanesh, J. H. Reibenspies, J. Blümel and J. A. Gladysz, *Chem. Asian J.*, 2018, **13**, 2632-2640.

11 (*a*) J. Chrzanowski, D. Krasowska and J. Drabowicz, *Heteroatom Chem*., 2018, **29**, e21476; (*b*) T. Kovacs and G. Keglevich, *Curr. Org. Chem*., 2017, **21**, 569-585; (*c*) D. Herault, D. H. Nguyen, D. Nuel and G. Buono, *Chem. Soc. Rev*., 2015, **44**, 2508-2528; (*d*) M. D. Fletcher, *Organophosphorus Reagents*, 2004, 171-214; (*e*) H. R. Hays and D. J. Peterson, *Org. Phosphorus Compounds*, 1972, **3**, 341-500; (*f*) H. Adams, R. C. Collins, S. Jones and C. J. A. Warner, *Org. Lett*., 2011, **13**, 6576-6579; (*g*) K. C. K. Swamy, N. N. B. Kumar, E. Balaraman and K. V. P. P. Kumar, *Chem. Rev.,* 2009, **109**, 2551-2651; (*h*) R. H. Beddoe, K. G. Andrews, V. Magné, J. D. Cuthbertson, J. Saska, A. L. Shannon-Little, S. E. Shanahan, H. F. Sneddon and R. M. Denton, *Science*, 2019, **365**, 910-914; (*i*) D. W. Stephan, *Science*, 2016, **354**, 1248; (*j*) J. M. Bayne and D. W. Stephan, *Chem. Soc. Rev.*, 2016, **45**, 765-774; (*k*) X. Cai, S. Majumdar, G. C. Fortman, L. M. Frutos, M. Temprado, C. R. Clough, C. C. Cummins, M. E. Germain, T. Palluccio, E. V. Rybak-Akimova, B. Captain and C. D. Hoff, *Inorg. Chem*., 2011, **50**, 9620-9630.

12 (*a*) S. J. Pike and C. A. Hunter, *Org. Biomol. Chem*., 2017, **15**, 9603-9610; (*b*) A. E. Stross, G. Iadevaia and C. A. Hunter, *Chem. Sci.*, 2016, **7**, 94-101; (*c*) G. Iadevaia, A. E. Stross, A. Neumann and C. A. Hunter, *Chem. Sci.*, 2016, **7**, 1760-1767; (*d*) R. Cuypers, E. J. R. Sudhölter and H. Zuilhof, *ChemPhysChem.*, 2010, **11**, 2230-2240; (*e*) D. Nunez-Villanueva, C. A. Hunter, *Chem. Sci*., 2017, **8**, 206--213.

13 N. A. Bewick, A. Arendt, Y. Li, S. Szafert, T. Lis, K. A. Wheeler, J. Young and R. Dembinski, *Curr. Org. Chem*., 2015, **19**, 469-474.

14 S. J. Pike and C. A. Hunter, *Org. Biomol. Chem*., 2017, **15**, 9603-9610.

15 N. J. Burke, A. D. Burrows, M. F. Mahon and J. E. Warren, *Inorg. Chim. Acta*, 2006, **359**, 3497-3506.

16 R. Joshi and S. P. Pasilis, *J. Mol. Liquids*, 2015, **209**, 381-386.

17 C. R. Hilliard, N. Bhuvanesh, J. A. Gladysz and J. Blümel, *Dalton Trans.,* 2012, **41**, 1742-1754.

18 F. F. Arp, N. Bhuvanesh and J. Blümel, *Dalton Trans*., 2019, **48**, 14312-14325.

19 S. Kharel, N. Bhuvanesh, J. A. Gladysz and J. Blümel, *Inorg. Chim. Acta*, 2019, **490**, 215-219.

20 (*a*) E. Y. Tupikina, M. Bodensteiner, P. M. Tolstoy, G. S. Denisov and I. G. Shenderovich, *J. Phys. Chem. C*, 2018, **122**, 1711-1720; (*b*) G. Begimova, E. Y. Tupikina,V. K. Yu, G. S. Denisov, M. Bodensteiner and I. G. Shenderovich, *J. Phys. Chem. C*, 2016, **120**, 8717-8729.

21 S. H. Ahn, K. J. Cluff, N. Bhuvanesh and J. Blümel, *Angew. Chem. Int. Ed.*, 2015, **54**, 13341-13345; *Angew. Chem*., 2015, **127**, 13539-13543.

22 S. H. Ahn, N. Bhuvanesh and J. Blümel, *Chem. Eur. J*., 2017, **23**, 16998-17009.

23 S. H. Ahn, D. Lindhardt, N. Bhuvanesh and J. Blümel, *ACS Sustainable Chem. Eng*., 2018, **6**, 6829-6840.

24 (*a*) "Handbook of Advanced Methods and Processes in Oxidation Catalysis", D. Duprey and F. Cavani, Imperial College Press, 2014; (*b*) F. Cavani, J. H. Teles, *ChemSusChem*, 2009, **2**, 508-534; (*c*) "Peroxides and Peroxide Compounds", A. E. Comyns in *Van Nostrand's Encyclopedia of Chemistry,* John Wiley & Sons, Inc., 2005.

25 Y. Lu, X. Zhao and S. Fang, *Foods*, 2019, **8**, 31, 1-12.

26 H. Ying, Y. Yang, K. Cai and J. Cheng, *Eur. J. Org. Chem.,* 2019, **2019**, 728-731.

27 (*a*) Nobel Foundation, The Nobel Prize in Physiology or Medicine 2015, 2015; (*b*) V. A. Vil, A. O. Terent'ev, N. Savidov, T. A. Gloriozova, V. V. Poroikov, T. A. Pounina and V. M. Dembitsky, *J. Steroid Biochem. Mol. Biol.*, 2019, **190**, 76-87.

28 (*a*) C. J. Legacy, A. Wang, B. J. O'Day and M. H. Emmert, *Angew. Chem. Int. Ed*. 2015, **54**, 14907–14910; (*b*) C. J. Legacy and M. H. Emmert, *Synlett* 2016, **27**, 1893–1897.

29 (*a*) P. C. B. Page, B. R. Buckley, C. Elliott, Y. Chan, N. Dreyfus and F. Marken, *Synlett*, 2016, **27**, 80-82; (*b*) D. Habibi, M. A. Zolfigol, M. Safaiee, A. Shamsian and A. Ghorbani-Choghamarani, *Catal. Commun.*, 2009, **10**, 1257–1260; (*c*) H. Golchoubian and F. Hosseinpoor, *Molecules*, 2007, **12***,* 304-311; (*d*) M. Amini, M. Bagherzadeh, Z. Moradi-Shoeili, D. M. Boghaei, A. Ellern and L. K. Woo, *J. Coord. Chem*., 2013, **66**, 464-472; (*e*) T. Okada, H. Matsumuro, S. Kitagawa, T. Iwai, K. Yamazaki, Y. Kinoshita, Y. Kimura and M. Kirihara, *Synlett*, 2015, **26**, 2547-2552; (*f*) J.-W. Chu and B. L. Trout, *J. Am. Chem. Soc.*, 2004, **126**, 900-908; (*g*) E. Wojaczynska and J. Wojaczynski, *Chem. Rev*., 2010, **110**, 4303-4356;

(*g*) B. Zhang, S. Li, M. Cokoja, E. Herdtweck, J. Mink, S.-L. Zang, W. A. Herrmann and F. E. Kühn, *Z. Naturforsch B*., 2014, **69b**, 1149-1163; (*h*) Y. Xie, Y. Li, S. Zhou, Y. Zhang, M. Chen and Z. Li, *Synlett*, 2018, **29**, 340-343.

30 (*a*) D. J. Covell and M. C. White, *Tetrahedron*, 2013, **69**, 7771-7778; (*b*) P. E. Gormisky and M. C. White, *J. Am. Chem. Soc.*, 2013, **135**, 14052−14055; (*c*) T. J. Osberger, D. C. Rogness, J. T. Kohrt, A. F. Stepan and M. C. White, *Nature*, 2016, **537**, 214–219; (*d*) J. M. Howell, K. Feng, J. R. Clark, L. J. Trzepkowski and M. C. White, *J. Am. Chem. Soc.*, 2015, **137**, 14590−14593; (*e*) B. H. Brodsky and J. Du Bois, *J. Amer. Chem. Soc.*, 2005, **127**, 15391-15393.

31 (*a*) J. Hou, Y. Chen, B. Cordes, D. Ma, J. Wang, X. Wang, F. E. Kühn, H. Guo and M. D. Zhou, *Chem. Commun*., 2015, **51**, 7439-7442; (*b*) M. D. Zhou, M. Liu, J. Huang, J. Zhang, J. Wang, X. Li, F. E. Kühn and S. L. Zang, *Green Chem*., 2015, **17**, 1186-1193; (*c*) M. Drees, S. A. Hauser, M. Cokoja and F. E. Kühn, *J. Organomet. Chem*., 2013, **748**, 36-45; (*d*) M. A. Goodman and M. R. Detty, *Synlett*, 2006, 1100-1104; (*e*) I. I. E. Markovits, W. A. Eger, S. Yue, M. Cokoja, C. J. Münchmeyer, B. Zhang, M.-D. Zhou, A. Genest, J. Mink, S.-L. Zang, N. Rösch and F. E. Kühn, *Chem. Eur. J.*, 2013, **19**, 5972-5979; (*f*) H. Yao and D. E. Richardson, *J. Am. Chem. Soc*., 2000, **122**, 3220-3221; (*g*) G. S. Owens and M. M. Abu-Omar, *Chem. Commun.*, 2000, 1165-1166.

32 (*a*) M. Uyanik and K. Ishihara, *ACS Catal*., 2013, **3**, 513-520; (*b*) L. Zhou, X. Liu, J. Ji, Y. Zhang, X. Hu, L. Lin and X. Feng, *J. Am. Chem. Soc*., 2012, **134**, 17023-17026; (*c*) L. Zhou, X. Liu, J. Ji, Y. Zhang, W. Wu, Y. Liu, L. Lin and X. Feng, *Org. Lett*., 2014, **16**, 2938-3941; (*d*) A. O. Terent'ev, M. M. Platonov, A. S. Kashin and G. I. Nikishin, *Tetrahedron*, 2008, **64**, 7944-7948; (*e*) A. Terent'ev, M. Platonov and A. Kutkin, *Cent. Eur. J. Chem.*, 2006, **4**, 207-215; (*f*) V. A. Vil', G. dos Passos Gomes, O. V. Bityukov, K. A. Lyssenko, G. I. Nikishin I. V. Alabugin and A. O. Terent'ev, *Angew. Chem. Int. Ed.*, 2018, **57**, 3372–3376.

33 (a) N. V. Klassen, D. Marchington and H. C. E. McGowan, *Anal. Chem*., 1994, **66**, 2921-2925; (*b*) Y. Cui, B. Zhang, B. Liu, H. Chen, G. Chen and D. Tang, *Microchim. Acta*, 2011, **174**, 137-144; (*c*) T. Tsuneda and T. Taketsugu, *Phys. Chem. Chem. Phys.*, 2018, **20**, 24992-24999.

34 (*a*) L. Ji, Y.-N. Wang, C. Qian and X.-Z. Chen, *Synthesis Commun.*, 2013, **43**, 2256-2264; (*b*) M. C. Ball and S. Massey, *Thermochim. Acta*, 1995, **261**, 95-106; (*c*) J. A. Dobado, J. Molina and D. Portal, *J. Phys. Chem. A*, 1998, **102**, 778-784; (*d*) S. Taliansky, *Synlett*, 2005, 1962–1963; (*f*) M. S. Cooper, H. Heaney, A. J. Newbold and W. R. Sanderson, *Synlett*, 1990, 533-535.

35 (*a*) N. Koukabi, *Synlett*, 2010, 2969-2970; (*b*) A. McKillop and W. R. Sanderson, *J. Chem. Soc., Perkin Trans. 1*, 2000, 471–476; (*c*) D. P. Jones and W. P. Griffith, *J. Chem. Soc., Dalton Trans.*, 1980, 2526-2532.

36 S. Bednarz, B. Ryś and D. Bogdał, *Molecules*, 2012, **17**, 8068-8078.

37 (*a*) C. Mühle, E.-M. Peters and M. Jansen, *Z. Naturforsch. B*, 2009, **64**, 111-115; (*b*) J. Cho, S. Jeon, S. A. Wilson, L. V. Liu, E. A. Kang, J. J. Braymer, M. H. Lim, B. Hedman, K. O. Hodgson, J. S. Valentine, E. I. Solomon and W. Nam, *Nature*, 2011, **478**, 502-505; (*c*) T. Schölkopf, N.-D. Van and T. Schleid, *Inorg. Chim. Acta*, 2011, **374**, 181-186; (*d*) A. Kunishita, J. D. Scanlon, H. Ishimaru, K. Honda, T. Ogura, M. Suzuki, C. J. Cramer and S. Itoh, *Inorg. Chem*., 2008, **47**, 8222-8232; (*e*) M. Schulz, J. H. Teles, J. Sundermeyer and G. Wahl, US Patent 6,054,407, 2000.

38 K. Korth, A. Schorm, J. Sundermeyer, H. Hermann and G. Boche, *Peroxo Complexes of Molybdenum, Tungsten and Rhenium with Phase Transfer Active Ligands: Catalysts for the Oxidation of Olefins and Aromatics by Hydrogen Peroxide and Bistrimethylsilyl Peroxide* in: *Organosilicon Chemistry IV*, Wiley-VCH, Weinheim, 2000, 238-244.

39 A. V. Arzumanyan, R. A. Novikov, A. O. Terent'ev, M. M. Platonov, V. G. Lakhtin, D. E. Arkhipov, A. A. Korlyukov, V. V. Chernyshev, A. N. Fitch, A. T. Zdvizhkov, I. B. Krylov, Y. V. Tomilov and G. I. Nikishin, *Organometallics*, 2014, **33**, 2230-2246, and refs. cited.

40 V. V. Mulloyarova, I. S. Giba, M. A. Kostin, G. S. Denisov, I. G. Shenderovich and P. M. Tolstoy, *Phys. Chem. Chem. Phys*. 2018, **20**, 4901-4910.

41 The following CCDC reference numbers contain the supplementary crystallographic data for the corresponding compounds **1**-**4** for this paper: CCDC 1945941 (**1**), 1449057 (**2**), 1449061 (**3**), and 1452863 (**4**). These data can be obtained free of charge from the Cambridge Crystallographic Data Centre via www.ccdc.cam.ac.uk/data_request/cif.

42 G. A. Jeffrey, *An Introduction to Hydrogen Bonding*; Oxford University Press: Oxford, **1997**;

43 E. N. Baker and R. E. Hubbard, Hydrogen Bonding in Globular Proteins, *Prog. Biophys. Mol. Biol.* 1984, **44**, 97-179.

44 N. A. Milas and A. Golubović, *J. Am. Chem. Soc.*, 1959, **81**, 5824-5826.

45 J. Zhang, W. Wu, G. Qian and X.-G. Zhou, *J. Haz. Mat.*, 2010, **181**, 1024–1030.

46 I. K. Liyanage, M. R. Navinan, A. C. A. Pathirana, H. R. I. S. Herath, J. Yudhishdran, N. Fernandopulle and A. Kulatunga, *J. Occup. Med. Toxicol.*, 2015, **10**, 26.

47 R.-H. Chang, C.-M. Shu, Y.-S. Duh and J.-M. Jehng, *J. Haz. Mat.*, 2007, **141**, 762-768.

48 F. Marchetti, C. Pettinari, A. Pizzabiocca, A. A. Drozdov, S. I. Troyanov, C. O. Zhuravlev, S. N.Semenov, Y. A. Belousov and I. G. Timokhin, *Inorg. Chim. Acta*, 2010, **363**, 4038-4047.

49 B. Schweitzer-Chaput, E. Boess, M. Klussmann, *Org. Lett.*, 2016, **18**, 4944-4947.

50 V. A. Vil', G. dos Passos Gomes, M. V. Ekimova, K. A. Lyssenko, M. A. Syroeshkin, G. I. Nikishin, I. V. Alabugin and A. O. Terent'ev, *J. Org. Chem.*, 2018, **83**, 13427-13445.

51 (*a*) A. O. Terent'ev, D. A. Borisov, V. V. Chernyshev and G. I. Nikishin, *J. Org. Chem.*, 2009, **74**, 3335-3340; (*b*) A. O. Terent'ev, I. A. Yaremenko, V. A. Vil', I. K. Moiseev, S. A. Kon'kov, V. M. Dembitsky, D. O. Levitsky and G. I. Nikishin, *Org. Biomol. Chem.*, 2013, **11**, 2613-2623.

52 V. Novikov and O. Shestak, *Russ. Chem. Bull*. 2013, **62**, 2171-2190.

53 A. T. Zdvizhkov, A. O. Terent'ev, P. S. Radulov, R. A. Novikov, V. A. Tafeenko, V. V. Chernyshev, A. I. Ilovaisky, D. O. Levitsky, F. Fleury and G. I. Nikishin, *Tetrahedron*, 2016, **57**, 949–952.

54 N.-D. H. Gamage, B. Stiasny, E. G. Kratz, J. Stierstorfer, P. D. Martin, G. A. Cisneros, T. M. Klapötke and C. H. Winter, *Eur. J. Inorg. Chem.*, 2016, **2016**, 5036–5043.

55 X-ray structure **4** (CCDC 1452863) was deposited at CCDC on Feb. 10, 2016. On Sept. 5, 2016, an equivalent structure with the same crystal system (monoclinic) and space group ($P2_1/n$) (CCDC 1487205, Refcode YAFDER), synthesized by using 50 wt% H_2O_2 and concentrated H_2SO_4, I_2, and $SnCl_2{\cdot}2H_2O$ as catalysts, and crystallized from a dichloromethane/ethyl acetate mixture, was published.[54] Unit cell parameters compare as follows (cited values) a = 5.5661(6) Å (5.5729(5) Å), b = 15.4167(15) Å (15.4498(12) Å), c = 8.8545(9) Å (8.7244(7) Å), β = 92.306(3)° (90.055(4)°), Volume = 759.20(13) Å^3 (751.17(11) Å^3), R_1 [I>2σ(I)] = 5.07% (6.18%), R_1 (all data) = 6.76% (8.03%).

56 (*a*) W. H. Hersh, P. Xu, B. Wang, J. W. Yom and C. K. Simpson, *Inorg. Chem*. 1996, **35**, 5453-5459; (*b*) W. H. Hersh, *J. Chem. Educ*. 1997, **74**, 1485-1488.

CHAPTER IV

DI(HYDROPEROXY)CYCLOALKANE ADDUCTS OF TRIARYLPHOSPHINE OXIDES: A COMPREHENSIVE STUDY INCLUDING SOLID-STATE STRUCTURES AND ASSOCIATION IN SOLUTION*

Introduction

General Introduction

Peroxides are ubiquitous in daily life.[1-3] They are active ingredients for bleaching in the production of goods and for disinfection in the household, in medicine,[4] and wastewater treatment.[5] Peroxides are also employed as radical initiators for polymerizations.[2,6] For synthetic chemistry oxidation reactions are crucial and inorganic and organic peroxides, either solo or in the presence of catalysts, play central roles.[1-3] Applications include the oxidation of amines to amides,[7,8] alkane activation,[9,10] epoxidation reactions,[11,12] selective transformations of sulfides to sulfoxides,[13,14] and catalyst-free oxidations of phosphines to their oxides.[15,16] Baeyer-Villiger oxidation is crucial for synthesizing esters from ketones.[17,18]

Aqueous H_2O_2 is a ubiquitous oxidizing agent, but it is not ideal. The major drawback is its abundance of water, which can lead to unwanted secondary reactions. Whenever reagents are not water soluble the oxidation reactions have to be performed in a biphasic system, slowing rates and requiring phase separations later. Water-free formulations of H_2O_2 such as urea hydrogen peroxide (UHP)[19,20] and peroxocarbonates[21]

---

* Reprinted (adapted) with permission from F. F. Arp, N. Bhuvanesh, J. Blümel, *Inorg. Chem.* 2020, *59*, 18, 13719-13732. Copyright 2020 American Chemical Society.

are used, but they are not very soluble in organic solvents. More promising are the previously described perhydrates.[22,23] Peroxoborates are industrially important oxidants with a world production of more than 550000 tons per year.[24] Peroxoborates have recently been applied, for example, for selective sulfide oxidation,[25] the stereodefined synthesis of lactones,[26] and the synthesis of flavones.[27] Peroxides like $(Me_3SiO)_2$ and $(CH_3)_2C(OO)$ (DMDO) are also in use, however, their synthesis and storage are not trivial.[28]

Phosphine oxides are important synthetic targets and intermediates.[29-31] For example, they are applied for Mitsunobu reactions,[32] and recently attracted attention as redox-free Mitsunobu organocatalysts.[33] On the other hand, phosphine oxides are co-products of Appel and Wittig reactions and unwanted byproducts of phosphine chemistry in general, especially when catalysts are immobilized on oxide supports via phosphine linkers.[34-37] They are applied to probe surface acidities[38,39] and receive attention in the decomposition of warfare agents.[40] From an analytical point of view, phosphine oxides display interesting mobilities on surfaces, that have recently been studied by solid-state NMR.[41-43]

One of the most important features of phosphine oxides with respect to this contribution is their ability to form hydrogen bonds with a variety of different donors. For example, phenols are used in combination with phosphine oxides to create extended hydrogen-bonded networks,[44-46] and hydrogen bonding with naphthol,[47] sulfonic acids,[48] and water has been reported.[43,48-50] Silanols and chloroform crystallize as hydrogen-bonded assemblies.[51] Besides single crystal X-ray diffraction, ^{31}P solid-state NMR

spectroscopy has been applied a powerful method to analyze the hydrogen bonding characteristics of diverse P(V) species.[41-43,52,53]

Combining the unique potential of phosphine oxides to form well-defined hydrogen bonding motifs with the quest for superior oxidizing agents, we recently discovered two new types of stabilized peroxides. The Hilliard hydrogen peroxide adducts $(R_3PO{\cdot}H_2O_2)_2$ (R = alkyl, aryl) can be obtained by combining phosphines with aqueous H_2O_2.[15,50,54,55] In the presence of ketones (R'COR"), di(hydroperoxy)alkane adducts $R_3PO{\cdot}(HOO)_2CR'R"$ (R,R',R" = alkyl, aryl) are generated (Ahn adducts).[54-57] For the sake of brevity, we will refer to Ahn adducts in the following.

Preliminary research has already indicated that Ahn adducts are solid, soluble in organic solvents, and that they exhibit well-defined structure and composition.[54-57] They are easy to synthesize and convenient to administer to reaction mixtures. No traces of potentially dangerous triacetone triperoxide (TATP) has ever been found in any preparation. Ahn adducts selectively and instantaneously oxidize phosphines to phosphine oxides, without insertion of oxygen into any P−C bond.[54-57] The additional merit of oxidations that can be performed in non-aqueous media has been demonstrated by the clean synthesis of the water-sensitive $Ph_2P(O)P(O)Ph_2$.[56] The ease of stoichiometric administration of the solid Ahn oxidizers has furthermore been demonstrated by the selective oxidation of sulfides into sulfoxides that is performed without overoxidation to sulfones.[55,56] The Baeyer-Villiger oxidation of cyclic ketones has been studied with representative Ahn adducts and lactones have been obtained

selectively, without adverse hydrolysis or polymerization, while only a trace amount of acid catalyst was needed.[57]

In this contribution, we broaden the basis of known di(hydroperoxy)cycloalkane adducts of triarylphosphine oxides with different steric demand and electronic properties. Their solid-state characteristics are explored by single crystal X-ray diffraction, IR, and Raman spectroscopy. In solution, ^{31}P NMR and natural abundance ^{17}O NMR serves to characterize all Ahn adducts. Furthermore, a systematic study has been undertaken to quantify the association of the Ahn adducts, i.e. the strength of the hydrogen bonding of di(hydroperoxy)cyclohexane and -heptane to the phosphine oxides with different electronic and steric properties. This study is supported by Diffusion Ordered Spectroscopy (DOSY).[58,59] Hereby, ^{1}H DOSY[60] that tracks the movements of both hydrogen-bound peroxides and phosphine oxide carriers is the most favorable method. The obtained Stokes diameters reveal the association of the adducts. Quantitative data gained with dynamic ^{31}P VT NMR spectroscopy yield for the first time the activation energies for the exchange of phosphine oxide carriers by the di(hydroperoxy)cycloalkanes.

Results and Discussion

Synthesis and Characterization

In order to broaden the range of available di(hydroperoxy)cycloalkane adducts (Ahn adducts) of triarylphosphine oxides, and further explore diverse analytical methods for their characterization, the triarylphosphine oxides **1** and **2**, and the adducts **3**-**6** have been synthesized (Figure 23). The syntheses of **1** and **2** were straightforward by combining dichloromethane solutions of the corresponding phosphines with 35% aqueous hydrogen peroxide, as described earlier.[15,61] The Ahn adducts **3**-**6** were obtained with stoichiometrically precise composition by combining **1** and **2** with di(hydroperoxy)cyclohexane and di(hydroperoxy)cycloheptane. The latter have been synthesized according to a literature procedure[62] and used for the adduct formation as soon as possible. The adducts were obtained pure and in high yields of 74 to 89% without elaborate purification operations.

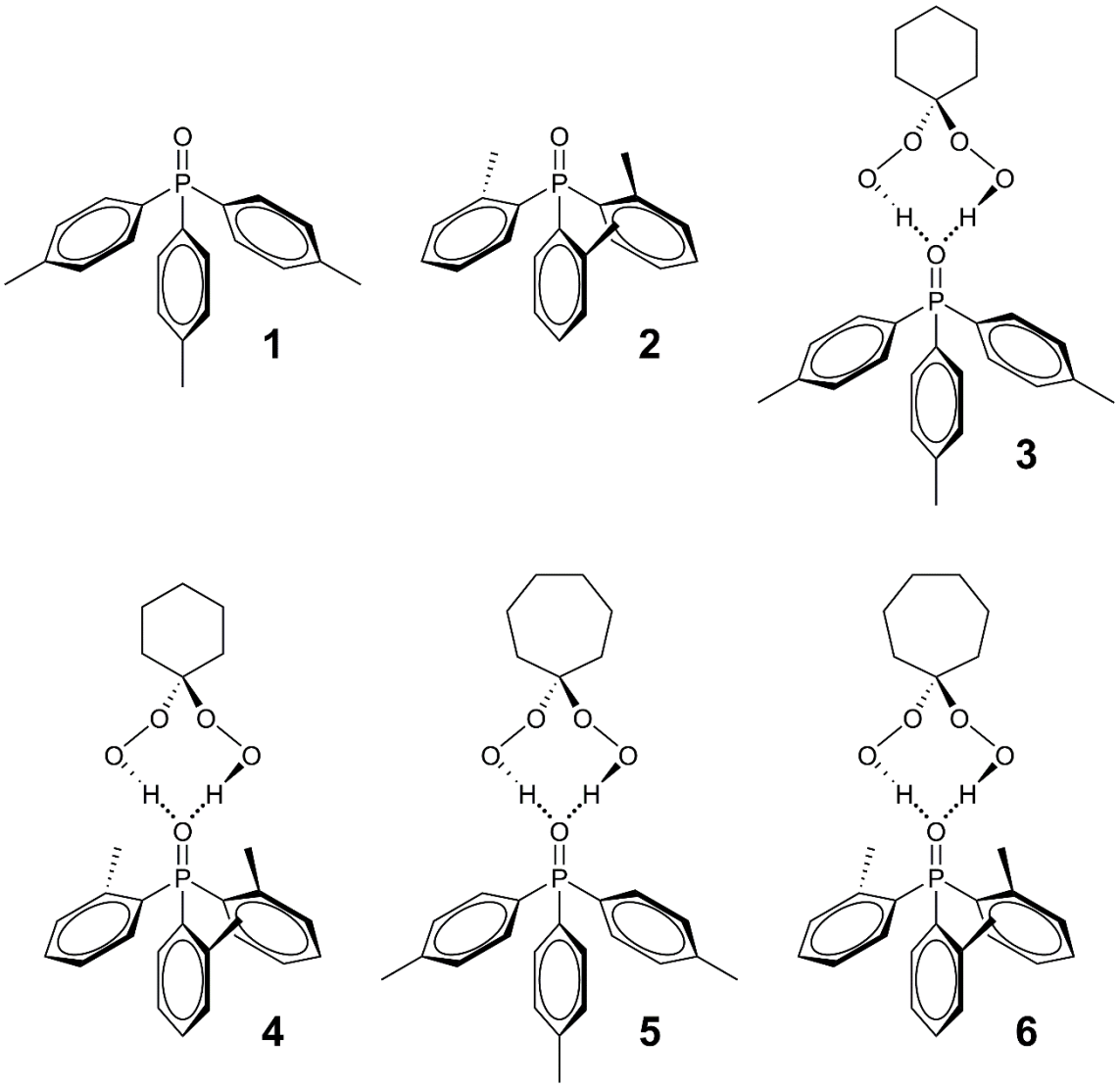

Figure 23 Phosphine oxides **1** and **2** and their Ahn adducts (di(hydroperoxy)alkane adducts) **3**-**6**.

All adducts **3**-**6** proved to be stable mechanically and thermally and their melting points or ranges could be determined. The characterization of the adducts was furthermore facilitated by their readiness to crystallize in large single crystals with dimensions in the cm range (Figure 24). Besides the single crystal X-ray structures, the

IR and Raman spectroscopic data are reported of the solid polycrystalline materials. The ^{31}P solution NMR data are in agreement with earlier results on Ahn adducts. Additionally, due to the high solubility of all adducts, high-quality natural abundance ^{17}O NMR spectra of **3**-**6** could be obtained for the first time with well-resolved signals for the di(hydroperoxy)cycloalkane and P=O oxygen nuclei. Competition and dynamic VT ^{31}P NMR investigations, as well as ^{1}H DOSY experiments elucidate the dissociation of the adducts in solution. The Gibbs energies of activation $\Delta G^{\ddagger}$, as well as the enthalpy $\Delta H^{\ddagger}$ and entropy of activation $\Delta S^{\ddagger}$ for these dynamic processes could be determined.

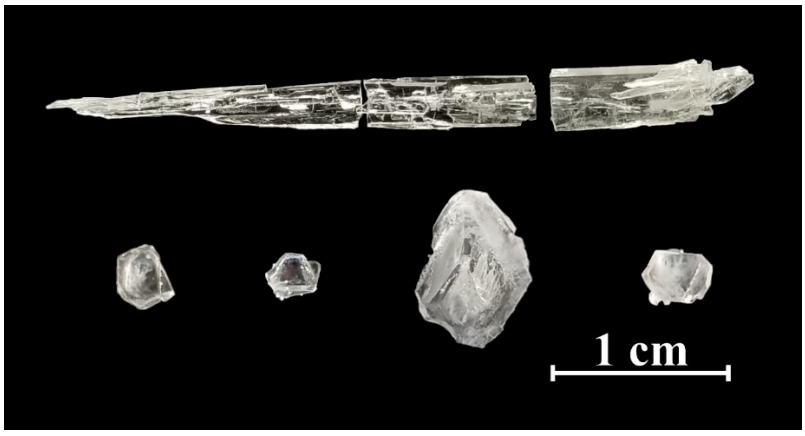

Figure 24 Representative single crystals of **3** (top) and **6** (bottom).

X-Ray Crystallography

All Ahn adducts **3**-**6** crystallize readily in large colorless specimens of high quality (Figure 24). Since Ph_3PO functions as a crystallization aid for amines,[63] it is assumed that the triarylphosphine oxide moieties are most probably responsible for the ease of

crystallization of the adducts. The single crystal X-ray structure of the neat phosphine oxide **1** has been obtained for comparison with the adduct structures (Figure 25).[64] In contrast to $^{n}Bu_3P{=}O$,[15] where the P=O groups are aligned in the same direction and the molecules are stacked on top of each other, the arrangement of **1** in the crystal lattice is dominated by the *p*-Tol substituents. The substituents of the phosphine oxide molecules face each other, while the P=O groups point in opposite directions (Figure 25). This motif has also been described recently for secondary and tertiary alkylphosphine oxides.[42]

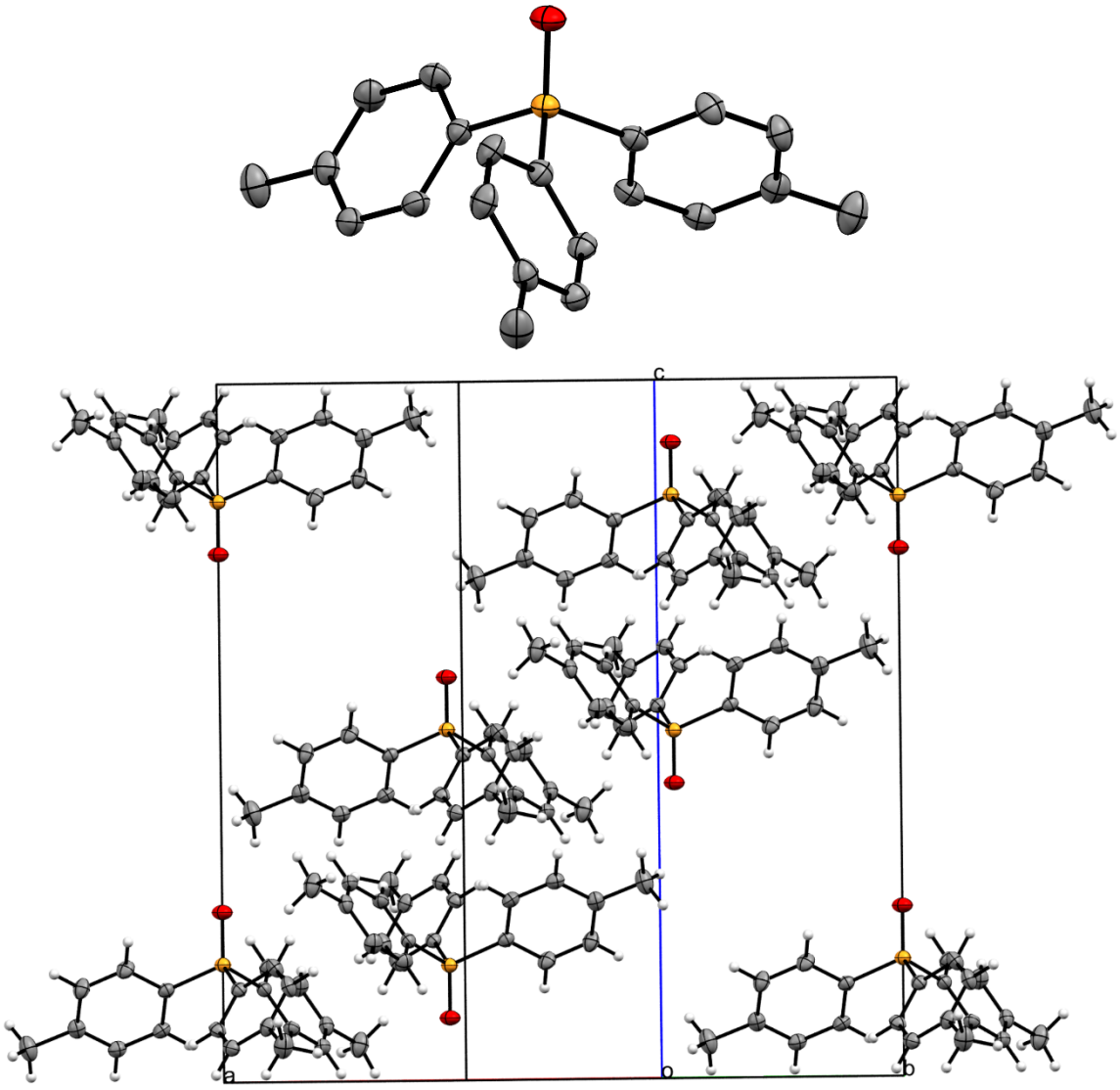

Figure 25 One molecule (top) and unit cell (bottom) of the single crystal X-ray structure of *p*-Tol3PO (**1**).[64]

The single crystal X-ray structures of the Ahn adducts **3**-**6** are displayed in Figures 26-29.[64] The relevant data are summarized in Tables 6 and 7.[64] Each adduct assembly of **3**-**6** incorporates two geminal hydroperoxy groups hydrogen-bonded to the oxygen atom of one P=O group. Therewith, the X-ray structures confirm the well-

defined adduct composition of one di(hydroperoxy)cycloalkane moiety per phosphine oxide molecule. As previously communicated for other Ahn adducts,[54-57] the crystal lattices of **3**-**6** are assembled by units of two adduct assemblies that are arranged in opposite directions (Figures 26-29). The steric ease of packing two adducts is nicely visible for **3** (Figure 26). The sterically compact nature of these double assemblies explains the ease of crystallization of all Ahn adducts.

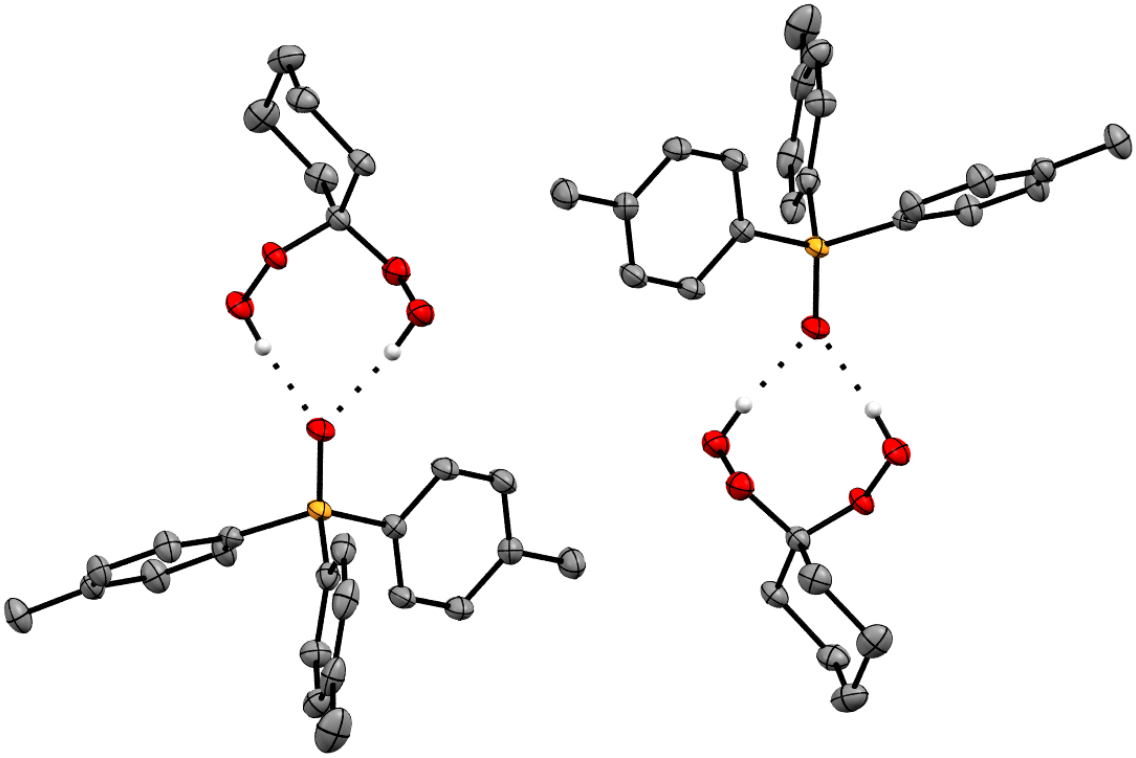

Figure 26 Single crystal X-ray structure of *p*-$Tol_3PO{\cdot}(HOO)_2C(CH_2)_5$ (**3**).[64]

The P=O bonds in the adducts **3-6** are all elongated as compared to the neat phosphine oxides (Table 6). The differences range between 0.0162 and 0.0234 Å.

Obviously, the hydrogen bonding of the di(hydroperoxy)cycloalkane moieties weakens the P=O bonds and therewith lengthens them. This result is corroborated by IR spectroscopy (see below). The lengthening of the P=O bonds is more substantial for the adducts with *ortho* methyl substituents (**4**, **6**) at the phenyl groups than for those with *para* methyl substituents (**3**, **5**). Since the X-ray structures do not indicate any steric crowding due to the substituents in the *ortho* positions it is assumed the electronic effects are responsible for this difference in the bond lengthening feature.

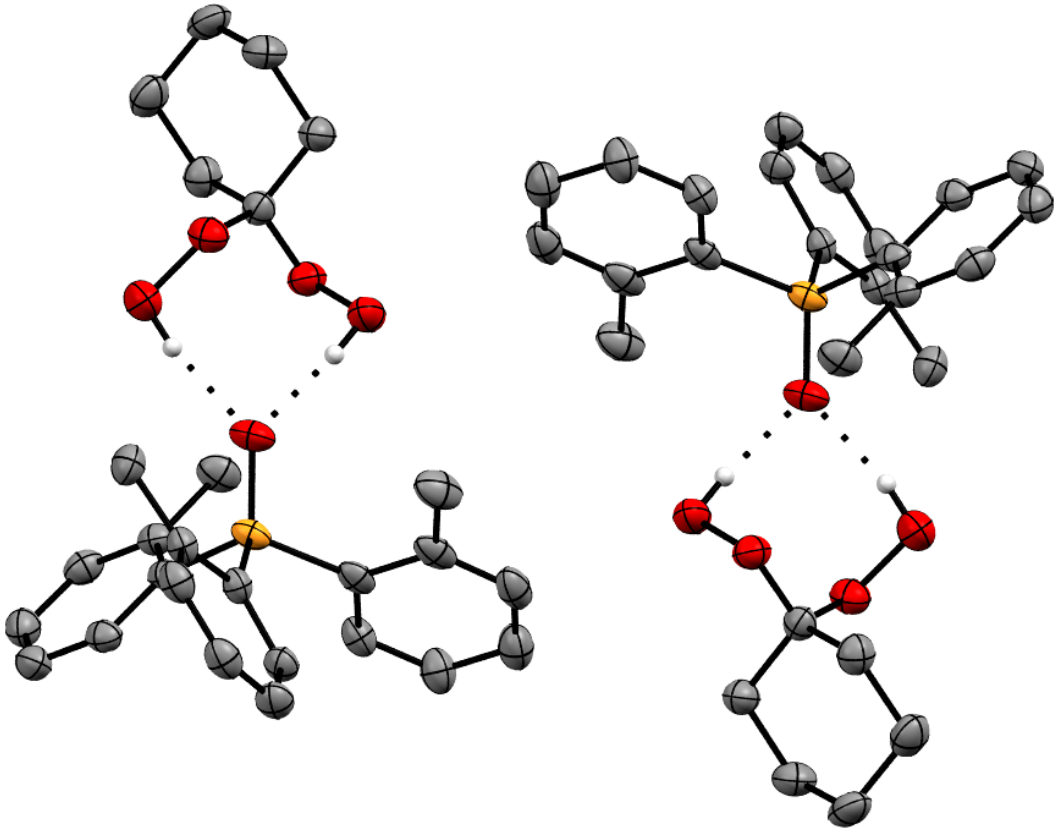

Figure 27 Single crystal X-ray structure of *o*-$Tol_3PO{\cdot}(HOO)_2C(CH_2)_5$ (**4**).[64]

The presence of strong hydrogen bonds in all adducts is corroborated by the short O···H distances (Table 6). All O···H distances in **3**-**6** are within the range of 1.842 to 1.951 Å (Table 6). Typically, hydrogen bonds exhibit O···H distances of 1.85 to 1.95 Å.[66] Additionally, the O···H−O distances of **3**-**6** have been determined using the single crystal X-ray data. These O···H−O distances represent another indicator for the formation of hydrogen bonds.[67] All values lie within the range of 2.686 to 2.7849 Å (Table 6). This again confirms strong hydrogen bonding, as most of the values are even smaller than the recognized range of 2.75 to 2.85 Å for O···H−O distances in hydrogen bonds.[67]

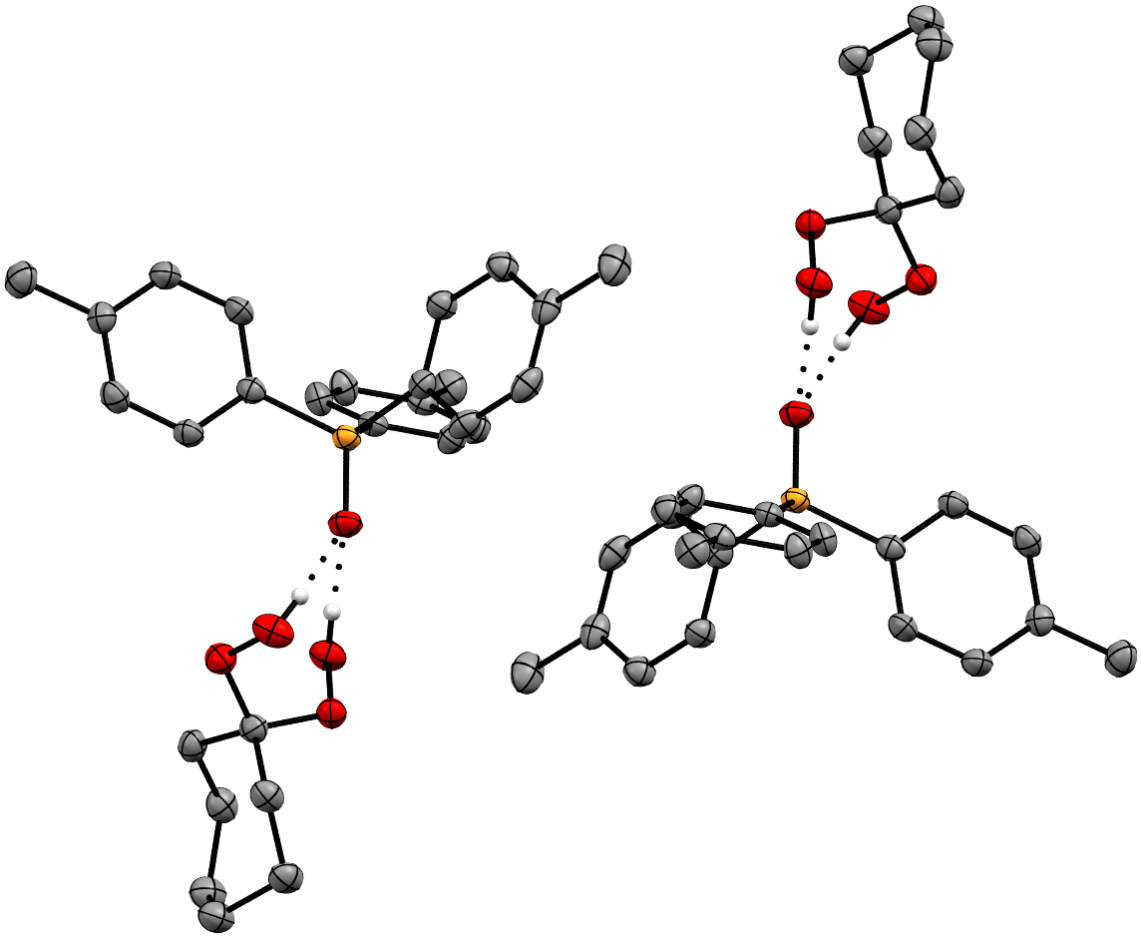

Figure 28 Single crystal X-ray structure of *p*-$Tol_3PO{\cdot}(HOO)_2C(CH_2)_6$ (**5**).[64]

Next, we analyzed the dihedral angles O···O–O–C in **3**-**6** (Table 7). Interestingly, one of the hydrogen bridges each in **3**-**6** displays a dihedral O···O–O–C angle between 89.25° and 92.44°. This is close to the value of 90.2(6)° found for solid H_2O_2. The other hydrogen bridge in each of the adducts **3**-**6** obviously has to accommodate the packing in the crystal lattice and is more distorted. These dihedral angles assume values within a remarkably narrow range from 94.42° to 96.23° (Table 7).

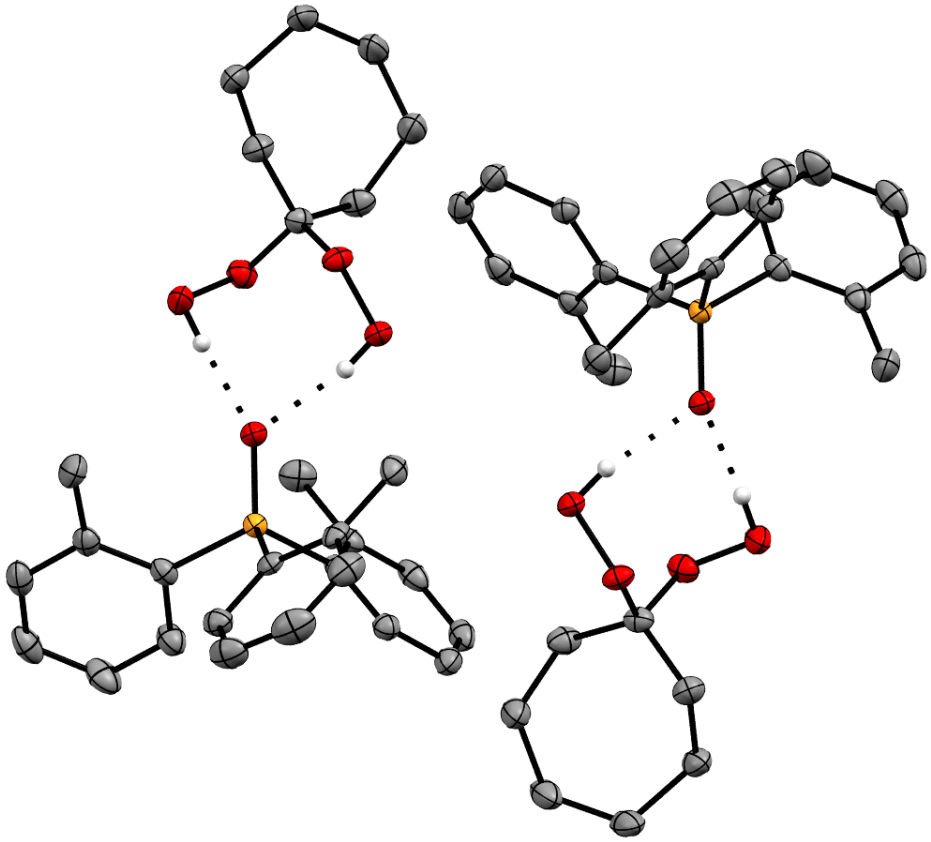

Figure 29 Single crystal X-ray structure of *o*-$Tol_3PO{\cdot}(HOO)_2C(CH_2)_6$ (**6**).[64]

Table 6 P=O bond lengths (Å), differences Δ(P=O) between the P=O bond lengths of the Ahn adducts **3**-**6** and the corresponding neat phosphine oxides **1** and **2** (Å), and the O···H and oxygen-oxygen distances of the hydrogen bonds O···H−O (Å) of the adducts **3**-**6**.[64]

Species	P=O bond length (Å)	Δ(P=O) (Å)	O···H distance (Å)	O···H−O distance (Å)
1	1.4885(17)[60]	–	–	–
2	1.478(2)/ 1.481(2)[61]	–	–	–
3	1.5047(10)	0.0162	1.862/1.920	2.7038(15)/2.7579(14)
4	1.4992(17)	0.0212/0.0182	1.842/1.881	2.686(2)/2.720(3)
5	1.5031(11)	0.0146	1.842/1.951	2.6889(17)/2.7849(17)
6	1.5014(11)	0.0234/0.0204	1.856/1.908	2.7057(16)/2.7245(16)

The cyclohexane and cycloheptane rings show the characteristic chair (**3**, **4**) and boat (**5**, **6**) conformations, respectively. Recently, a conformational analysis of $Ph_3P=O$ has been undertaken using theoretical calculations.[68] According to the theory, the energetic minima of the dihedral angle C−C−P=O should be ±33° or ±25° of 0° or 180°, depending on the method used for the calculations. The experimental distribution of dihedral angles in $Ph_3P=O$ containing, metal-free compounds is concentrated in the regions (±15-30°) on either side of 0° and 180°.[68] Since **1**-**6** are the perfect candidates to test the theory, this research sparked our interest in the dihedral C−C−P=O angles (Table 7). The values in Table 7 indicate that the methyl groups in the *ortho* positions lead to massive deviations from theory and the experimental distribution due to their steric impact in **2**, **4**, and **6**. The phenyl groups are rotated out of the positions of energetic minima that the phenyl groups in $Ph_3P=O$ would assume and display larger dihedral C−C−P=O angles. For **3** and **5**, with the methyl substituents in the *para*

positions, the theory and experimental dihedral angle distributions are closer. Two of the three *p*-Tol groups for each, **3** and **5**, lie within the expected range with values from 1.35° to 7.15°. But the third dihedral angle deviates for **3** and **5**, with 70.83° and 70.64°, respectively. Interestingly, different patterns for the dihedral angles C−C−P=O have been observed for the Hilliard adducts ((*p*-$Tol_3P{=}O{\cdot}H_2O_2)_2$ 9.14°/27.26°/81.04°; (*o*-$Tol_3P{=}O{\cdot}H_2O_2)_2$ 46.82°/47.07°/55.35°).[50]

Table 7 Dihedral angles (°) of the phosphine oxides **1** and **2** and the Ahn adducts **3**-**6**.[64]

Species	O···O−O−C	C−C−P=O
1	–	39.77(12)
2	–	40.8(3)/ 42.6(3)/53.4(3) 35.3(3)/47.3(3)/48.6(3)*,[61]
3	92.44(9)/94.42(9)	1.69(14)/7.15(13)/70.83(13)
4	91.17(15)/94.44(15)	36.3(4)/49.2(2)/53.1(2)
5	90.85(11)/95.45(11)	1.35(16)/3.31(15)/70.64(15)
6	89.25(10)/96.23(10)	42.0(2)/48.96(14)/52.12(14)

* Two independent molecules in the asymmetric unit.[61]

^{31}P NMR Spectroscopy

The Ahn adducts **3**-**6** are highly soluble in organic solvents (see also below).[54-57] Therefore, the ^{31}P NMR spectra can be recorded with just a few scans. A capillary with neat, liquid $ClPPh_2$, centered within the NMR tubes conveniently serves as a standard. The ^{31}P chemical shifts of the adducts **3**-**6** show increased values as compared with those of the corresponding phosphine oxides **1** and **2** (Table 8). The trend of the adduct chemical shifts consists of a downfield shift between 2.44 and 5.48 ppm, corroborating

earlier results on different Ahn adducts.[54-57] This downfield shift can be explained by the hydrogen bonds to the ddi(hydroperoxy)cycloalkane moieties, which lead to deshielding of the ^{31}P nuclei. The latter can be attributed to the electron density being drawn towards the oxygen atom in the P=O group. This is why the chemical shift values of Ahn[54-57] and hydrogen peroxide adducts[50] are generally higher than the $\delta(^{31}P)$ of the parent phosphine oxides.

Table 8 ^{31}P NMR chemical shifts of **1**-**6** in $CDCl_3$ and the differences of the chemical shift values $\Delta\delta(^{31}P)$ between the adducts **3**-**6** and their corresponding phosphine oxides **1** and **2**.

Species	$\delta(^{31}P)$ (ppm)	$\Delta\delta(^{31}P)$ (ppm)
1	29.28	–
2	37.51	–
3	34.76	5.48
4	42.47	4.96
5	32.51	3.23
6	39.95	2.44

In contrast to the ^{31}P chemical shifts, the changes of the ^{1}H and ^{13}C NMR data when forming the Ahn adducts from the phosphine oxides is minimal. This can be seen, for example, by comparing the $\delta(^{13}C)$ and $J(^{31}P\text{-}^{13}C)$ values of **1** with those of **3**.

^{17}O NMR Spectroscopy

^{17}O NMR poses more challenges than routine ^{31}P NMR spectroscopy. The Larmor frequency of ^{17}O lies within an easily accessible range, but the natural abundance of this nucleus is only 0.037%, which is about half of the value for deuterium. The nuclear spin of the ^{17}O isotope is I = 5/2, and therewith it is quadrupolar

in nature. The quadrupole moment Q = $-2.6 \cdot 10^{-26}$ is moderate,[69] which leads to ^{17}O resonances that are typically broader than 100 Hz for species with unsymmetric electronic surroundings of the ^{17}O nucleus. Most ^{17}O NMR investigations have been carried out with isotopically enriched samples to facilitate the measurements. Examples include studies of organic peroxides[70] and alkyl hydrotrioxides.[71] Furthermore, the peroxide binding to the active center of an enzyme[72] and polymer degradation mechanisms have been studied using ^{17}O NMR.[73] Enriched samples were also applied for studying polymorphs of triphenylphosphine oxide[74] and the hydrogen bonding in carboxylic acids by ^{17}O solid-state NMR.[75]

However, the fast quadrupolar relaxation[69] allows for the scans to be administered in rapid succession and compounds without isotopic enrichment, but with sufficient solubility in non-aqueous liquids are accessible to natural abundance ^{17}O NMR.

Fortunately, the adducts **3**-**6** are highly soluble in organic solvents (see below). Especially their excellent solubility in benzene is advantageous because it allows the measurement of very concentrated samples in a solvent that can be heated up to reduce its viscosity. The lower viscosity of benzene at elevated temperatures shortens the correlation times of the dissolved adducts and therefore diminishes the halfwidths of the quadupolar ^{17}O NMR resonances.[69]

A representative ^{17}O NMR spectrum is shown in Figure 30. The ^{17}O NMR data of the Ahn adducts **3**-**6** and the original phosphine oxides **1** and **2** are summarized in Table 9. The spectrum in Figure 30 shows the three expected signals of **4**. Although the

halfwidths are substantial and of triple digit magnitude in units of Hz, most resonances are resolved because of the large chemical shift dispersion of ^{17}O. The oxygen nucleus of the P=O group resonates at 60.36 ppm, which is well within the region for phosphine oxides (Table 9).[50] The two ^{17}O NMR signals of the di(hydroperoxy)cycloalkane moiety are found at 234.89 and 216.31 ppm. The signal assignment given in Figure 30 is based on a comparison with $\delta(^{17}O)$ of ^{t}BuOO^{t}Bu (269 ppm) and ^{t}BuOOH (243 ppm for C−O, 208.5 ppm for O−H).[70]

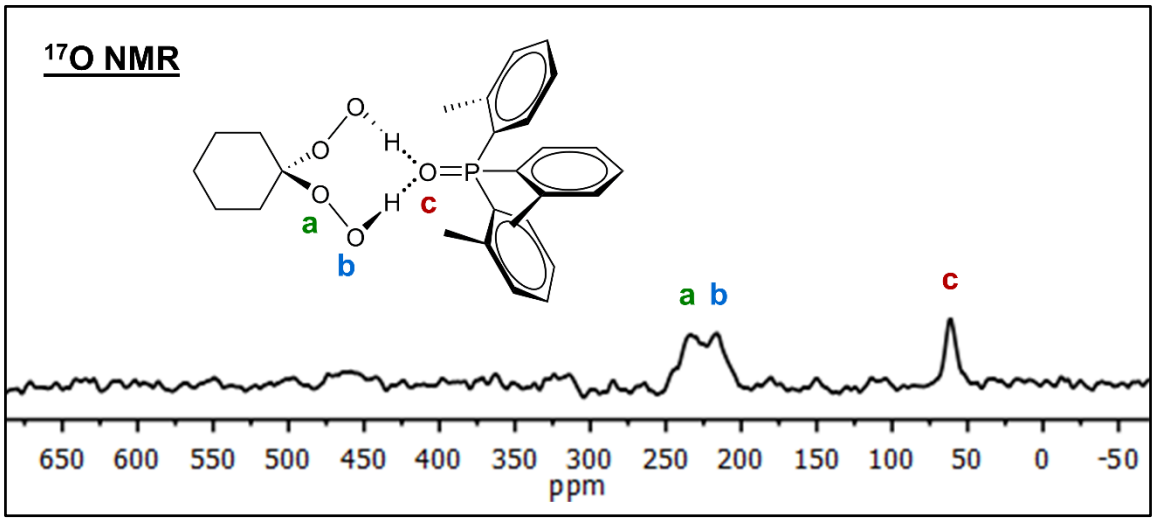

Figure 30 Natural abundance ^{17}O NMR spectrum of *o*-Tol$_3$PO·(HOO)$_2$C(CH$_2$)$_5$ (**4**) in benzene, recorded at 70 °C.

Table 9 ^{17}O NMR chemical shifts $\delta(^{17}O)$ (signal halfwidths $\Delta\nu_{1/2}$ (Hz)) of the phosphine oxides **1** and **2**, and the Ahn adducts **3**-**6** in C_6H_6 at 70 °C.

Adduct	$\delta(^{17}O)$ (ppm) of bound $R(OOH)_2$ ($\Delta\nu_{1/2}$ (Hz))		$\delta(^{17}O)$ (ppm) of **P=O** group ($\Delta\nu_{1/2}$ (Hz))
	C−O	**O−H**	
1	–	–	50.35* (235)
2	–	–	66.16 (379)
3	229.3 (979)	217.9 (516)	48.37 (644)
4	234.9 (815)	216.3 (1017)	61.36 (545)
5	246.2[#] (820)	246.2[#] (820)	48.89 (611)
6	188.9[§] (391)	188.9[§] (391)	63.73 (441)

* signal is split into a doublet with $^1J(^{31}P–^{17}O)$ = 129.9 Hz.
[#,§] C−O and O−H signals are not resolved.

It is important to note that the Ahn adducts do not decompose during the measurement at 70 °C. No signals corresponding to the decomposition products, free water (0 ppm) or water hydrogen-bound to phosphine oxide,[50] hydrogen peroxide (179.3 ppm),[70,72] or any of the parent ketones,[69] have been found.

The $\delta(^{17}O)$ of the P=O groups of the Ahn adducts **3**-**6** are found within the range of 48.37 to 63.73 ppm (Table 9), in accordance with the range for the hydrogen peroxide (Hilliard) adducts of the same phosphine oxides (46.60 to 60.04 ppm),[50] and with other compounds incorporating phosphorus-oxygen double bonds.[76] As compared to the $\delta(^{17}O)$ of the P=O group of **1** (50.35 ppm) (Table 9) the chemical shift for the oxygen nucleus of $Ph_3P=O$ in $CDCl_3$ has been reported as 43.3 ppm.[77] The deviation from this value for **1** and the variation of the $\delta(^{17}O)$ for the P=O group in **2** reflects the presence of

substituents at the aromatic rings, and the change of the solvent, since the solvent dependence of ^{17}O NMR chemical shifts can be substantial.[79]

Comparing the $\delta(^{17}O)$ of the P=O groups in the adducts **3**-**6** with those of the corresponding phosphine oxides **1** and **2** measured in the same solvent, benzene, shows that hydrogen bonding leads to a slight, but consistent upfield shift of the signals, amounting to 1.98 (**1**/**3**), 1.46 (**1**/**5**), 4.80 (**2**/**4**) and 2.43 (**2**/**6**) ppm (Table 9). A similar upfield shift had been observed for the Hilliard adducts earlier.[50] This result can be interpreted in terms of the electron density around the phosphorus nucleus being increased by the pull of electrons from the aromatic rings towards oxygen and the hydrogen bond. This leads to a shielding of the ^{31}P nucleus and the observed upfield shift. Regarding the ^{17}O NMR signals of the hydrogen-bonded di(hydroperoxy)cycloalkane moieties in **3**-**6**, comparisons with literature values are limited to the case of ^{t}BuOOH mentioned above[70] because the data displayed here are the first for Ahn adducts.

The $\Delta\nu_{1/2}$ values are in most of the cases presented larger for the hydroperoxy oxygen nuclei than for oxygen in the P=O groups (Table 9). The halfwidth $\Delta\nu_{1/2}$ of the ^{17}O phosphine oxide signal of **1** is even small enough to reveal its splitting into a doublet with $^{1}J(^{31}P\text{-}^{17}O)$ = 129.9 Hz. This value is in accordance with that of $Ph_3P=O$ in $CDCl_3$ (160 Hz).[77] The correlation time of the hydrogen-bonded di(hydroperoxy)cycloalkane moieties and the carrier phosphine oxides has to be the same, as the adduct assembly moves in unison. Therefore, the larger halfwidths of the peroxy oxygen signals

compared with the P=O resonance must have its origin in a greater electronic unsymmetry.

DOSY NMR Spectroscopy

The adducts **3**-**6** feature di(hydroperoxy)cycloalkane moieties hydrogen-bonded to phosphine oxides in a 1 : 1 ratio in the solid state. Although the affinity of the components in the solids is obvious, no information about the dissociation of **3**-**6** in a solvent has been reported so far. In contrast to the Hilliard adducts, for the Ahn adducts each assembly of two components is held together by two intramolecular hydrogen bonds.

While a certain degree of dissociation has been found for the Hilliard adducts,[50] no prediction is feasible for the Ahn adducts in solution. In order to get insight into this issue, we sought to employ Diffusion-Ordered NMR Spectroscopy (DOSY) to probe the hydrogen bond association in **3**-**6**.[58,59] For this purpose, the straightforward ^{1}H DOSY experiments have been employed.[60] The obtained Stokes diameters can then be compared with the expected diameters of **1**-**6** based on their maximal extensions in the X-ray structures. Although the associates **3**-**6** are not entirely spherically symmetric, but somewhat elongated (Figures 26 to 29), the resulting values for the Stokes diameters should lie within an error margin of ±2 Å. For the phosphine oxides **1** and **2** larger deviations of the Stokes diameters from the largest H···H distances have to be acknowledged because their shape is more of an umbrella type than spherical (Figure 25), which increases their resistance towards diffusion. The Stokes diameters of the adducts **3**-**6** and the corresponding phosphine oxides **1** and **2** have been compared to

the maximal sizes of the species, as defined by the largest H···H distance in their X-ray structures (Table 10). Indeed, the obtained Stokes diameters for the umbrella-shaped phosphine oxides are somewhat larger than the structural data would imply. However, the values are still within the error margins for monomers, and the presence of stacks of phosphine oxides, as found for example, in solid $^{n}Bu_3PO$,[15] can be excluded in solution. For the Ahn adducts **3**-**6** the Stokes diameters fit very well the assumption that in solution the 1 : 1 adduct assemblies as a whole, consisting of the phosphine oxide and di(hydroperoxy)cycloalkane moiety, as found in the solid state, are diffusing through the solution in unison.

Table 10 Stokes diameters of the phosphine oxides **1** and **2**, and the Ahn adducts **3**-**6** obtained from ^{1}H DOSY measurements in C_6D_6. The maximal H···H distances were obtained from the atomic positions in the X-ray structures of the adduct assemblies **3**-**6** and include two times the van der Waals radius of H. The last column reports the differences between the Stokes diameters and the maximal H···H distances in **1**-**6**.

Species	Stokes Diameter (Å)	Maximal H···H distance (Å)	Difference (Å)
1	15.1	13.677	1.4
2	14.5	11.867	2.6
3	17.4	16.299	1.1
4	17.0	15.349	1.7
5	17.9	16.942	1.0
6	15.4	15.880	0.5

The DOSY result that the adducts **3**-**6** do not completely dissociate into R_3PO and $(HOO)_2C(CH_2)_{5/6}$ moieties is also corroborated by the fact that the adducts show

solubilities in most organic solvents that are different from those of the parent phosphine oxides (see solubilities below).

Dynamic NMR Spectroscopy of Ahn Adducts

Competition Experiments

The DOSY experiments described above prove that the adducts **3**-**6** diffuse through solution as hydrogen-bonded assemblies with the phosphine oxides and di(hydroperoxy)cycloalkane components in a 1 : 1 ratio. Therefore, most of the time, the assemblies stay together.

However, this does not mean that exchange between the components could not happen that is fast as compared to the DOSY NMR time scale. In other words, the peroxy moiety could jump from one phosphine oxide carrier to the next. In order to probe this possibility, competition experiments have been performed, as depicted for one representative example in Scheme 3. Hereby, the potential migration of the di(hydroperoxy)cycloalkane moiety from one phosphine oxide carrier to another one of the same (Scheme 4) or of a different sort (Scheme 3) is monitored.

In practical terms, an equimolar excess of the same or a different phosphine oxide is offered to the solution of an adduct and the resulting ^{31}P NMR spectrum is evaluated. For example, when adduct **3** is combined with an equal amount of the phosphine oxide Cy_3PO (**7**), the phosphine oxide **1** could be liberated completely, and adduct **8** could be formed quantitatively (Scheme 3). Alternatively, no changes could occur, in which case **3** and **7** would persist as the only species in the mixture. Of course,

there could also be an equilibrium with all four entities, **1**, **3**, **7**, and **8**, present in an equilibrium that is not shifted entirely to the right or left side.

In order to quantitatively probe the ability of the peroxy moiety to migrate, exact amounts of adducts and competing phosphine oxides have been weighed in. For obtaining precise ^{31}P NMR chemical shifts, capillaries containing pure liquid Ph_2PCl were centered in the NMR tubes. In a first step, the $\delta(^{31}P)$ of the pure phosphine oxides **1**, **2**, and **7**, as well as all adducts were determined in benzene (Table 10). The latter was chosen as a nonprotic and unpolar solvent to avoid complications due to exchange with solvent molecules. The representative examples displayed in figure 31 will be discussed here, the NMR spectra and all data of the other competition experiments are provided for in Tables 10 and 11 and in appendix C.

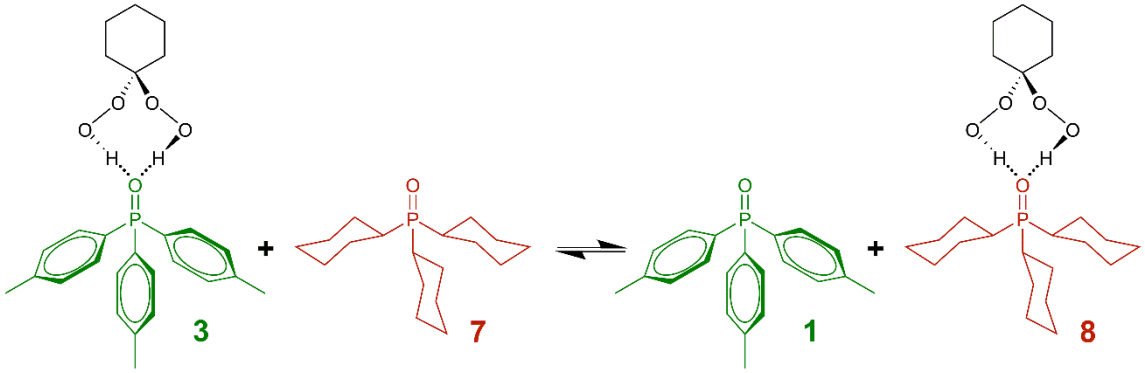

Scheme 3 Equilibrium of a 1 : 1 mixture of *p*-$Tol_3PO\cdot(HOO)_2C(CH_2)_5$ (**3**) and Cy_3PO (**7**) with the products *p*-Tol_3PO (**1**) and $Cy_3PO\cdot(HOO)_2C(CH_2)_5$ (**8**).

When an equal amount of **1** is added to a solution of **3**, a sharp signal is obtained at 29.63 ppm, which is about halfway in between the chemical shifts of **1** (25.53 ppm)

and **3** (33.06 ppm) (Figure 31, Table 11). The position and small halfwidth of the one resulting resonance indicate that the exchange of the di(hydroperoxy)cycloalkane moiety between the phosphine oxide carriers is fast on the ^{31}P NMR time scale at room temperature. Very slow exchange, with **1** and **3** coexisting in solution, would have allowed both signals of the phosphine oxide and adduct to be visible and sharp in the spectrum. A moderate exchange rate on the time scale of ^{31}P NMR would have resulted in individual broad lines. Analogous results were obtained for 1 : 1 mixtures of **1** and **5**, **2** and **4**, and **2** and **6** (Table 11 and appendix C).

Next, we sought to investigate the relative affinities of di(hydroperoxy)cyclohexane and di(hydroperoxy)cycloheptane to *p*-*T*ol$_3$PO (**1**), *o*-Tol$_3$PO (**2**), and Cy$_3$PO (**7**). The affinities were assessed by experiments probing the competition between the adducts **3**-**6** and different phosphine oxides. For example, an equal amount of Cy$_3$PO (**7**) has been added to *p*-*T*ol$_3$PO·(HOO)$_2$C(CH$_2$)$_5$ (**3**) (Figure 31, bottom spectrum, Table 11). In this case an equilibrium mixture is obtained. The original signal of **3** at 33.06 ppm is shiefted upfield to 27.02 ppm, but not quite reaching the chemical shift of pure **1** (25.53 ppm). This indicates that **3** lost some, but not all of the hydrogen-bonded di(hydroperoxy)cyclohexane. At the same time, **7** undergoes a downfield shift from originally 45.99 ppm to 53.48 ppm, which proves the formation of a certain amount of Cy$_3$PO·(HOO)$_2$C(CH$_2$)$_5$ (**8**). Overall, the mixture contains **3** and **7**, as well as **1** and **8**, so the equilibrium outlined in Scheme 3 does not pivot entirely to the right or left side.

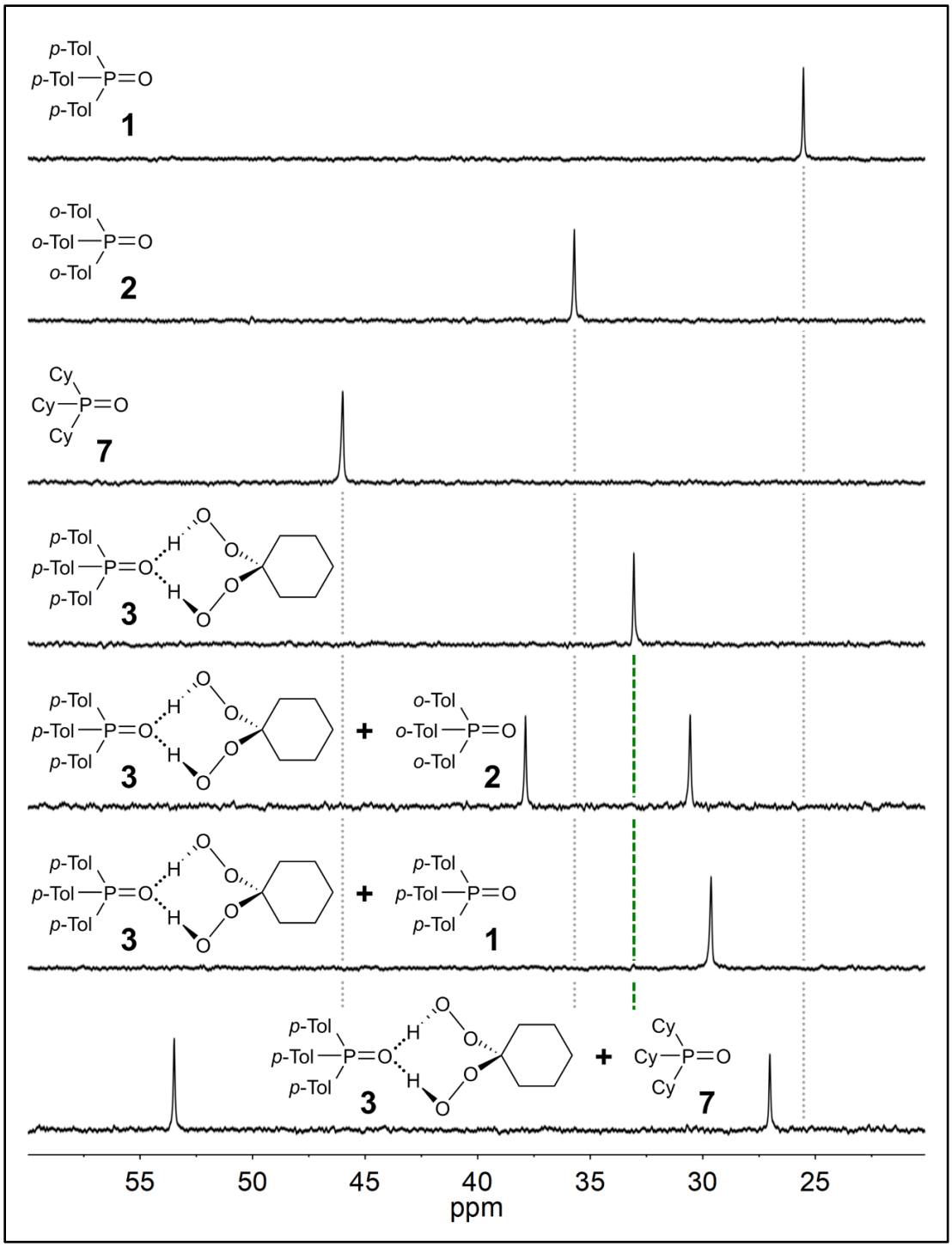

Figure 31 Competition experiments: ^{31}P NMR spectra of the phosphine oxides *p*-Tol_3PO (**1**), *o*-Tol_3PO (**2**), and Cy_3PO (**7**), the pure adduct *p*-$Tol_3PO{\cdot}(HOO)_2C(CH_2)_5$ (**3**), and of 1 : 1 mixtures of **3** with the phosphine oxides **1**, **2**, and **7** in benzene at ambient temperature.

Table 11 ^{31}P NMR chemical shifts obtained in competition experiments when the Ahn adducts **3**-**6** are combined with equal amounts of the phosphine oxides **1**, **2**, and **7** in benzene. The $\delta(^{31}P)$ of the phosphine oxides in benzene are 25.53 ppm (**1**), 37.71 ppm (**2**), and 45.99 ppm (**7**).

Adduct	$\delta(^{31}P)$ (ppm)	$\delta(^{31}P)$ (ppm) of adduct after adding an equal amount of the phosphine oxide		
		p-Tol$_3$PO (**1**)	*o*-Tol$_3$PO (**2**)	Cy$_3$PO (**7**)
3	33.06	29.63	30.56	27.02
4	41.57	38.17	38.98	36.50
5	32.48	29.34	30.24	26.60
6	40.11	37.35	38.05	36.03

As the next step, we sought to estimate the affinities of the peroxy moieties to the different phosphine oxides in a qualitative manner. For this purpose we contemplated the ^{31}P chemical shift changes that all adducts **3**-**6** undergo when equimolar amounts of the phosphine oxides **1**, **2**, and **7** are added (Table 12). When **7** was added to the adducts **3**-**6**, their signals shifted 4.08−6.04 ppm upfield. Adding **1** or **2** led to upfield shifts of 2.76−3.43 ppm, and 2.06−2.59 ppm, respectively. The shift differences are largest for **7** and smallest for **2**. Therefore, the relative affinities of both di(hydroperoxy)cycloalkanes with respect to hydrogen bonding are increasing from **2** over **1** to **7**.

Table 12 ^{31}P NMR chemical shift differences between the adducts **3**-**6** and the $\delta(^{31}P)$ that result when an equal amount of **1**, **2**, and **7** is added to their benzene solution.

Adduct	$\Delta\delta(^{31}P)$ = [$\delta(^{31}P)$ of adduct] − [$\delta(^{31}P)$ of adduct in 1 : 1 mixture with phosphine oxide]		
	p-Tol$_3$PO (**1**)	*o*-Tol$_3$PO (**2**)	Cy$_3$PO (**7**)
3	3.43	2.50	6.04
4	3.40	2.59	5.07
5	3.14	2.24	5.88
6	2.76	2.06	4.08

Variable Temperature ^{31}P NMR Experiments

While the competition experiments discussed above served well for gaining some insight into the adduct association in a qualitative manner, in the following a quantitative approach is described.

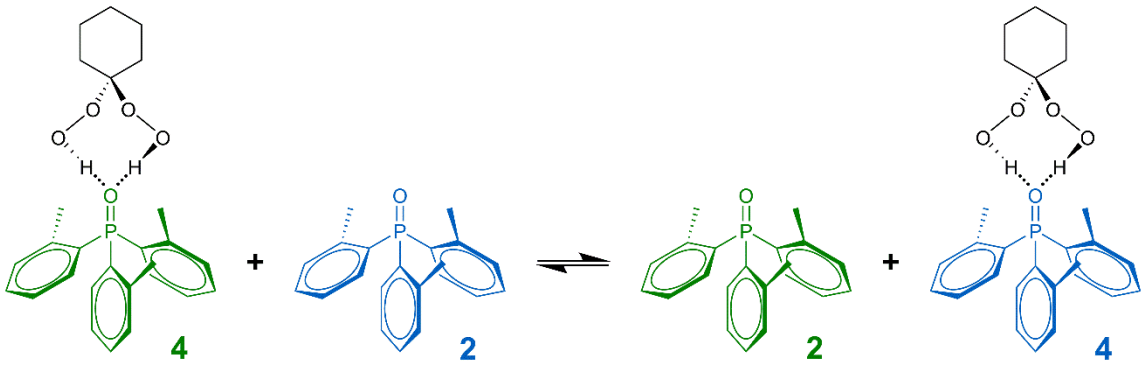

Scheme 4 Exchange equilibrium for a 1 : 1 mixture of *o*-Tol$_3$PO (**2**) and *o*-Tol$_3$PO·(HOO)$_2$C(CH$_2$)$_5$ (**4**).

In order to quantify the dissociation of the Ahn adducts in solution, ^{31}P NMR spectra of 1 : 1 mixtures of **3**-**6** with their corresponding phosphine oxides **1** and **2**, as

despicted for one example in Scheme 4, have been recorded at variable temperatures. At 20 °C all mixtures show fast exchange of the di(hydroperoxy)cycloalkane moieties between the phosphine oxides, as also described above. Upon cooling, coalescence is reached at about −75 °C (**3**), −70 °C (**5**), −60 °C (**6**), and −50 °C (**4**). At −80 °C the exchange is slowed down substantially (Figure 32 and appendix C). However, the signals are still broad and therefore the low temperature limit with complete resolution of the adduct and phosphine oxide peaks presumably lies much lower. Fortunately, the ^{31}P NMR spectra of the pure phosphine oxides **1** and **2** and the Ahn adducts **3**-**6** could be recorded separately to obtain the precise values for the chemical shifts and linewidths at all temperatures (Appendix C, Table S3). Therefore, a need to reach the low temperature limit did not arise. Simulations[79] were performed using these chemical shifts and linewidth values, iterating solely on the rate constant of exchange (k_r).

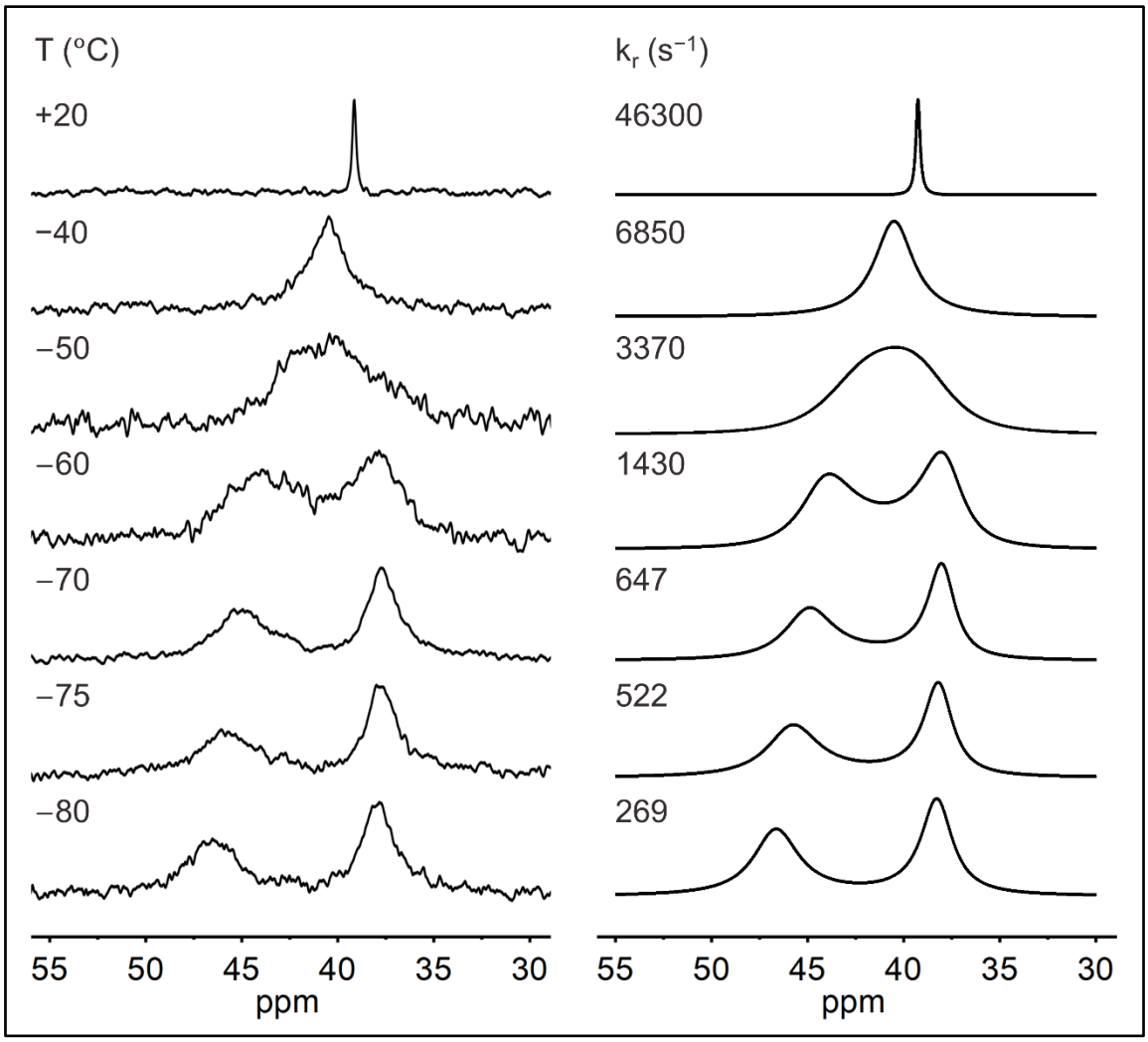

Figure 32 Variable temperature ^{31}P NMR spectra of a 1 : 1 mixture of *o*-Tol$_3$PO (**2**) and *o*-Tol$_3$PO·(HOO)$_2$C(CH$_2$)$_5$ (**4**) in dichloromethane, recorded at the indicated temperatures (left) and the respective simulations (right).

Using the Eyring equation, the Gibbs energy of activation ($\Delta G^{\ddagger}$)[80] values summarized in Table 13 were obtained assuming a transmission coefficient of $\kappa = 1$.[80,81] At 20 °C these $\Delta G^{\ddagger}$ values range from 44.0 kJ/mol for the pair **2**/**6** to 45.6 kJ/mol for **1**/**5**. At this point a comparison with similar, well-known scenarios is interesting. For

example, the energy barrier of a hydrogen bond breakage in an isolated protein β-sheet corresponds to a $\Delta G^{\ddagger}$ of 20 kJ/mol,[82] while the energy needed to initiate a proton transfer in water amounts to 21 kJ/mol.[83] The activation barrier for the transfer of a di(hydroperoxy)cycloalkane from one phosphine oxide to another, identical one, is about twice as large.

Table 13 $\Delta G^{\ddagger}$ values for the exchange reaction of a di(hydroperoxy)alkane between two identical phosphine oxides at the corresponding temperatures.

Mixture (1 : 1)	**1/3**	**2/4**	**1/5**	**2/6**
T (°C)	**$\Delta G^{\ddagger}$ (kJ/mol)**			
20	45.5	45.6	45.6	44.0
−40	–	39.5	–	38.0
−50	–	39.0	–	38.1
−60	35.5	38.7	36.2	37.8
−70	35.3	38.2	35.5	37.1
−75	34.7	37.5	35.2	36.7
−80	34.4	37.6	35.1	36.5

The values for the activation enthalpy ($\Delta H^{\ddagger}$) and entropy ($\Delta S^{\ddagger}$) have been obtained from Eyring plots[80] (Figure 33 and appendix C) and summarized in Table 14. The pairs **1**/**3** and **1**/**5** with the more tightly hydrogen-bonded *p*-Tol_3PO feature lower enthalpies of activation ($\Delta H^{\ddagger}$) than the mixtures **2**/**4** and **2**/**6**. Considering the hydrogen-bonding of another phosphine oxide molecule during the transition state, the overall number of hydrogen bonds stays the same. Firm hydrogen-bonding with the more basic *p*-Tol_3PO (see IR spectroscopy below) explains the lower enthalpy loss in those transition states as compared to the cases involving *o*-Tol_3PO.

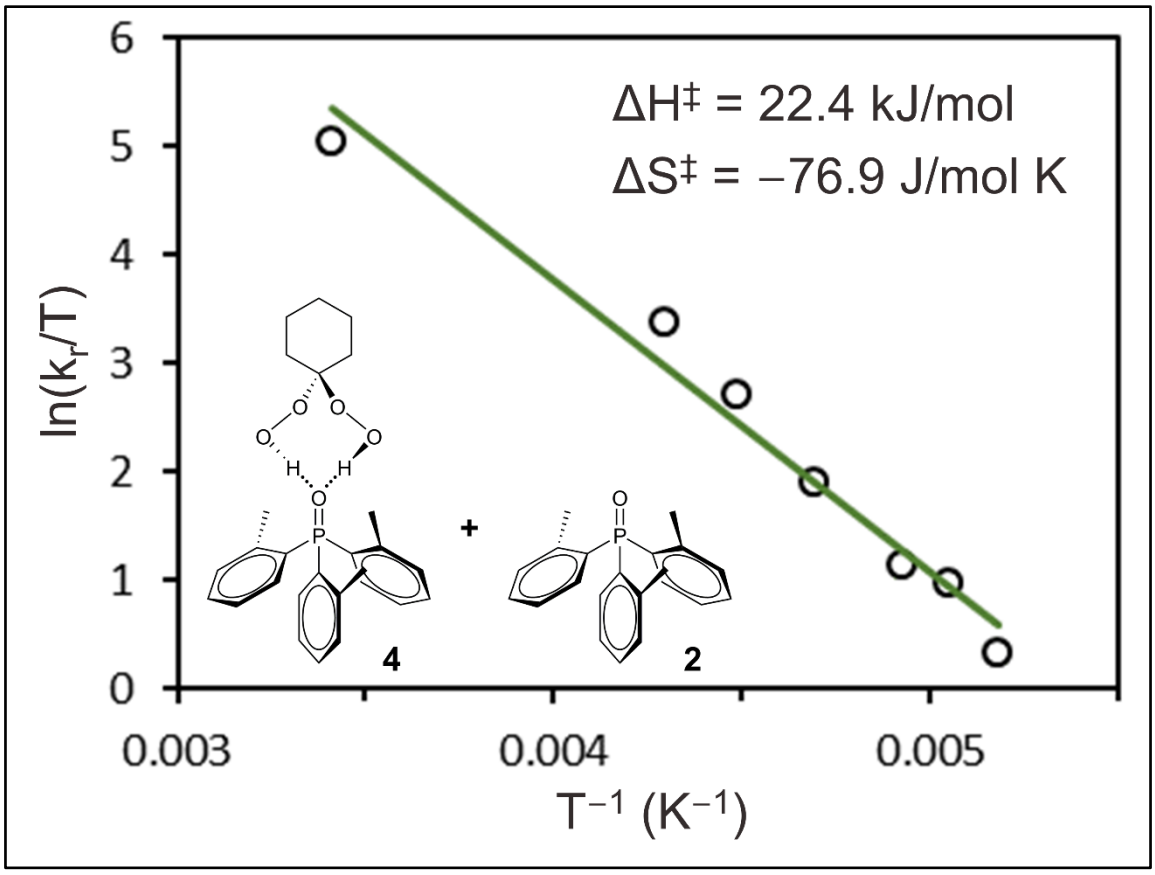

Figure 33 Temperature dependence of the exchange rate constant k_r, depicted as $\ln(k_r/T)$ versus T^{-1}, of a 1 : 1 mixture of *o*-Tol_3PO (**2**) and *o*-$Tol_3PO{\cdot}(HOO)_2C(CH_2)_5$ (**4**) in dichloromethane.

Table 14 $\Delta H^{\ddagger}$ and $\Delta S^{\ddagger}$ values for the exchange reaction of a di(hydroperoxy)alkane between two identical phosphine oxides.

Mixture (1 : 1)	**1/3**	**2/4**	**1/5**	**2/6**
$\Delta H^{\ddagger}$ (kJ/mol)	12.4	22.4	14.0	22.5
$\Delta S^{\ddagger}$ (J/(mol·K))	−112.0	−76.9	−107.0	−71.0

The low entropies of activation ($\Delta S^{\ddagger}$) range from −71.0 J/(mol K) to −112.0 J/(mol K) (Table 14). They are close to values observed for highly polar

transition states that can be as low as −175 J/(mol K).[80] The latter are well solvated and thus highly ordered, leading to a very negative entropy of activation. A mostly associated nature of the adducts **3**-**6**, when dissolved in the only moderately polar solvent dichloromethane, can be assumed based, for example, on the DOSY (above) and solubility (below) experiments. Therefore, the negative entropies of activation for **3**-**6** are most probably not caused by a highly ordered solvent shell, but by an otherwise highly ordered transition state. This transition state could, for example, be an assembly of the general form $[R_3PO{\cdot}HOOCR_2OOH{\cdot}OPR_3]^{‡}$. The entropies of activation ($\Delta S^{‡}$) of the pairs **1**/**3** and **1**/**5** are more negative than those of **2**/**4** and **2**/**6**. As in the case of $\Delta H^{‡}$ discussed above, this result most probably reflects the stronger hydrogen bonds that di(hydroperoxy)cycloalkanes form with **1** as compared with **2**.

IR and Raman Spectroscopy

The IR spectra[85] of the Ahn adducts **3**-**6** and the pure phosphine oxides **1** and **2** are in accordance with the ^{31}P NMR spectroscopy results (Table 15). The stretching frequencies and wavenumbers for the P=O groups are 6 to 35 cm^{-1} lower for **3**-**6** as compared to **1** and **2** because the hydrogen bonding of the oxygen atom with the di(hydroperoxy)cycloalkane moieties weakens the double bond. Therefore, less energy is required to excite the stretching mode of the bond in the adducts, the bond order is diminished and lower wavenumbers are observed. The differences Δν(P=O) are in the range of 6 to 35 cm^{-1}, in accordance with an earlier study of Hilliard H_2O_2 adducts.[50] It should also be noted that hydrogen bonding to **1** leads to a lower ν(P=O) value in both **3** and **5** (Δν(P=O) = 35 cm^{-1}), as compared to bonding to **2** (Δν(P=O) = 6 and 12 cm^{-1})

(Table 15). This corroborates the assumption that **1** is hydrogen-bound more firmly to di(hydroperoxy)cycloalkanes, which corresponds well to the results of the activation enthalpy $\Delta H^{\ddagger}$ for the adduct exchange discussed above.

Table 15 IR stretching frequencies ν(P=O) (cm^{-1}) of the P=O groups of the neat phosphine oxides **1** and **2** and the Ahn adducts **3**-**6**. Δν(P=O) (cm^{-1}) stands for the wavenumber differences between the adducts and the corresponding neat phosphine oxides. Additionally, the IR stretching frequencies ν(O−H) and the Raman ν(O−O) stretching frequencies of **3**-**6** are summarized.

Species	**ν(P=O) (cm^{-1})**	**Δν(P=O) (cm^{-1})**	**ν(O−H) (cm^{-1})**	**ν(O−O) (cm^{-1})**
1	1185	0	–	–
2	1158	0	–	–
3	1150	35	3254	866
4	1146	12	3240	863
5	1150	35	3275	873
6	1152	6	3246	868

The ν(O−H) stretching bands of the hydrogen-bonded di(hydroperoxy)-cycloalkane moieties in **3**-**6** display wavenumbers of 3240 to 3275 cm^{-1} which can be clearly distinguished from potential water bands at about 3400 cm^{-1}.[15,84] The hydrogen bonding of the O−H hydrogen atoms to the P=O group weakens the O−H bonds, which leads to lower ν(O−H) wavenumbers.

Due to the favorable symmetry of the adducts **3**-**6**, the Raman spectra show the O−O stretching bands (Table 15). The intensities of these bands are lower as compared to those from the entirely symmetric Hilliard hydrogen peroxide adducts,[50] but they are still discernable. The ν(O−O) values are found within the narrow range from 863 to

873 cm^{-1}, in agreement with the Raman data of Hilliard adducts,[50] and with theoretically predicted values for $(Ph_3PO{\cdot}H_2O_2)_2$.[85] As expected, due to the bond order of one, the wavenumbers are much lower than those found for O_2 gas (1556 cm^{-1})[86] and O_2^- (1139 cm^{-1}).[87] Basically, the ν(O−O) for hydrogen-bonded di(hydroperoxy)cycloalkanes in **3**-**6** lies in the region of values for aqueous (99.5%) H_2O_2 (880 cm^{-1})[88] and H_2O_2 vapor (864 cm^{-1}).[89] However, the O−O bonds in **3**-**6** are still stronger than those in alkali peroxides (736-790 cm^{-1})[90] or the oxidizing agent ^{t}BuOOH (847 cm^{-1}).[91] Overall, the IR and Raman data of **3**-**6** corroborate the results of the low-temperature ^{31}P NMR experiments.

Solubilities

From a practical point of view, the most attractive characteristic of the Ahn adducts **3**-**6** is their high solubility in most organic solvents (Figure 34). They are soluble in aromatic solvents like benzene, in polar solvents with electron donation capabilities, such as THF, dichloromethane (DCM), and dimethylformamide (DMF), as well as in protic solvents like alcohols. Interestingly, in contrast to the Hilliard adducts of the same phosphine oxides,[50] the solubilities of all Ahn adducts are lowest in methanol (Figure 34). In fact, the solubilities of **3**-**6** in methanol are roughly two orders of magnitude lower than those of the corresponding Hilliard adducts.[50] The solubilities of the Ahn adducts **3**-**6** in methanol (5-7 g/L) are also much lower than the solubilities of the corresponding phosphine oxides **1** (25 g/L) and **2** (45 g/L) in this solvent. We assume that, in accordance with the exchange and competition experiments described above, the

solvent does not lead to prolonged dissociation of the adducts and the solubilities obtained (Figure 34) reflect the fact that **3**-**6** overall have an unpolar character.

Overall, for adducts containing *o*-Tol substituents (**4**, **6**) the solubilities in nonprotic solvents like THF or CH_2Cl_2 are higher for adducts incorporating seven-membered alkyl rings as compared to those with six-membered rings (**3**, **4**). For adducts with *p*-Tol groups no trend for the dependence on the alkyl ring size is discernible.

The high solubilities of **3**-**6** in organic solvents are beneficial for many oxidation reactions. For example, the selective oxidations of phosphines to phosphine oxides[54-57] or sulfides to sulfoxides[55,56] can be performed in one organic phase, rendering a biphasic reaction mixture obsolete. Especially in cases where a large amount of water in the aqueous phase could lead to unwanted secondary products this is advantageous. For example, it has been described earlier that cyclic ketones could selectively be oxidized to lactones via Baeyer-Villiger reactions without hydrolysis and polymerization when using Ahn adducts.[57] Whenever all educts are dissolved in one phase, the reactions also proceed faster as compared to processes that only take place at phase boundaries. Furthermore, no phase separations or cumbersome drying procedures for the products are required when reactions with **3**-**6** are performed in organic solvents. The one water molecule formed per P=O group for **3**-**6** in case all peroxy groups have reacted remains firmly bound to the phosphine oxide carriers and will not interfere with the product or the progress of the reaction. The structures and characteristic data of representative water adducts of phosphine oxides have been reported earlier.[43,50] Once the above-mentioned oxidation reactions are complete, the phosphine oxide carriers can easily be removed

from the reaction mixtures by precipitating them with hexanes. The phosphine oxides can also be bound to insoluble inorganic supports like silica[34-36] and separated from the supernatant reaction mixtures containing the products by decanting. After recharging with H_2O_2 and ketones the Ahn adducts of the tethered phosphine oxides can be reused.

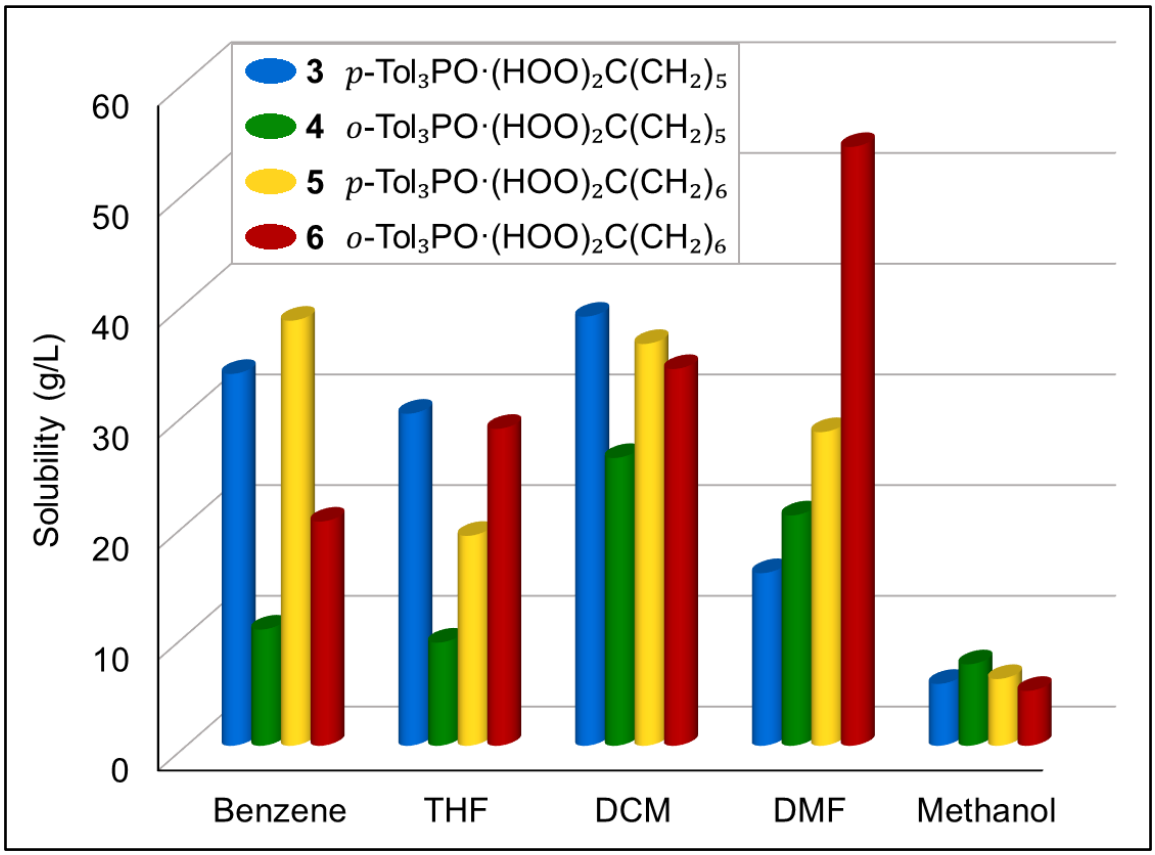

Figure 34 Solubilities of the Ahn adducts **3-6** in selected organic solvents.

Shelf Lives

The Ahn adducts **3-6** are stable when subjected to dry grinding. They do not react to sudden impact like hammering. Even when the powders are brought directly into a

flame oxygen is released slowly without any violent audible or visual effect. Furthermore, the adducts can be molten without initial decomposition, and oxygen slowly effervesces in tiny bubbles at higher temperatures.

Table 16 Oxidative power of the solids **3**-**6** after storage between −13 °C and −18 °C for 250 days. 100% oxidative power corresponds to two active oxygen atoms per adduct assembly.

Adduct	Residual Oxidative Power (%)
3	99
4	100
5	80
6	68

As solids, the adducts **3**-**6** remain oxidatively active over weeks at ambient and months at low temperatures (Table 16). The oxidative power has been determined by a convenient and standardized *in situ* ^{31}P NMR test.[50,54-57] Hereby, for **3-6**, 100% oxidative power corresponds to two active oxygen atoms per P=O group in one adduct assembly. The data show that all adducts can be conveniently handled at ambient temperatures and that they allow storage in a freezer for months. Since the Ahn adducts can be generated also from water adducts of phosphine oxides,[56] old batches can easily be restored to 100% oxidative power by reaction with H_2O_2 and ketone and crystallization.

Conclusions

The presented studies allow the following generalizations. (**a**) The composition of all Ahn adducts **3**-**6** is well-defined and reproducible, with one di(hydroperoxy)cycloalkane moiety hydrogen-bonded to one phosphine oxide group. (**b**) All adducts are solid and crystallize readily in large habits. (**c**) The single crystal X-ray diffraction studies of **3**-**6** show that there is a common structural motif with two hydroperoxy groups hydrogen-bound to the oxygen of one P=O group. (**d**) All adducts are safe and robust towards high temperatures and mechanical stress inflicted by hammering and grinding, with shelf lives of months in a refrigerator. (**e**) The one-step synthesis of **3**-**6** is straightforward. (**f**) The high solubility of all adducts in organic solvents allows for natural abundance ^{17}O NMR spectroscopy. (**g**) The adducts can also be characterized by Raman and IR spectroscopy, both of which corroborate the hydrogen bonding of intact hydroperoxy groups. (**h**) ^{1}H DOSY spectroscopy revealed that the adducts **3**-**6** do not dissociate in solvents, but diffuse through solutions as 1 : 1 assemblies. (**i**) Competition experiments using various phosphine oxides allowed to estimate the relative strengths of the hydrogen bonds between the di(hydroperoxy)cycloalkanes and the phosphine oxides with different electronic and steric properties. (**j**) Variable temperature ^{31}P NMR spectroscopy led to quantitative results on the migration of the di(hydroperoxy)cycloalkanes from on phosphine oxide carrier to the next, and the Gibbs energy of activation $\Delta G^{\ddagger}$, as well as the enthalpy and entropy of activation, $\Delta H^{\ddagger}$ and $\Delta S^{\ddagger}$, could be determined.

In the future, the toolbox of phosphine oxides for all adducts can be further expanded by including the oxides of tripodal phosphines[37] and tetraphosphines[36,92] as carriers to increase their specific peroxide contents.

In conclusion, the presented work greatly expands the general understanding, fundamental chemistry and characterization, as well as solution dynamics of a new important class of peroxides that are stabilized by novel $P{=}O(\cdots HOO)_2$ hydrogen bonding motifs. They possess many of the most desirable attributes for oxidizing agents and are primed to have a significant positive impact on diverse problems in synthetic chemistry.

Experimental Section

General Considerations

All reactions were carried out using standard Schlenk techniques and a purified N_2 atmosphere, if not stated otherwise. Reagents purchased from Sigma Aldrich or VWR were used without further purification. Aqueous H_2O_2 solution (35% w/w) was obtained from Acros Organics and used as received. Solvents were dried by boiling over sodium, then they were distilled and stored under purified nitrogen. Acetone, dichloromethane (Aldrich, ACS reagent grade) and ethanol (200 proof) were dried over 3 Å molecular sieves (EMD Chemical Inc.) prior to use. The latter were also used for drying **1** and **2**. The phosphine oxides were obtained according to literature procedures.[15,61] 1,1-di(hydroperoxy)cyclohexane and 1,1-di(hydroperoxy)cycloheptane were synthesized from cyclohexanone and cycloheptanone according to a literature procedure.[62]

*Solubility Measurements of **3-6***

The adduct (5-12 mg) was placed into a tared 20 mL vial. The desired solvent was added in dropsized portions while shaking the vial vigorously at 20 °C. Once all solid was dissolved, the overall weight gain was recorded, and the solvent volume was calculated.

NMR Spectroscopy

The ^{1}H, ^{13}C, and ^{31}P NMR spectra at ambient and variable temperature were recorded at 499.70, 125.66, and 202.28 MHz on a 500 MHz Varian spectrometer. The ^{13}C and ^{31}P NMR spectra were recorded with ^{1}H decoupling if not stated otherwise. Neat Ph_2PCl ($\delta(^{31}P)$ = +81.92 ppm) in a capillary centered in the 5 mm NMR tubes was used for referencing the ^{31}P chemical shifts of dissolved compounds. For referencing the ^{1}H and ^{13}C chemical shifts, the residual proton and the carbon signals of the solvents were used (C_6D_6: $\delta(^{1}H)$ = 7.16 ppm, $\delta(^{13}C)$ = 128.00 ppm; $CDCl_3$: $\delta(^{1}H)$ = 7.26 ppm, $\delta(^{13}C)$ = 77.00 ppm). The signal assignments were based on comparisons with analogous phosphine oxides and 2D NMR spectra.[15,50,54-57]

^{17}O NMR Spectroscopy

The natural abundance ^{17}O NMR spectra were recorded using 0.3 to 0.5 molar benzene (C_6H_6) solutions of the compounds at 70 °C. A Varian 500 NMR spectrometer equipped with a 5 mm broad band probe operating at 67.79 MHz was employed. The following measurement parameters have been optimized to yield spectra of good quality with $0.8 \cdot 10^6$ to $1 \cdot 10^6$ scans: spectral window (73.5 kHz), number of data points (2206), measurement pulse length (20 μs), pulse angle (90°), relaxation delay (1 ms), and acquisition time (30 ms). The chemical shifts were referenced externally using pure D_2O ($\delta(^{17}O) = 0$ ppm).

^{1}H DOSY

The ^{1}H DOSY NMR measurements were performed using a Varian 500 NMR spectrometer equipped with a 5 mm broad band probe operating at 499.84 MHz. 0.015 molar solutions of the compounds in C_6D_6 were investigated at 25 °C. Hereby, 15 gradient increments were measured after optimizing the following parameters: pulse sequence (Dbppste), diffusion gradient length (1.75 ms), diffusion delay (50 ms), spectral window (8 kHz), complex points (16384), measurement pulse length (15 μs), pulse angle (90°), relaxation delay (1 s), acquisition time (2.045 s), number of scans (64), and number of steady state pulses (8). The measurements were performed using tetramethylsilane (TMS) as an internal size reference.[60] The diffusion (D) of the sample molecule was determined as the averaged values of D of all aromatic hydrogen atoms in the molecule, determined by integration. The ratio of the reference and sample diffusion

($\Delta r = D^{TMS}/D$) was multiplied with the Van der Waals radius of TMS (7.34 Å) to give the hydrodynamic radius of the sample molecule.

IR Spectroscopy

The IR spectra of the neat powders of all adducts and compounds were recorded with a Shimadzu IRAffinity-1 FTIR spectrometer equipped with a Pike Technologies MIRacle ATR plate.

Raman Spectroscopy

The Raman spectra were acquired using a Jobin-Yvon Horiba Labram HR instrument coupled to an Olympus BX41 microscope with 514.51 nm laser excitation from an Ar-ion laser. A 600 lines/mm grating and an acquisition time of 2 s were applied. 60 scans gave spectra of good quality.

X-Ray Diffraction

See appendix C.

Synthesis and Characterization

Synthesis of *p-T*ol$_3$PO (1). *p*-Tol$_3$PO was synthesized according to a modified literature procedure.[93] *p*-Tol$_3$P (450 mg, 1.48 mmol) is dissolved in dichloromethane (14 mL) and aqueous H_2O_2 (6 mL, 35%, 70 mmol) is added while vigorously stirring. After 30 min the phases are separated and dry molecular sieves (550 mg) are added to the organic phase. After standing over the molecular sieves for 18 h, the solution is filtered and the solvent is allowed to slowly evaporate. A colorless powder (467 mg, 1.46 mmol, 99% yield) is collected. Melting range 142-146 °C.

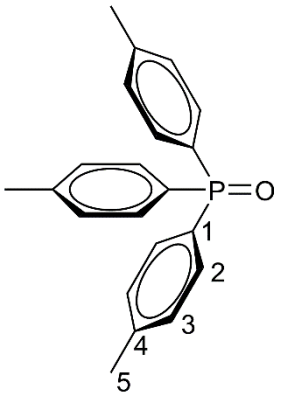

NMR (δ, $CDCl_3$), $^{31}P\{^1H\}$ 29.28 (s); ^1H 7.52 (dd, $^3J(^{31}P–^1H)$ = 11.8 Hz, $^3J(^1H–^1H)$ = 8.1 Hz, 6H, H2), 7.21 (dd, $^3J(^1H–^1H)$ = 8.1 Hz, $^4J(^{31}P–^1H)$ = 2.4 Hz, 6H, H3), 2.34 (s, 9H, H5); ^{13}C 142.18 (d, $^4J(^{31}P–^{13}C)$ = 2.8 Hz, C4), 132.04 (d, $^2J(^{31}P–^{13}C)$ = 10.2 Hz, C2), 129.13 (d, $^3J(^{31}P–^{13}C)$ = 12.5 Hz, C3), 128.58 (d, $^1J(^{31}P–^{13}C)$ = 80.8 Hz, C1), 21.56 ppm (d, $^5J(^{31}P–^{13}C)$ =1.3 Hz, C5). IR: ν(P=O) = 1185 cm^{-1}.

Synthesis of *o*-Tol$_3$PO (2). The synthesis of **2** was performed according to a modified literature procedure.[93] (*o*-$Tol_3PO{\cdot}H_2O_2)_2$ (6.99 g, 9.86 mmol) is dissolved in dichloromethane (100 mL) and dry molecular sieves (7 g) are added to the organic phase. After standing over molecular sieves for 18 h, the solution is filtered and the solvent is allowed to slowly evaporate. A colorless powder (5.98 g, 18.7 mmol, 95% yield) is collected. Melting range 134-137 °C. The crystal structure of **2** has been reported previously.[65] The NMR values are in correspondence with those given in the literature,[93] but no assignments had been provided.

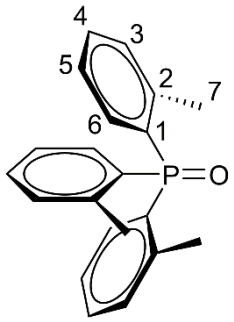

NMR (δ, $CDCl_3$), $^{31}P\{^1H\}$ 37.51 (s); ^1H 7.44 (t, $^3J(^1H–^1H)$ = 7.4 Hz, 3H, H4), 7.32 (dd, $^3J(^1H–^1H)$ = 7.6 Hz, $^4J(^{31}P–^1H)$ = 4.1 Hz, 3H, H3), 7.20 – 7.16 (m, 3H, H5), 7.10 (ddd, $^3J(^{31}P–^1H)$ = 13.8 Hz, $^3J(^1H–^1H)$ = 7.7 Hz, $^4J(^1H–^1H)$ = 1.3 Hz, 3H, H6), 2.50 (s, 9H, H7); ^{13}C 143.69 (d, $^2J(^{31}P–^{13}C)$ = 7.8 Hz, C2), 133.07 (d, $^2J(^{31}P–^{13}C)$ = 12.8 Hz, C6), 132.17 (d, $^3J(^{31}P–^{13}C)$ = 10.4 Hz, C3), 132.05 (d, $^4J(^{31}P–^{13}C)$ = 2.6 Hz, C4), 128.77 (d, $^1J(^{31}P–^{13}C)$ = 81.5 Hz, C1), 125.65 (d, $^3J(^{31}P–^{13}C)$ = 12.8 Hz, C5), 22.15 ppm (d, $^3J(^{31}P–^{13}C)$ = 4.1 Hz, C7). IR: ν(P=O) = 1158 cm^{-1}.

Synthesis of *p*-$Tol_3PO·(HOO)_2C(CH_2)_5$ (3). *p*-Tol_3PO (450 mg, 1.40 mmol) is dissolved in dichloromethane (10 mL) and 1,1-di(hydroperoxy)cyclohexane (250 mg, 1.69 mmol) is added under stirring. Hexanes (10 mL) is added to the mixture and the solvent is allowed to evaporate slowly. Large colorless crystals (487 mg, 1.04 mmol, 74% yield) are obtained. Melting range 114-115 °C.

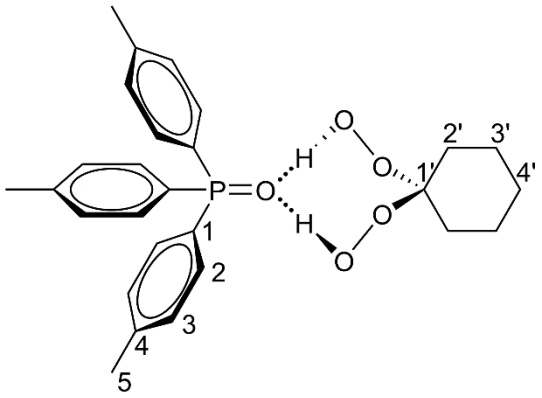

NMR (δ, $CDCl_3$), $^{31}P\{^1H\}$ 34.76 (s); ^1H 9.31–8.35 (br s, O*H*), 7.54 (dd, $^3J(^{31}P–^1H)$ = 12.1 Hz, $^3J(^1H–^1H)$ = 7.8 Hz, 6H, H2), 7.28 (d, $^3J(^1H–^1H)$ = 7.6 Hz, 6H, H3), 2.41 (s, 9H, H5), 1.85 (t, $^3J(^1H–^1H)$ = 6.1 Hz, 4H, H2'), 1.60 (quint., $^3J(^1H–^1H)$ = 6.1 Hz, 4H, H3'), 1.52–1.43 (m, 2H, H4'); ^{13}C 143.00 (d, $^4J(^{31}P–^{13}C)$ = 2.6 Hz, C4), 132.26 (d, $^2J(^{31}P–^{13}C)$ = 10.7 Hz, C2), 129.52 (d, $^3J(^{31}P–^{13}C)$ = 12.8 Hz, C3), 128.15 (d, $^1J(^{31}P–^{13}C)$ = 108.3 Hz, C1), 109.50 (s, C1'), 29.94 (s, C2'), 25.82 (s, C4'), 22.75 (s, C3'), 21.74 ppm (d, $^5J(^{31}P–^{13}C)$ =1.3 Hz, C5). IR: ν(O-H) = 3254 cm^{-1}, ν(P=O) = 1150 cm^{-1}.

Synthesis of *o*-$Tol_3PO{\cdot}(HOO)_2C(CH_2)_5$ (4). *o*-Tol_3PO (450 mg, 1.40 mmol) is dissolved in dichloromethane (10 mL) and 1,1-di(hydroperoxy)cyclohexane (250 mg, 1.69 mmol) is added while stirring. Hexanes (10 mL) is added to the mixture and the solvent is allowed to evaporate slowly. Colorless crystals (587 mg, 1.25 mmol, 89% yield) are collected. Melting range 138-140 °C.

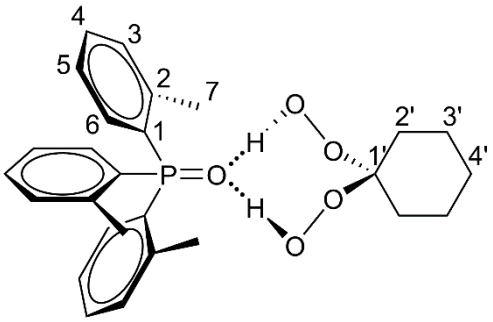

NMR (δ, $CDCl_3$), $^{31}P\{^1H\}$ 42.47 (s); ^1H 9.74–8.20 (br s, O*H*), 7.46 (t, $^3J(^1H–^1H)$ = 7.5 Hz, 3H, H4), 7.34 (dd, $^3J(^1H–^1H)$ = 7.4 Hz, $^4J(^{31}P–^1H)$ = 4.4 Hz, 3H, H3), 7.17 (t, $^3J(^1H–^1H)$ = 7.2 Hz, 3H, H5), 7.06 (dd, $^3J(^{31}P–^1H)$ = 14.5 Hz, $^3J(^1H–^1H)$ = 7.7 Hz, 3H, H6),2.47 (s, 9H, H7), 1.79 (t, $^3J(^1H–^1H)$ = 6.2 Hz, 4H, H2'), 1.62–1.52 (m, 4H, H3'), 1.44–1.39 (m, 2H, H4');^{13}C 143.77 (d, $^2J(^{31}P–^{13}C)$ = 7.7 Hz, C2), 133.17 (d, $^2J(^{31}P–^{13}C)$ = 13.5 Hz, C6), 132.60 (d, not fully resolved, C4), 132.45 (d, $^3J(^{31}P–^{13}C)$ = 10.5 Hz, C3), 129.07 (d, $^1J(^{31}P–^{13}C)$ = 101.1 Hz, C1), 125.85 (d, $^3J(^{31}P–^{13}C)$ = 13.2 Hz, C5), 109.40 (s, C1'), 29.88 (s, C2'), 25.78 (s, C4'), 22.73 (s, C3'), 22.14 ppm (d, $^3J(^{31}P–^{13}C)$ = 4.3 Hz, C7). IR: ν(O-H) = 3240 cm^{-1}, ν(P=O) = 1146 cm^{-1}.

Synthesis of *p*-$Tol_3PO·(HOO)_2C(CH_2)_6$ (5). *p*-Tol_3PO (450 mg, 1.40 mmol) is dissolved in dichloromethane (10 mL) and 1,1-di(hydroperoxy)cycloheptane (226 mg, 1.4 mmol) is added under stirring. Hexanes (10 mL) is added to the reaction mixture and the solvent is allowed to evaporate slowly. Colorless crystals (523 mg, 1.08 mmol, 78% yield) have been collected. Melting range 120-122 °C. After melting, oxygen was released at 126 °C.

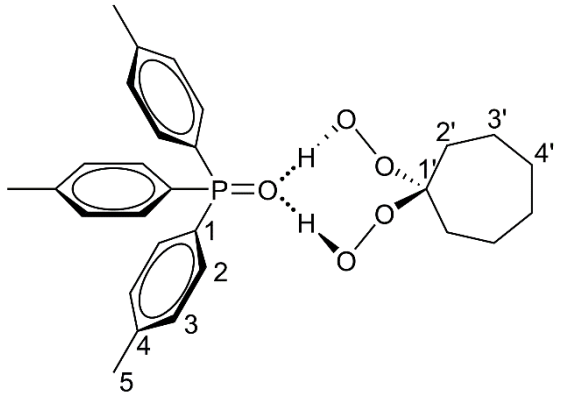

NMR (δ, $CDCl_3$), $^{31}P\{^1H\}$ 32.51 (s); ^1H 7.49 (dd, $^3J(^{31}P–^1H)$ = 12.0 Hz, $^3J(^1H–^1H)$ = 7.9 Hz, 6H, H2), 7.22 (d, $^3J(^1H–^1H)$ = 7.7 Hz, 6H, H3), 6.35–5.33 (br s, O*H*), 2.36 (s, 9H, H5), 1.94–1.90 (m, 4H, H2'), 1.59–1.50 (m, 8H, H3', H4'); ^{13}C 142.78 (d, $^4J(^{31}P–^{13}C)$ = 2.3 Hz, C4), 132.27 (d, $^2J(^{31}P–^{13}C)$ = 10.5 Hz, C2), 129.44 (d, $^3J(^{31}P–^{13}C)$ = 12.7 Hz, C3), 128.76 (d, $^1J(^{31}P–^{13}C)$ = 106.5 Hz, C1), 114.71 (s, C1'), 32.56 (s, C2'), 30.31 (s, C4'), 23.04 (s, C3'), 21.75 ppm (d, $^5J(^{31}P–^{13}C)$ =1.3 Hz, C5). IR: ν(O-H) = 3275 cm^{-1}, ν(P=O) = 1150 cm^{-1}.

Synthesis of *o*-$Tol_3PO{\cdot}(HOO)_2C(CH_2)_6$ (6). *o*-Tol_3PO (450 mg, 1.40 mmol) is dissolved in dichloromethane (10 mL) and 1,1-di(hydroperoxy)cycloheptane (226 mg, 1.4 mmol) is added while stirring. Hexanes (10 mL) is added to the reaction mixture and the solvent is allowed to slowly evaporate. Colorless crystals (504 mg, 1.04 mmol, 75% yield) are collected. Melting range 119-130 °C.

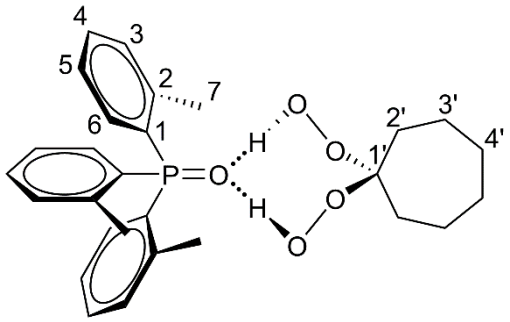

NMR (δ, $CDCl_3$), $^{31}P\{^1H\}$ 39.95 (s); ^1H 7.44 (t, $^3J(^1H–^1H)$ = 7.5 Hz, 3H, H4), 7.32 (dd, $^3J(^1H–^1H)$ = 7.6 Hz, $^4J(^{31}P–^1H)$ = 4.2 Hz, 3H, H3), 7.15 (t, $^3J(^1H–^1H)$ = 7.2 Hz, 3H, H5), 7.07 (dd, $^3J(^{31}P–^1H)$ = 14.3 Hz, $^3J(^1H–^1H)$ = 7.5 Hz, 3H, H6), 2.48 (s, 9H, H7), 1.92–1.90 (m, 4H, H2'), 1.59–1.50 (m, 8H, H3', H4'); ^{13}C 143.72 (d, $^2J(^{31}P–^{13}C)$ = 7.7 Hz, C2), 133.10 (d, $^2J(^{31}P–^{13}C)$ = 13.1 Hz, C6), 132.29 (d, $^3J(^{31}P–^{13}C)$ = 10.5 Hz, C3), 132.28 (d, $^4J(^{31}P–^{13}C)$ = 2.6 Hz, C4), 129.91 (d, $^1J(^{31}P–^{13}C)$ = 102.2 Hz, C1), 125.72 (d, $^3J(^{31}P–^{13}C)$ = 13.0 Hz, C5), 114.60 (s, C1'), 32.44 (s, C2'), 30.33 (s, C4'), 22.99 (s, C3'), 22.11 ppm (d, $^3J(^{31}P–^{13}C)$ = 4.1 Hz, C7). IR: ν(O-H) = 3246 cm^{-1}, ν(P=O) = 1152 cm^{-1}.

References

1 D. Duprey and F. Cavani, *Handbook of Advanced Methods and Processes in Oxidation Catalysis*, 2014.

2 F. Cavani and J. H. Teles, *ChemSusChem*, 2009, **2**, 508.-534.

3 A. E. Comyns, *Van Nostrand's Encyclopedia of Chemistry*, 2005.

4 N. M. Todorović, M. Stefanovic, B. Tinant, J.-P. Declercq, M. T. Makler and B. A. Šolaja, *Steroids*, 1996, **61**, 688-696.

5 C. A. Bettenhausen, *Chem. Eng. News*, 2020, **98**, 16-17.

6 I. B. Krylov, A. S. Budnikov, A. V. Lastovko, Y. A. Ibatov, G. I. Nikishin and A. O. Terent'ev, *Russ. Chem. Bull.*, 2019, **68**, 1454–1457.

7 C. J. Legacy, A. Wang, B. J. O'Day and M. H. Emmert, *Angew. Chem. Int. Ed.*, 2015, **54**, 14907–14910.

8 C. J. Legacy and M. H. Emmert, *Synlett*, 2016, **27**, 1893-1897.

9 T. J. Osberger, D. C. Rogness, J. T. Kohrt, A. F. Stepan and M. C. White, *Nature*, 2016, **537**, 214-219.

10 J. M. Howell, K. Feng, J. R. Clark, L. J. Trzepkowski and M. C. White, *J. Am. Chem. Soc.*, 2015, **137**, 14590-14593.

11 M. D. Zhou, M. Liu, J. Huang, J. Zhang, J. Wang, X. Li, F. E. Kühn and S. L. Zang, *Green Chem.*, 2015, **17**, 1186-1193.

12 I. I. E. Markovits, W. A. Eger, S. Yue, M. Cokoja, C. J. Münchmeyer, B. Zhang, M.-D. Zhou, A. Genest, J. Mink, S.-L. Zang, N. Rösch and F. E. Kühn, *Chem. - Eur. J.*, 2013, **19**, 5972-5979.

13 E. Wojaczynska and J. Wojaczynski, *Chem. Rev.*, 2010, **110**, 4303-4356.

14 P. B. Page, B. Buckley, C. Elliott, Y. Chan, N. Dreyfus and F. Marken, *Synlett*, 2015, **27**, 80-82.

15 C. R. Hilliard, N. Bhuvanesh, J. A. Gladysz and J. Blümel, *Dalton Trans.*, 2012, **41**, 1742-1754.

16 J. Chrzanowski, D. Krasowska and J. Drabowicz, *Heteroat. Chem.*, 2018, **29**, e21476.

17 M. Uyanik and K. Ishihara, *ACS Catal.*, 2013, **3**, 513-520.

18 L. Zhou, X. Liu, J. Ji, Y. Zhang, X. Hu, L. Lin and X. Feng, *J. Am. Chem. Soc.*, 2012, **134**, 17023-17026.

19 L. Ji, Y.-N. Wang, C. Qian and X.-Z. Chen, *Synth. Commun.*, 2013, **43**, 2256-2264.

20 D. Kaur and B. R. Chhabra, *J. Chem. Biol., Phys. Sci. A*, 2013, **3**, 980-987.

21 N. Koukabi, *Synlett*, 2010, **2010**, 2969-2970.

22 A. V. Churakov, P. V. Prikhodchenko and J. A. K. Howard, *CrystEngComm*, 2005, **7**, 664-669.

23 A. V. Churakov, D. A. Grishanov, A. G. Medvedev, A. A. Mikhaylov, M. V. Vener, M. A. Navasardyan, T. A. Tripol'skaya, O. Lev and P. V. Prikhodchenko, *CrystEngComm*, 2020, **22**, 2866-2872.

24 A. McKillop and W. R. Sanderson, *J. Chem. Soc. Perkin 1*, 2000, 471-476.

25 M. V. Gómez, R. Caballero, E. Vázquez, A. Moreno, A. de la Hoz and Á. Díaz-Ortiz, *Green Chem.*, 2007, **9**, 331-336.

26 Z. Elkhayat, I. Safir, Z. Gandara, P. Retailleau and S. Arseniyadis, *Eur. J. Org. Chem.*, 2010, **2010**, 4851-4860.

27 N. C. Ganguly, S. Chandra and S. K. Barik, *Synth. Commun.*, 2013, **43**, 1351-1361.

28 A. V. Arzumanyan, R. A. Novikov, A. O. Terent'ev, M. M. Platonov, V. G. Lakhtin, D. E. Arkhipov, A. A. Korlyukov, V. V. Chernyshev, A. N. Fitch, A. T. Zdvizhkov, I. B. Krylov, Y. V. Tomilov and G. I. Nikishin, *Organometallics*, 2014, **33**, 2230-2246.

29 S. Kharel, T. Jia, N. Bhuvanesh, J. H. Reibenspies, J. Blümel and J. A. Gladysz, *Chem. - Asian J.*, 2018, **13**, 2632-2640.

30 M. D. Fletcher, *Organophosphorus Reagents*, 2004, 171-214.

31 H. Adams, R. C. Collins, S. Jones and C. J. A. Warner, *Org. Lett.*, 2011, **13**, 6576-6579.

32 K. C. K. Swamy, N. N. B. Kumar, E. Balaraman and K. V. P. P. Kumar, *Chem. Rev.*, 2009, **109**, 2551-2651.

33 R. H. Beddoe, K. G. Andrews, V. Magne, J. D. Cuthbertson, J. Saska, A. L. Shannon-Little, S. E. Shanahan, H. F. Sneddon and R. M. Denton, *Science*, 2019, **365**, 910-914.

34 J. Guenther, J. Reibenspies and J. Blümel, *Mol. Catal.*, 2019, **479**, 110629.

35 J. C. Pope, T. Posset, N. Bhuvanesh and J. Blümel, *Organometallics*, 2014, **33**, 6750-6753.

36 J. H. Baker, N. Bhuvanesh and J. Blümel, *J. Organomet. Chem.*, 2017, **847**, 193-203.

37 K. J. Cluff, N. Bhuvanesh and J. Blümel, *Chem. - Eur. J.*, 2015, **21**, 10138-10148.

38 A. Zheng, S.-B. Liu and F. Deng, *Chem. Rev.*, 2017, **117**, 12475−12531.

39 S. Machida, M. Sohmiya, Y. Ide and Y. Sugahara, *Langmuir*, 2018, **34**, 12694−12701.

40 A. R. Wilmsmeyer, W. O. Gordon, E. D. Davis, B. A. Mantooth, T. A. Lalain and J. R. Morris, *Rev. Sci. Instrum.*, 2014, **85**, 014101.

41 P. J. Hubbard, J. W. Benzie, V. I. Bakhmutov and J. Blümel, *J. Chem. Phys.*, 2020, **152**, 054718.

42 S. Kharel, K. J. Cluff, N. Bhuvanesh, J. A. Gladysz and J. Blümel, *Chem. - Asian J.*, 2019, **14**, 2704-2711.

43 C. R. Hilliard, S. Kharel, K. J. Cluff, N. Bhuvanesh, J. A. Gladysz and J. Blümel, *Chem. - Eur. J.*, 2014, **20**, 17292-17295.

44 A. E. Stross, G. Iadevaia and C. A. Hunter, *Chem. Sci.*, 2016, **7**, 94-101.

45 D. Nunez-Villanueva and C. A. Hunter, *Chem. Sci.*, 2017, **8**, 206-213.

46 N. A. Bewick, A. Arendt, Y. Li, S. Szafert, T. Lis, K. A. Wheeler, J. Young and R. Dembinski, *Curr. Org. Chem.*, 2015, **19**, 469-474.

47 S. J. Pike and C. A. Hunter, *Org. Biomol. Chem.*, 2017, **15**, 9603-9610.

48 N. J. Burke, A. D. Burrows, M. F. Mahon and J. E. Warren, *Inorganica Chim. Acta*, 2006, **359**, 3497-3506.

49 R. Joshi and S. P. Pasilis, *J. Mol. Liq.*, 2015, **209**, 381-386.

50 F. F. Arp, N. Bhuvanesh and J. Blümel, *Dalton Trans.*, 2019, **48**, 14312-14325.

51 S. Kharel, N. Bhuvanesh, J. A. Gladysz and J. Blümel, *Inorganica Chim. Acta*, 2019, **490**, 215-219.

52 E. Y. Tupikina, M. Bodensteiner, P. M. Tolstoy, G. S. Denisov and I. G. Shenderovich, *J. Phys. Chem. C*, 2018, **122**, 1711-1720.

53 G. Begimova, E. Y. Tupikina, V. K. Yu, G. S. Denisov, M. Bodensteiner and I. G. Shenderovich, *J. Phys. Chem. C*, 2016, **120**, 8717-8729.

54 F. F. Arp, S. H. Ahn, N. Bhuvanesh and J. Blümel, *New J. Chem.*, 2019, **43**, 17174-17181.

55 S. H. Ahn, K. J. Cluff, N. Bhuvanesh and J. Blümel, *Angew. Chem. Int. Ed.*, 2015, **54**, 13341-13345.

56 S. H. Ahn, N. Bhuvanesh and J. Blümel, *Chem. - Eur. J.*, 2017, **23**, 16998-17009.

57 S. H. Ahn, D. Lindhardt, N. Bhuvanesh and J. Blümel, *ACS Sustainable Chem. Eng.*, 2018, **6**, 6829-6840.

58 J. L. Cook, C. A. Hunter, C. M. R. Low, A. Perez-Velasco and J. G. Vinter, *Angew. Chem. Int. Ed.*, 2007, **46**, 3706-3709.

59 G. Kagan, W. Li, R. Hopson and P. G. Williard, *Org. Lett.*, 2009, **11**, 4818-4821.

60 E. J. Cabrita and S. Berger, *Magn. Reson. Chem.*, 2001, **39**, S142-S148.

61 A. Burger and N. D. Dawson, *J. Org. Chem.*, 1951, **16**, 1250–1254.

62 A. O. Terent'ev, M. M. Platonov, Y. N. Ogibin and G. I. Nikishin, *Synth. Commun.*, 2007, **37**, 1281-1287.

63 M. C. Etter and P. W. Baures, *J. Am. Chem. Soc.*, 1988, **110**, 639-640.

64 The following CCDC reference numbers contain the supplementary crystallographic data for the corresponding compounds **1** and **3**-**6** for this paper: 1937469 (*p*-Tol_3PO, **1**), 1960850 (*p*-$Tol_3PO{\cdot}(HOO)_2C(CH_2)_5$, **3**), 1960851 (*o*-$Tol_3PO{\cdot}(HOO)_2C(CH_2)_5$, **4**), 1960852 (*p*-$Tol_3PO{\cdot}(HOO)_2C(CH_2)_6$, **5**), 1960853 (*o*-$Tol_3PO{\cdot}(HOO)_2C(CH_2)_6$, **6**). These data can be obtained free of charge from the Cambridge Crystallographic Data Centre via www.ccdc.cam.ac.uk/data_request/cif.

65 F. R. Fronczek, CCDC 1021095, *CSD Communication* **2014**. DOI: 10.5517/cc138jkg.

66 G. A. Jeffrey, *An Introduction to Hydrogen Bonding*, 1997.

67 E. N. Baker and R. E. Hubbard, *Prog. Biophys. Mol. Biol.*, 1984, **44**, 97-179.

68 N. De Silva, F. Zahariev, B. P. Hay, M. S. Gordon and T. L. Windus, *J. Phys. Chem. A*, 2015, **119**, 8765-8773.

69 H. C. E. McFarlane, W. McFarlane and J. Mason, *Oxygen in Multinuclear NMR*, 1987.

70 J. J. Barieux and J. P. Schirmann, *Tetrahedron Lett.*, 1987, **28**, 6443.

71 B. Plesničar, J. Cerkovnik, T. Tekavec and J. Koller, *Chem. - Eur. J.*, 2000, **6**, 809-819.

72 M. Căsný, D. Rehder, H. Schmidt, H. Vilter and V. Conte, *J. Inorg. Biochem.*, 2000, **80**, 157-160.

73 T. M. Alam, M. Celina, R. A. Assink, R. L. Clough, K. T. Gillen and D. R. Wheeler, *Macromolecules*, 2000, **33**, 1181–1190.

74 D. L. Bryce, K. Eichele and R. E. Wasylishen, *Inorg. Chem.*, 2003, **42**, 5085-5096.

75 A. Wong, K. J. Pike, R. Jenkins, G. J. Clarkson, T. Anupõld, A. P. Howes, D. H. G. Crout, A. Samoson, R. Dupree and M. E. Smith, *J. Phys. Chem. A*, 2006, **110**, 1824-1835.

76 H. Dahn, V. Van Toan and M.-N. Ung-Truong, *Magn. Reson. Chem.*, 1992, **30**, 1089-1096.

77 R. D. Sammons, P. A. Frey, K. Bruzik and M.-D. Tsai, *J. Am. Chem. Soc.*, 1983, **105**, 5455.

78 A. L. Baumstark, P. C. Vasquez and P. Balakrishnan, *Tetrahedron Lett.*, 1985, **26**, 2051-2054.

79 P. H. M. Budzelaar, *gNMR 5.0.6.0; IvorySoft: Centennial*, 2006.

80 S. Ašperger, *Chemical Kinetics and Inorganic Reaction Mechanisms*, 2003.

81 D. K. Zimmer, R. Shoemaker and R. R. Ruminski, *Inorganica Chim. Acta*, 2006, **359**, 1478-1484.

82 S.-Y. Sheu, D.-Y. Yang, H. L. Selzle and E. W. Schlag, *Proc. Natl. Acad. Sci. U. S. A.*, 2003, **100**, 12683-12687.

83 J. P. Guthrie, *J. Am. Chem. Soc.*, 1996, **118**, 12886–12890.

84 H. Günzler and H.-U. Gremlich, *IR Spektroskopie*, 2003.

85 T. Tsuneda, J. Miyake and K. Miyatake, *ACS Omega*, 2018, **3**, 259-265.

86 W. H. Fletcher and J. S. Rayside, *J. Raman Spectrosc.*, 1974, **2**, 3-14.

87 M. Hayyan, M. A. Hashim and I. M. AlNashef, *Chem. Rev.*, 2016, **116**, 3029-3085.

88 R. C. Taylor and P. C. Cross, *J. Chem. Phys.*, 1956, **24**, 41-44.

89 P. A. Giguére and T. K. K. Srinivasan, *J. Raman Spectrosc.*, 1974, **2**, 125-132.

90 H. H. Eysel and S. Thym, *Z. Anorg. Allg. Chem.*, 1975, **411**, 97-102.

91 V. Vacque, B. Sombret, J. P. Huvenne, P. Legrand and S. Suc, *Spectrochim. Acta, Part A*, 1997, **53**, 55-66.

92 Y. Yang, B. Beele and J. Blümel, *J. Am. Chem. Soc.*, 2008, **130**, 3771-3773.

93 R. M. Denton, J. An, B. Adeniran, A. J. Blake, W. Lewis and A. M. Poulton, *J. Org. Chem.*, 2011, **76**, 6749-6767.

CHAPTER V

CONCLUSIONS

The syntheses described in this work and the X-ray single crystal analyses confirm the consistently preferred binding modes between phosphine oxides and hydrogen peroxide or di(hydroperoxy)alkanes respectively. Deviations of the chair type arrangement were found in hydrogen peroxide adducts if a molecule of hydrogen peroxide was removed using heat, or if the two phosphine oxide moieties could sterically only accommodate one hydrogen peroxide. The twist boat type arrangement of di(hydroperoxy)alkanes was found consistently throughout all synthesized species.

The influence of hydrogen bonding on the chemical shift of ^{31}P NMR resonances of the phosphine oxides was extensively studied and discussed. The high solubility of the adducts also allowed to perform natural abundance ^{17}O NMR studies, whereas both phosphine oxide and peroxide oxygens could be observed. In the case of Ahn adducts complete resolution of the peroxide oxygens allowed to exclude the theoretical possibility of equilibria that could lead to the intermediate formation of condensed peroxide species, such as triacetone peroxide (TATP).

While the ^{31}P and ^{17}O studies confirmed the presence of hydrogen bonds of dissolved adducts, ^{1}H and ^{31}P DOSY NMR studies were performed in order to assess the extent of dissociation in solution. Hilliard adducts were confirmed to dissociate incompletely depending on the hydrogen bond affinity of the employed phosphine oxide, while Ahn adducts were found to be more resistant to dissociation.

A qualitative dynamic NMR assay was developed, using competing phosphine oxides. While the nature of bonding for Ahn adducts was found to be dynamic, there was a clear preference for alkylphosphine oxides over arylphosphine oxides. Variable temperature NMR assays using Ahn adducts with excess phosphine oxides allowed to quantify the enthalpy and entropy of the transition states of peroxide exchange equilibria. While the enthalpies were found to be in the typical range for breaking hydrogen bonds, the very negative entropies suggested a highly ordered transition state. This suggests stepwise breaking of one hydrogen bond, leaving one hydroperoxy group free to from a bond to another phosphine oxide, and subsequent breakage of the hydrogen bond of the other hydroperoxy group. This behavior confirms the lack of unbound di(hydroperoxy)alkane in solution, which suggests that these adducts have altered reactivity compared to pristine di(hydroperoxy)alkanes.

This curious behavior of di(hydroperoxy)alkanes in the presence of phosphine oxides was exploited to template the formation of methylethylketone peroxide (MEKPO). MEKPO is synthesized from butanone (methylethylketone) and hydrogen peroxide. A mixture of seven different oligomers and some starting material is obtained. However, if the difunctional dppe (bis(diphenylphosphino)ethane) dioxide is present in the reaction, an adduct of the MEKPO dimer only can be easily isolated.

Further work in our group will focus on the synthesis of bulky Ahn adducts, and the application of Ahn adducts in oxidation reactions, especially the oxidative esterification of aldehydes.

APPENDIX A

SUPPLEMENTARY DATA CHAPTER II

X-Ray Crystallography

Adduct 1. A solution of **1** in dichloromethane and pentane (2:1) was concentrated by slow evaporation. Colorless blocks with well-defined faces were collected and data obtained as outlined in Table **S1**. Sixty data frames were taken at widths of 1.0°. These reflections were used in the auto-indexing procedure to determine the unit cell. A suitable cell was found and refined by nonlinear least squares and Bravais lattice procedures. The unit cell was verified by examination of the h k l overlays on several frames of data. No super-cell or erroneous reflections were observed. After careful examination of the unit cell, an extended data collection procedure (4 sets) was initiated using omega scans.

Integrated intensity information for each reflection was obtained by reduction of the data frames with the program APEX2.[S1] The integration method employed a three dimensional profiling algorithm and all data were corrected for Lorentz and polarization factors, and for crystal decay effects. Finally, the data was merged and scaled to produce a suitable data set. The absorption correction program SADABS[S2] was employed to correct the data for absorption effects.

Systematic reflection conditions and statistical tests of the data suggested the space group $P2_1/n$. A solution was obtained readily using XT/XS in APEX2.[S1,S3] Hydrogen atoms were placed in idealized positions and were set riding on the respective parent atoms. All non-hydrogen atoms were refined with anisotropic thermal parameters. Unusual thermal

ellipsoids on O2 and O3 indicated a possible disorder, and was modeled successfully between two positions with an occupancy ratio of 0.75:0.25. Appropriate restraints were used to keep the bond distances and the thermal ellipsoids meaningful.

Absence of additional symmetry and voids were confirmed using PLATON (ADDSYM).[S4] The structure was refined (weighted least squares refinement on F2) to convergence.[S3,S5] Olex2 was employed for the final data presentation and structure plots.[S5]

Adduct 2. A solution of **2** in dichloromethane was concentrated by slow evaporation. Colorless blocks with well-defined faces were collected, data were obtained and the structure was solved as described for **1** (20732 reflections).

Adduct 3. Assembly **3** was crystallized as **2**. Data were obtained and the structure was solved as described for **1** (68772 reflections). After careful examination of the unit cell, an extended data collection procedure (7 sets) was initiated using omega and phi scans. Integrated intensity information for each reflection was obtained by reduction of the data frames with the program APEX3.[S6] The H_2O_2 molecule was found disordered between two sites and was modeled successfully with an occupancy ratio of 0.54:0.46. In the thermal ellipsoid plot only the molecule occupying 54% is shown

Adduct 4. Adduct **4** was crystallized as **1**. Data were obtained as outlined in Table **S2** and the structure was solved as described for **1** (28153 reflections). Integrated intensity

information for each reflection was obtained by reduction of the data frames with the program APEX3.[S6] The compound crystallizes in *C*2/*c* with Z = 4, Z' = 0.5.

Adduct 5. Adduct **5** was crystallized as **2**. Data were obtained as outlined in Table **S2** and the structure was solved as described for **1** (34408 reflections). After careful examination of the unit cell, an extended data collection procedure (7 sets) was initiated using omega and phi scans. Atom C7 is found disordered (attached to C2 and C19) and was modeled successfully with an occupancy ratio of 0.76:0.24. The H_2O_2 molecule was found disordered between two sites and was modeled successfully with an occupancy ratio of 0.92:0.08. In the thermal ellipsoid plot disordered atoms are not shown, only the model with higher occupancy.

Adduct 6. A solution of **6** in toluene was concentrated by slow evaporation. Colorless blocks with well-defined faces were collected and data were obtained as outlined in Table **S2**. The structure was solved as described for **1** (13684 reflections). Integrated intensity information for each reflection was obtained by reduction of the data frames with the program APEX3.[S6] A molecule of water was found solvated. An unusual thermal ellipsoid suggested partial occupancy. The latter refined to a value close to 0.75 to which it was fixed for final refinement.

Table S1. Crystallographic data for **1**, **2**, and **3**.

	1	**2**	**3**
empirical formula	$C_{21}H_{23}O_3P$	$C_{21}H_{23}O_3P$	$C_{20}H_{21}O_3P$
formula weight	354.36	354.36	340.34
temperature [K]	110	110	100
diffractometer	Bruker APEX 2	Bruker APEX 2	Bruker Quest
wavelength [Å]	0.71073	0.71073	0.71073
crystal system	monoclinic	monoclinic	monoclinic
space group	$P2_1/n$	$P2_1/c$	$P2_1/c$
unit cell dimensions:			
a [Å]	10.937(3)	9.133(2)	8.9873(5)
b [Å]	17.920(4)	15.855(4)	15.7070(7)
c [Å]	10.968(3)	12.790(3)	12.4419(6)
α [°]	90	90	90
β [°]	117.255(2)	101.117(3)	100.431(2)
γ [°]	90	90	90
V [Å^3]	1911.1(8)	1817.4(7)	1727.32(15)
Z	4	4	4
ρ_{calc} [Mg/m^3]	1.232	1.295	1.309
μ [mm^{-1}]	0.160	0.168	0.174
F(000)	752	752	720
crystal size [mm^3]	0.565 × 0.482 × 0.212	0.772 × 0.582 × 0.396	0.233 × 0.142 × 0.133
Θ limit [°]	2.178 to 27.636	2.070 to 27.655	2.110 to 27.628
index range (h, k, l)	–14, 14; –21, 23; –14, 14	–11, 11; –20, 20; –16, 16	–11, 11; –20, 20; –16, 16
reflections collected	19083	20732	68772
independent reflections	4416	4199	4000
R(int)	0.0487	0.0373	0.0626
completeness to Θ	100.0 %	99.9 %	100 %
max. and min. transmission	0.7456 and 0.6095	0.7456 and 0.6787	0.7411 and 0.6956
data/restraints/parameters	4416 / 43 / 248	4199 / 0 / 229	4000 / 42 / 239
goodness-of-fit on F^2	1.034	1.026	1.100
R indices (final) [$I > 2\sigma(I)$]			
R_1	0.0465	0.0438	0.0550
wR_2	0.1202	0.1056	0.1221
R indices (all data)			
R_1	0.0628	0.0571	0.0754
wR_2	0.1316	0.1138	0.1325
largest diff. peak and hole [eÅ^{-3}]	0.833 and -0.274	0.481 and -0.387	0.494 and -0.444

Table S2. Crystallographic data for **4**, **5**, and **6**.

	4	**5**	**6**
empirical formula	$C_{42}H_{44}O_4P_2$	$C_{19}H_{18}O_2P$	$C_{20}H_{20.5}O_{1.75}P$
formula weight	674.71	309.30	319.83
temperature [K]	110.0	110.0	110.0
diffractometer	Bruker Quest	Bruker APEX 2	Bruker Quest
wavelength [Å]	0.71073	0.71073	0.71073
crystal system	monoclinic	triclinic	monoclinic
space group	*C*2/*c*	*P*-1	$P2_1/c$
unit cell dimensions:			
a [Å]	15.5361(11)	8.606(3)	8.7455(6)
b [Å]	12.2423(9)	10.259(3)	15.6756(10)
c [Å]	19.5371(14)	18.844(6)	12.2448(9)
α [°]	90	94.697(5)	90
β [°]	104.688(2)	90.536(5)	98.131(2)
γ [°]	90	102.113(5)	90
V [Å^3]	3594.5(4)	1620.7(9)	1661.8(2)
Z	4	4	4
ρ_{calc} [Mg/m^3]	1.247	1.268	1.278
μ [mm^{-1}]	0.163	0.174	0.171
F(000)	1432	652	678
crystal size [mm^3]	0.432 × 0.415 × 0.372	0.526 × 0.481 × 0.226	0.438 × 0.216 × 0.198
Θ limit [°]	2.146 to 24.998	1.085 to 27.613	2.688 to 24.998
index range (*h*, *k*, *l*)	–18, 18; –14, 14; –23, 23	–11, 11; –13, 13; –24, 24	–7, 10; –18, 18; –14, 14
reflections collected	28153	34408	13684
independent reflections	3170	7421	2925
R(int)	0.0944	0.0286	0.0464
completeness to Θ	100.0 %	99.7 %	99.7 %
max. and min. transmission	0.7456 and 0.4820	0.7456 and 0.6707	0.7456 and 0.6127
data/restraints/parameters	3170 / 0 / 220	7421 / 91 / 421	2925 / 0 / 213
goodness-of-fit on F^2	1.084	1.214	1.167
R indices (final) [$I > 2\sigma(I)$]			
R_1	0.0595	0.0632	0.0489
wR_2	0.1406	0.1214	0.0997
R indices (all data)			
R_1	0.0744	0.0735	0.0650
wR_2	0.1501	0.1259	0.1151
largest diff. peak and hole [eÅ^{-3}]	0.569 and -0.511	0.656 and -0.428	0.378 and -0.396

References

[S1] Bruker (2012). *APEX2*. Bruker AXS Inc., Madison, Wisconsin, USA.

[S2] Bruker (2001). *SADABS*. Bruker AXS Inc., Madison, Wisconsin, USA.

[S3] Sheldrick, G. M. (2008). *Acta Cryst*. A**64**, 112-122. Sheldrick, G. M. (2015), *Acta Cryst*. A**71**, 3-8. XT, XS, BRUKER AXS Inc., 5465 East Cheryl Parkway, Madison, WI 53711-5373 USA.

[S4] Spek, A. L. (2009). *Acta Cryst*. D**65**, 148-155.

[S5] Dolomanov, O. V; Bourhis, L. J.; Gildea, R. J.; Howard, J. A. K.; Puschmann, H. J. (2009) *Appl. Cryst*., **42**, 339-341.

[S6] Bruker (2013). *APEX3*. Bruker AXS Inc., Madison, Wisconsin, USA.

APPENDIX B

SUPPLEMENTARY DATA CHAPTER III

X-Ray Crystallography

1. A solution of **1** in dichloromethane was layered with pentane, and then concentrated by slow evaporation. A colorless block with very well-defined faces from a representative sample of crystals of the same habit was collected and data obtained as outlined in Table **S1**. The sample was optically centered with the aid of a video camera such that no translations were observed as the crystal was rotated through all positions. The X-ray radiation employed was generated from a Mo-Iμs X-ray tube (K_α = 0.71073 Å). 45 data frames were taken at widths of 1.0°. These reflections were used to determine the unit cell. The unit cell was verified by examination of the *h k l* overlays on several frames of data. No super-cell or erroneous reflections were observed. After careful examination of the unit cell, an extended data collection procedure (4 sets) was initiated using omega scans.

Integrated intensity information for each reflection was obtained by reduction of the data frames with the program *APEX3*.[S1] The integration method employed a three dimensional profiling algorithm and all data were corrected for Lorentz and polarization factors, as well as for crystal decay effects. Finally, the data was merged and scaled to produce a suitable data set. The absorption correction program *SADABS*[S2] was employed to correct the data for absorption effects.

Systematic reflection conditions and statistical tests of the data were used to determine the space group. A solution was obtained readily using *XT/XS* in *APEX3*.[S1,S3] Hydrogen

atoms were placed in idealized positions and were set riding on the respective parent atoms. All non-hydrogen atoms were refined with anisotropic thermal parameters.

Absence of additional symmetry and voids were confirmed using *PLATON (ADDSYM)*.[S4] The structure was refined (weighted least squares refinement on F^2) to convergence.[S3,S5] *Olex2* and *Mercury* were employed for the final data presentation and structure plots.[S5,S6]

2. A solution of **2** in toluene was concentrated by slow evaporation. A colorless block with very well-defined faces from a representative sample of crystals of the same habit was collected and data were obtained, and the structure was solved as in **1**. The X-ray radiation employed was generated from a Cu-Iμs X-ray tube (K_α = 1.5418 Å with a potential of 50 kV and a current of 1.0 mA). After careful examination of the unit cell, an extended data collection procedure (30 sets) was initiated using omega and phi scans. Residual electron density peak near (~1.5 Å) C17 indicated a possibility of disorder of the ethyl (C15-C16) and the methyl (C17) groups which were modeled successfully between two positions with an occupancy ratio of 0.85:0.15. Appropriate restraints and or constraints were added to keep the bond distances, angles, and thermal ellipsoids of the disordered atoms meaningful.

3. A solution of **3** in acetylacetone was concentrated by slow evaporation. A colorless block with very well-defined faces from a representative sample of crystals of the same habit was collected and data were obtained, and the structure was solved as in **1**. The X-

ray radiation employed was generated from a Cu sealed X-ray tube (K_α = 1.5418 Å with a potential of 40 kV and a current of 40 mA) fitted with a graphite monochromator in the parallel mode (175 mm collimator with 0.5 mm pinholes). 180 data frames were taken at widths of 0.5°. These reflections were used to determine the unit cell using Cell_Now.[S7] After careful examination of the unit cell, an extended data collection procedure (26 sets) was initiated using omega and phi scans.

Integrated intensity information for each reflection was obtained by reduction of the data frames with *APEX2*.[S8]

4. A solution of **4** in acetylacetone was layered with benzene. A colorless block with very well-defined faces from a representative sample of crystals of the same habit was collected and data were obtained, and the structure was solved as in **1**. The absorption correction program *TWINABS* was employed to correct the data for absorption effects, as well as to separate files: twin4.hkl, containing reflections from only the major component, and twin5.hkl, containing reflections from both the twin components.[S9] While the former was used for structure solution, the latter was used for final least squares refinement.

Table S1. Crystallographic data for **1** and **2**.

	1	**2**
empirical formula	$C_{26}H_{50}O_4P_2$	$C_{34}H_{42}O_8P_2$
formula weight	488.60	640.61
temperature [K]	110.0	100.01
diffractometer	Bruker Quest	Bruker Venture
wavelength [Å]	0.71073	1.54178
crystal system	monoclinic	triclinic
space group	*C*2/*c*	*P*-1
unit cell dimensions:		
a [Å]	24.4329(13)	8.6352(2)
b [Å]	11.0268(6)	9.0229(2)
c [Å]	10.9841(6)	11.5477(3)
α [°]	90	85.762(2)
β [°]	114.110(2)	81.565(2)
γ [°]	90	67.8510(10)
V [Å^3]	2701.1(3)	824.16(3)
Z	4	1
ρ_{calc} [Mg/m^3]	1.201	1.291
μ [mm^{-1}]	0.190	1.611
F(000)	1072	340
crystal size [mm^3]	0.519 × 0.122 × 0.106	0.249 × 0.1 × 0.045
Θ limit [°]	2.619 to 27.543	3.870 to 70.148
index range (*h*, *k*, *l*)	–31, 31; –14, 14; –13, 14	–9, 10; –11, 11; –14, 14
reflections collected	27843	19043
independent reflections	3109	3099
R(int)	0.0532	0.0686
completeness to Θ	99.9 %	99.4 %
max. and min. transmission	0.7431 and 0.6901	0.7533 and 0.6466
data/restraints/parameters	3109 / 0 / 145	3099 / 124 / 231
goodness-of-fit on F^2	1.049	1.101
R indices (final) [$I > 2\sigma(I)$]		
R_1	0.0435	0.0534
wR_2	0.0945	0.0990
R indices (all data)		
R_1	0.0597	0.0718
wR_2	0.1016	0.1072
largest diff. peak and hole [eÅ^{-3}]	0.427 and -0.362	0.391 and -0.287

Table S2. Crystallographic data for **3** and **4**.

	3	**4**
empirical formula	$C_5H_{10}O_4$	$C_5H_{10}O_6$
formula weight	134.13	166.13
temperature [K]	110.15	100.03
diffractometer	Bruker GADDS	Bruker Quest
wavelength [Å]	1.54178	0.71073
crystal system	tetragonal	monoclinic
space group	$P4_32_12$	$P2_1/n$
unit cell dimensions:		
a [Å]	8.9845(4)	5.5661(6)
b [Å]	8.9845(4)	15.4167(15)
c [Å]	8.5007(5)	8.8545(9)
α [°]	90	90
β [°]	90	92.306(3)
γ [°]	90	90
V [Å^3]	686.19(7)	759.20(13)
Z	4	4
ρ_{calc} [Mg/m^3]	1.298	1.453
μ [mm^{-1}]	0.975	0.136
F(000)	288	352
crystal size [mm^3]	0.18 × 0.13 × 0.1	0.225 × 0.214 × 0.104
Θ limit [°]	6.970 to 60.489	2.642 to 25.000
index range (h, k, l)	–10, 10; –10, 10; –9, 9	–6, 6; 0, 18; 0, 10
reflections collected	15337	2327
independent reflections	518	2327
R(int)	0.0584	0.0545
completeness to Θ	83.8 %	97.5 %
max. and min. transmission	0.7388 and 0.6510	0.745 and 0.555
data/restraints/parameters	518 / 0 / 45	2327 / 0 / 103
goodness-of-fit on F^2	1.195	1.036
R indices (final) [$I > 2\sigma(I)$]		
R_1	0.0246	0.0507
wR_2	0.0555	0.1094
R indices (all data)		
R_1	0.0261	0.0676
wR_2	0.0557	0.1186
largest diff. peak and hole [eÅ^{-3}]	0.116 and -0.092	0.183 and -0.266

References

[S1] Bruker (2015), *APEX3*, Bruker AXS Inc., Madison, Wisconsin, USA.

[S2] Bruker (2001), *SADABS*, Bruker AXS Inc., Madison, Wisconsin, USA.

[S3] G. M. Sheldrick (2008), *XT*, *XS* Acta Cryst. A**64**, 112-122. G. M. Sheldrick (2015), Acta Cryst. A**71**, 3-8. G. M. Sheldrick (2015), Acta Cryst. C**71**, 3-8. BRUKER AXS Inc., 5465 East Cheryl Parkway, Madison, WI 53711-5373 USA.

[S4] A. L. Spek (2009), *PLATON*, Acta Cryst. D**65**, 148-155.

[S5] O. V. Dolomanov, L. J. Bourhis, R. J. Gildea, J. A. K. Howard, H. J. Puschmann (2009), *OLEX2*, Appl. Cryst., **42**, 339-341.

[S6] R. Taylor, C. F. Macrae (2001), *Mercury*, Acta Cryst., B**57**, 815-827.

[S7] G. M. Sheldrick (2008), *Cell_Now*, University of Göttingen, Göttingen, Germany.

[S8] Bruker (2012). *APEX2*. Bruker AXS Inc., Madison, Wisconsin, USA.

[S9] G. M. Sheldrick (2012), *TWINABS*, University of Göttingen, Göttingen, Germany.

APPENDIX C

SUPPLEMENTARY DATA CHAPTER IV

X-Ray Crystallography

1. A solution of **1** in dry dichloromethane was concentrated by slow evaporation in a nitrogen stream under an inert atmosphere. A colorless block with very well-defined faces from a representative sample of crystals of the same habit was collected and data were obtained as outlined in Table **S1**. The X-ray radiation employed was generated from a Mo-Iμs X-ray tube (K_α = 0.71073 Å with a potential of 50 kV and a current of 1.0 mA). 45 data frames were taken at widths of 1.0°. These reflections were used to determine the unit cell. The unit cell was verified by examination of the *h k l* overlays on several frames of data. No super-cell or erroneous reflections were observed. After careful examination of the unit cell, an extended data collection procedure (4 sets) was initiated using omega and phi scans.

Integrated intensity information for each reflection was obtained by reduction of the data frames with the program *APEX3*.[S1] The integration method employed a three-dimensional profiling algorithm and all data were corrected for Lorentz and polarization factors, as well as for crystal decay effects. Finally, the data was merged and scaled to produce a suitable data set. The absorption correction program *SADABS*[S2] was employed to correct the data for absorption effects.

Systematic reflection conditions and statistical tests of the data were used to determine the space group. A solution was obtained readily using *XT/XS* in *APEX3*.[S1,S3] Hydrogen

atoms were placed in idealized positions and were set riding on the respective parent atoms.[1] All non-hydrogen atoms were refined with anisotropic thermal parameters. Absence of additional symmetry and voids were confirmed using *PLATON (ADDSYM)*.[S4] The structure was refined (weighted least squares refinement on F^2) to convergence.[S3,S5] *Olex2* and *Mercury* were employed for the final data presentation and structure plots.[S5,S6]

3. A solution of **3** in a mixture of dichloromethane and hexanes (1:1) was concentrated by slow evaporation. A colorless block with very well-defined faces from a representative sample of crystals of the same habit was collected and data were obtained as outlined in Table S1, and the structure was solved as in **1**. 45 data frames were taken at widths of 1.0°. These reflections were used to determine the unit cell. The unit cell was verified by examination of the *h k l* overlays on several frames of data. No super-cell or erroneous reflections were observed. After careful examination of the unit cell, an extended data collection procedure (6 sets) was initiated using omega and phi scans.

4. A solution of **4** in a mixture of dichloromethane and hexanes (1:1) was concentrated by slow evaporation. A colorless block with very well-defined faces from a

[1] The refinement was stabilized (zero shift) before the H atoms were added to the OOH groups. The latter H atoms were placed in one of the following ways: (a) If residual electron densities accounting for the corresponding H atoms were found, they were assigned as H atoms, and then were set riding on the parent O atoms. (b) If the H atoms could not be located from residual electron densities, they were placed geometrically with respect to the O atoms they were hydrogen-bonded to, and then were set riding on the parent O atoms. The last step was carried out after all remaining atoms were stabilized and confirming there were no major shifts in those atoms after the addition of the hydrogen atoms in question.

representative sample of crystals of the same habit was collected and data were obtained as outlined in Table **S1**, and the structure was soved as in **1**. The X-ray radiation employed was generated from a Cu-X-ray sealed tube (K_α = 1.5418 Å with a potential of 50 kV and a current of 40.0 mA). 60 data frames were taken at widths of 1.0°. These reflections were used in the auto-indexing procedure to determine the unit cell. The unit cell was verified by examination of the *h k l* overlays on several frames of data. No super-cell or erroneous reflections were observed. After careful examination of the unit cell, an extended data collection procedure (3 sets) was initiated using omega scans.

Elongated ellipsoids on one *o*-Tol group (C15-C21) and the residual electron density near the group suggested disorder and was modeled successfully between two positions with an occupancy ratio of 0.75:0.25. Appropriate restraints and constraints were placed to keep the bond distances, angles, and thermal ellipsoids meaningful.

5. A solution of **5** in a mixture of dichloromethane and hexanes (1:1) was concentrated by slow evaporation. A colorless block with very well-defined faces from a representative sample of crystals of the same habit was collected and data were obtained as outlined in Table **S2**, and the structure was solved as in **1**. The X-ray radiation employed was generated from a Cu-Iμs X-ray tube (K_α = 1.5418 Å with a potential of 50 kV and a current of 1.0 mA). 45 data frames were taken at widths of 1.0°. These reflections were used to determine the unit cell. The unit cell was verified by examination of the *h k l* overlays on several frames of data. No super-cell or erroneous

reflections were observed. After careful examination of the unit cell, an extended data collection procedure (28 sets) was initiated using omega and phi scans.

6. A solution of **6** in a mixture of dichloromethane and hexanes (1:1) was concentrated by slow evaporation. A colorless block with very well-defined faces from a representative sample of crystals of the same habit was collected and data were obtained as outlined in Table **S2**, and the structure was solved as in **1**. The X-ray radiation employed was generated from a Cu- X-ray sealed tube (K_α = 1.5418 Å with a potential of 50 kV and a current of 40.0 mA). 60 data frames were taken at widths of 1.0°. These reflections were used in the auto-indexing procedure to determine the unit cell. The unit cell was verified by examination of the *h k l* overlays on several frames of data. No super-cell or erroneous reflections were observed. After careful examination of the unit cell, an extended data collection procedure (3 sets) was initiated using omega scans.
Elongated ellipsoids on one *o*-Tol group (C15-C21) and the residual electron density near the group suggested disorder and was modeled successfully between two positions with an occupancy ratio of 0.94:0.06. Appropriate restraints and constraints were placed to keep the bond distances, angles, and thermal ellipsoids meaningful.

Table S1. Crystallographic data for **1**, **3**, and **4**.

	1	**3**	**4**
empirical formula	$C_{21}H_{21}OP$	$C_{27}H_{33}O_5P$	$C_{27}H_{33}O_5P$
formula weight	320.35	468.50	468.50
temperature [K]	110.0	110.0	110.0
diffractometer	Bruker Quest	Bruker Quest	Bruker APEX II
wavelength [Å]	0.71073	0.71073	0.71073
crystal system	trigonal	monoclinic	monoclinic
space group	*R*-3	$P2_1/n$	$P2_1/n$
unit cell dimensions:			
a [Å]	12.4223(6)	12.6252(4)	9.3858(15)
b [Å]	12.4223(6)	12.7293(4)	17.367(3)
c [Å]	19.7979(11)	15.4253(5)	15.469(3)
α [°]	90	90	90
β [°]	90	98.9660(10)	101.076(2)
γ [°]	120	90	90
V [Å^3]	2645.8(3)	2448.71(14)	2474.4(7)
Z	6	4	4
ρ_{calc} [Mg/m^3]	1.206	1.271	1.258
μ [mm^{-1}]	0.158	0.148	0.146
F(000)	1020	1000	1000
crystal size [mm^3]	0.459 × 0.402 × 0.259	0.527 × 0.351 × 0.327	0.403 × 0.358 × 0.341
Θ limit [°]	2.796 to 27.463	2.085 to 27.478	2.632 to 23.997
index range (*h*, *k*, *l*)	–16, 16; –16, 16; –25, 25	–16, 16; –16, 16; –20, 19	–10, 10; –19, 19; –17, 17
reflections collected	10958	54167	22281
independent reflections	1354	5595	3860
R(int)	0.0343	0.0512	0.0297
completeness to Θ	99.7 %	99.9 %	99.4 %
max. and min. transmission	0.4305 and 0.3923	0.4286 and 0.4002	0.7450 and 0.6568
data/restraints/parameters	1354 / 0 / 71	5595 / 0 / 301	3860 / 334 / 360
goodness-of-fit on F^2	1.085	1.022	1.066
R indices (final) [$I > 2\sigma(I)$]			
R_1	0.0368	0.0373	0.0460
wR_2	0.0844	0.0881	0.0979
R indices (all data)			
R_1	0.0421	0.0494	0.0521
wR_2	0.0890	0.0944	0.1010
largest diff. peak and hole [eÅ^{-3}]	0.313 and -0.381	0.343 and -0.302	0.326 and -0.338

Table S2. Crystallographic data for **5** and **6**.

	5	**6**
empirical formula	$C_{28}H_{35}O_5P$	$C_{28}H_{35}O_5P$
formula weight	482.53	482.53
temperature [K]	110.0	110.0
diffractometer	Bruker Venture	Bruker APEX II
wavelength [Å]	1.54178	0.71073
crystal system	monoclinic	monoclinic
space group	$P2_1/n$	$P2_1/n$
unit cell dimensions:		
a [Å]	12.5053(5)	10.5015(14)
b [Å]	13.0669(5)	10.0377(14)
c [Å]	15.4366(6)	24.760(3)
α [°]	90	90
β [°]	98.165(2)	98.9405(15)
γ [°]	90	90
V [Å^3]	2496.86(17)	2578.2(6)
Z	4	4
ρ_{calc} [Mg/m^3]	1.284	1.243
μ [mm^{-1}]	1.272	0.142
F(000)	1032	1032
crystal size [mm^3]	0.382 × 0.044 × 0.035	0.322 × 0.266 × 0.204
Θ limit [°]	4.265 to 70.039	2.625 to 24.996
index range (h, k, l)	–15, 15; –14, 15; –18, 18	–12, 12; –11, 11; –28, 29
reflections collected	22061	18831
independent reflections	4702	4527
R(int)	0.0313	0.0346
completeness to Θ	99.8 %	99.7 %
max. and min. transmission	0.4684 and 0.3815	0.7456 and 0.7025
data/restraints/parameters	4702 / 0 / 310	4527 / 340 / 375
goodness-of-fit on F^2	1.082	1.024
R indices (final) [$I > 2\sigma(I)$]		
R_1	0.0387	0.0347
wR_2	0.0966	0.0769
R indices (all data)		
R_1	0.0451	0.0451
wR_2	0.1041	0.0834
largest diff. peak and hole [eÅ^{-3}]	0.389 and -0.231	0.308 and -0.302

References

[S1] Bruker (2015), *APEX3*, Bruker AXS Inc., Madison, Wisconsin, USA.

[S2] Bruker (2001), *SADABS*, Bruker AXS Inc., Madison, Wisconsin, USA.

[S3] G. M. Sheldrick (2008), *XT*, *XS* Acta Cryst. A64, 112-122. G. M. Sheldrick (2015), Acta Cryst. A71, 3-8. G. M. Sheldrick (2015), Acta Cryst. C71, 3-8. BRUKER AXS Inc., 5465 East Cheryl Parkway, Madison, WI 53711-5373 USA.

[S4] A. L. Spek (2009), *PLATON*, Acta Cryst. D**65**, 148-155.

[S5] O. V. Dolomanov, L. J. Bourhis, R. J. Gildea, J. A. K. Howard, H. J. Puschmann (2009), *OLEX2*, Appl. Cryst., **42**, 339-341.

[S6] R. Taylor, C. F. Macrae (2001), *Mercury*, Acta Cryst., B**57**, 815-827.

Dynamic NMR Experiments

Competition Experiments

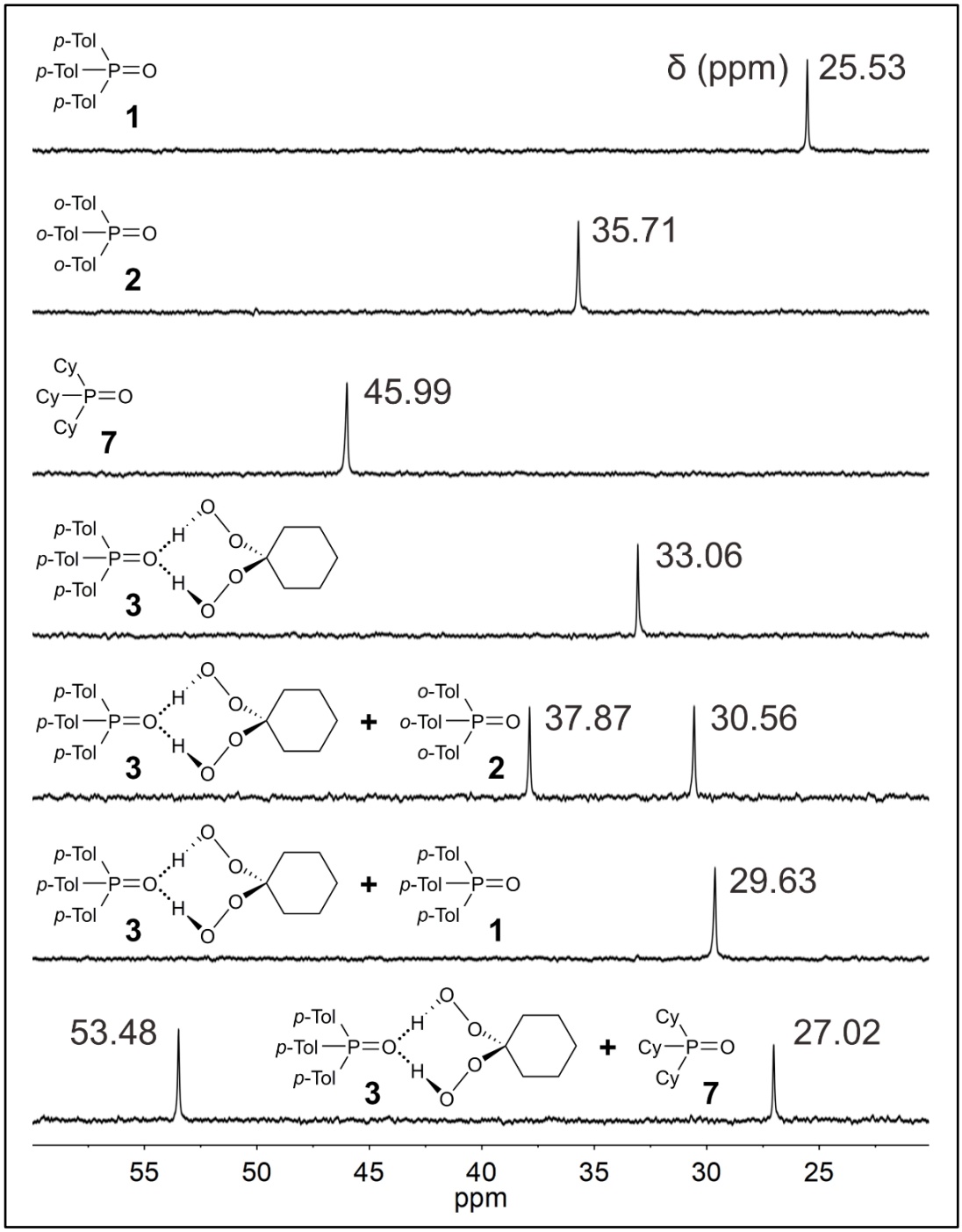

Figure S1. ^{31}P NMR competition experiments of 1 : 1 mixtures of *p*-Tol$_3$PO·(HOO)$_2$C(CH$_2$)$_5$ (**3**) and phosphine oxides *p*-Tol$_3$PO (**1**), *o*-Tol$_3$PO (**2**), and Cy$_3$PO (**7**) in benzene.

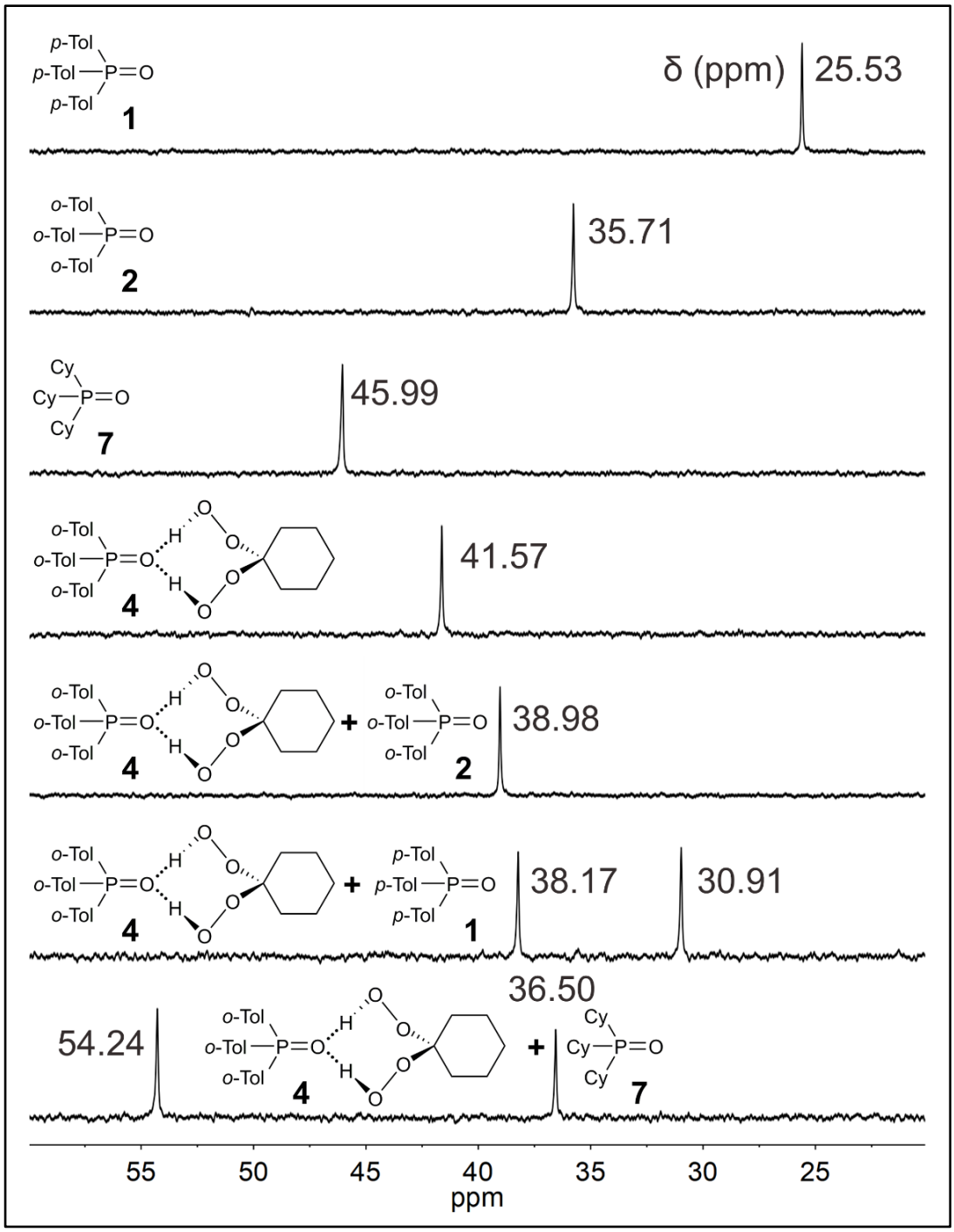

Figure S2. ^{31}P NMR competition experiments of 1 : 1 mixtures of *o*-$Tol_3PO{\cdot}(HOO)_2C(CH_2)_5$ (**4**) and phosphine oxides *p*-Tol_3PO (**1**), *o*-Tol_3PO (**2**), and Cy_3PO (**7**) in benzene.

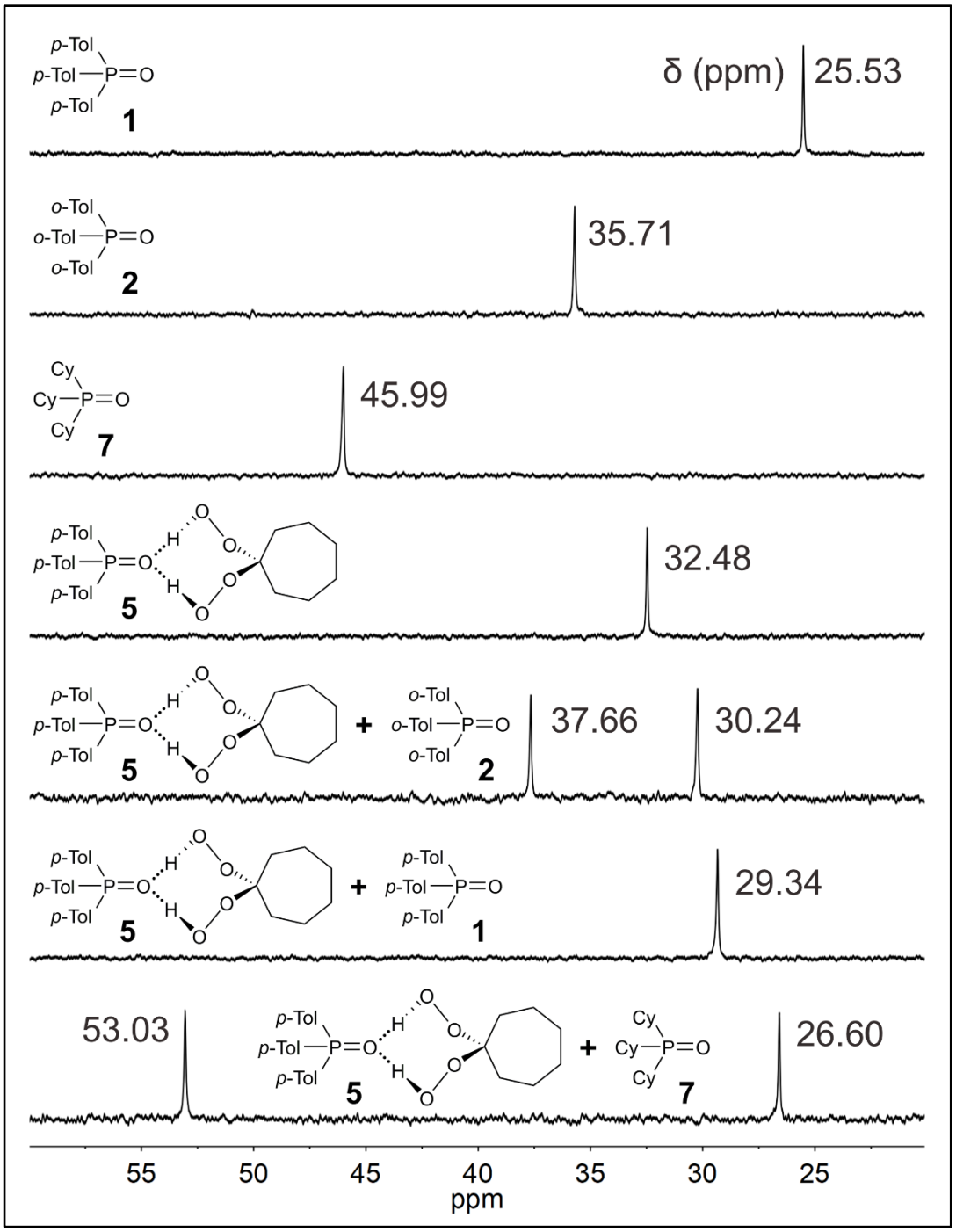

Figure S3. ^{31}P NMR competition experiments of 1 : 1 mixtures of *p*-Tol$_3$PO·(HOO)$_2$C(CH$_2$)$_6$ (**5**) and phosphine oxides *p*-Tol$_3$PO (**1**), *o*-Tol$_3$PO (**2**), and Cy$_3$PO (**7**) in benzene.

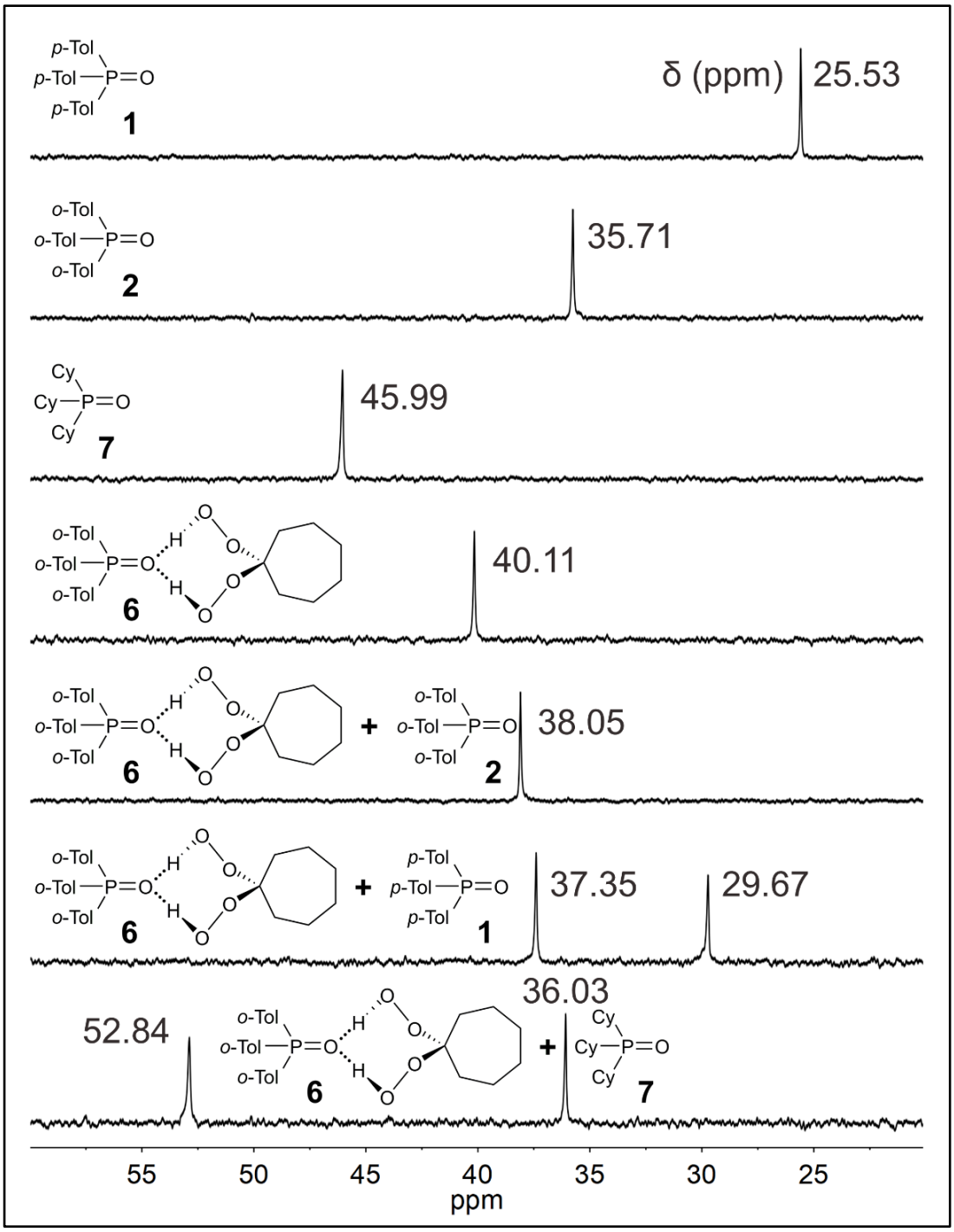

Figure S4. ^{31}P NMR competition experiments of 1 : 1 mixtures of *o*-Tol$_3$PO·(HOO)$_2$C(CH$_2$)$_6$ (**6**) and phosphine oxides *p*-Tol$_3$PO (**1**), *o*-Tol$_3$PO (**2**), and Cy$_3$PO (**7**) in benzene.

Variable Temperature NMR Experiments

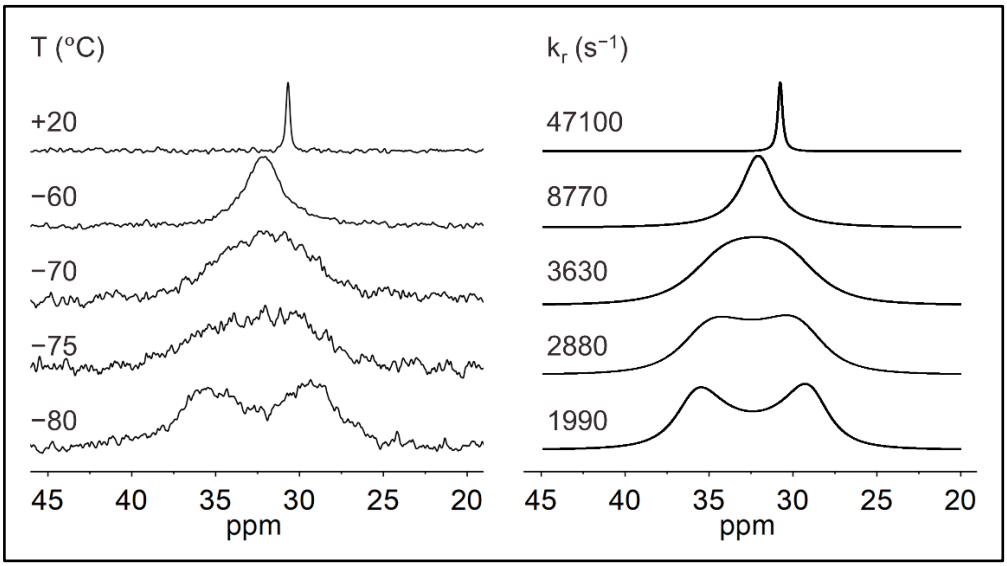

Figure S5. ^{31}P NMR spectra of a 1 : 1 mixture of *p*-Tol_3PO (**1**) and *p*-$Tol_3PO{\cdot}(HOO)_2C(CH_2)_5$ (**3**) in dichloromethane, recorded at varying temperatures (left) and the corresponding simulations (right).

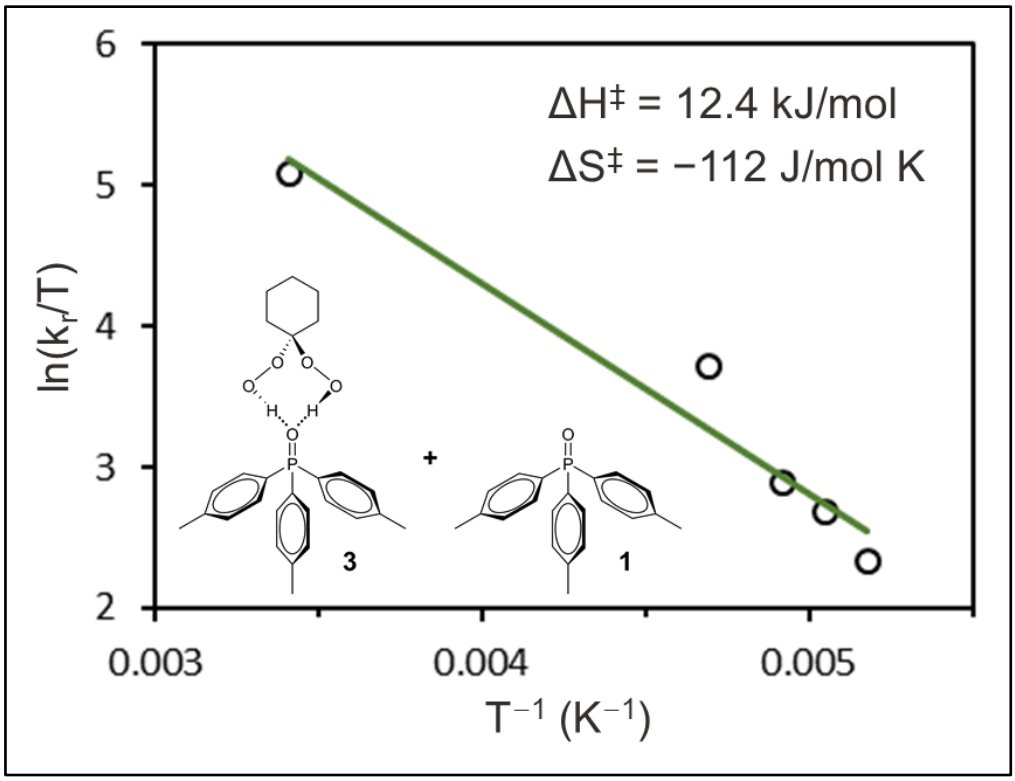

Figure S6. Temperature dependence of the exchange rate constant k_r depicted as $\ln(k_r/T)$ versus T^{-1} of a 1 : 1 mixture of *p*-Tol_3PO (**1**) and *p*-$Tol_3PO{\cdot}(HOO)_2C(CH_2)_5$ (**3**) in dichloromethane.

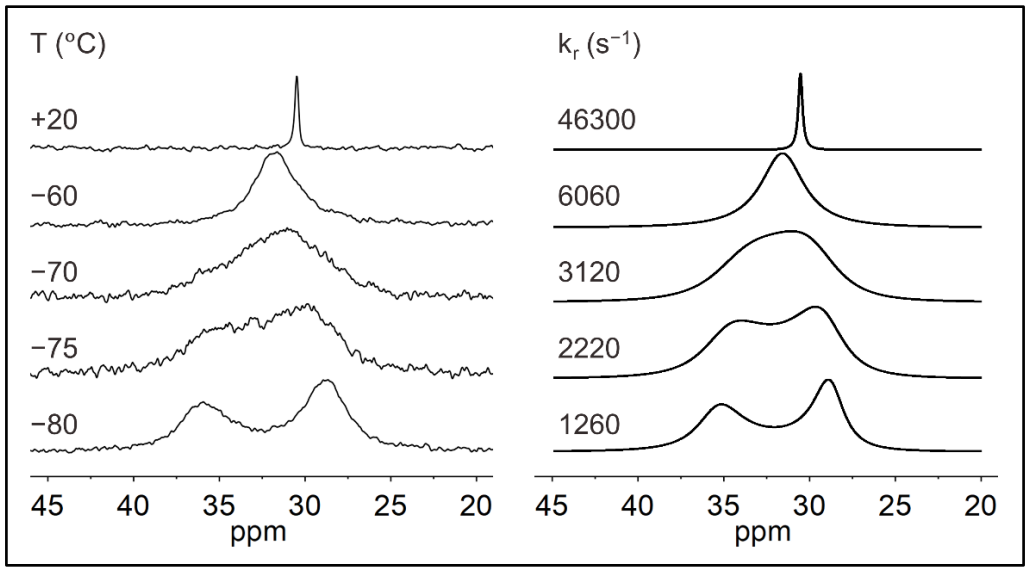

Figure S7. ^{31}P NMR spectra of a 1 : 1 mixture of *p*-Tol$_3$PO (**1**) and *p*-Tol$_3$PO·(HOO)$_2$C(CH$_2$)$_6$ (**5**) in dichloromethane, recorded at varying temperatures (left) and the corresponding simulations (right).

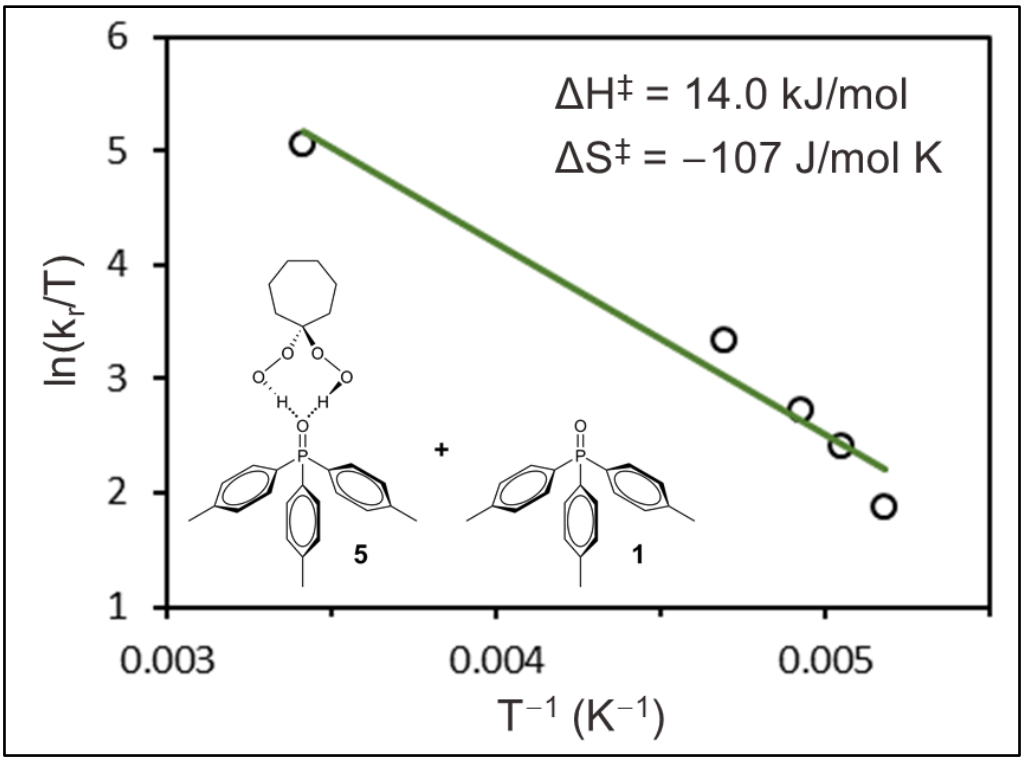

Figure S8. Temperature dependence of the exchange rate constant k_r depicted as $\ln(k_r/T)$ versus T^{-1} of a 1 : 1 mixture of *p*-Tol_3PO (**1**) and *p*-$Tol_3PO{\cdot}(HOO)_2C(CH_2)_6$ (**5**) in dichloromethane.

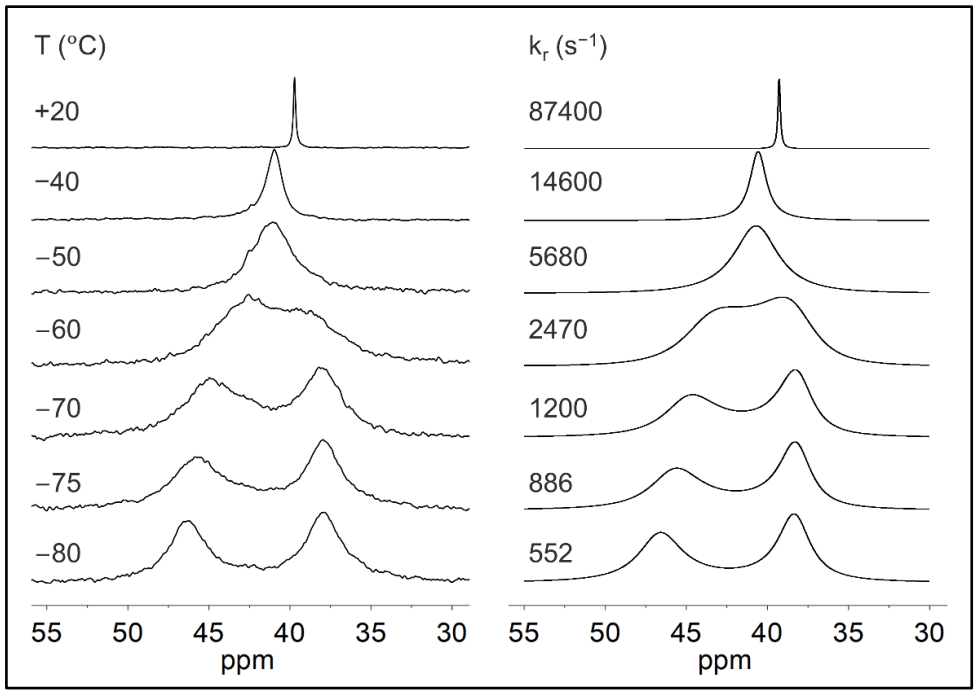

Figure S9. ^{31}P NMR spectra of a 1 : 1 mixture of *o*-Tol_3PO (**2**) and *o*-$Tol_3PO{\cdot}(HOO)_2C(CH_2)_6$ (**6**) in dichloromethane, recorded at varying temperatures (left) and the corresponding simulations (right).

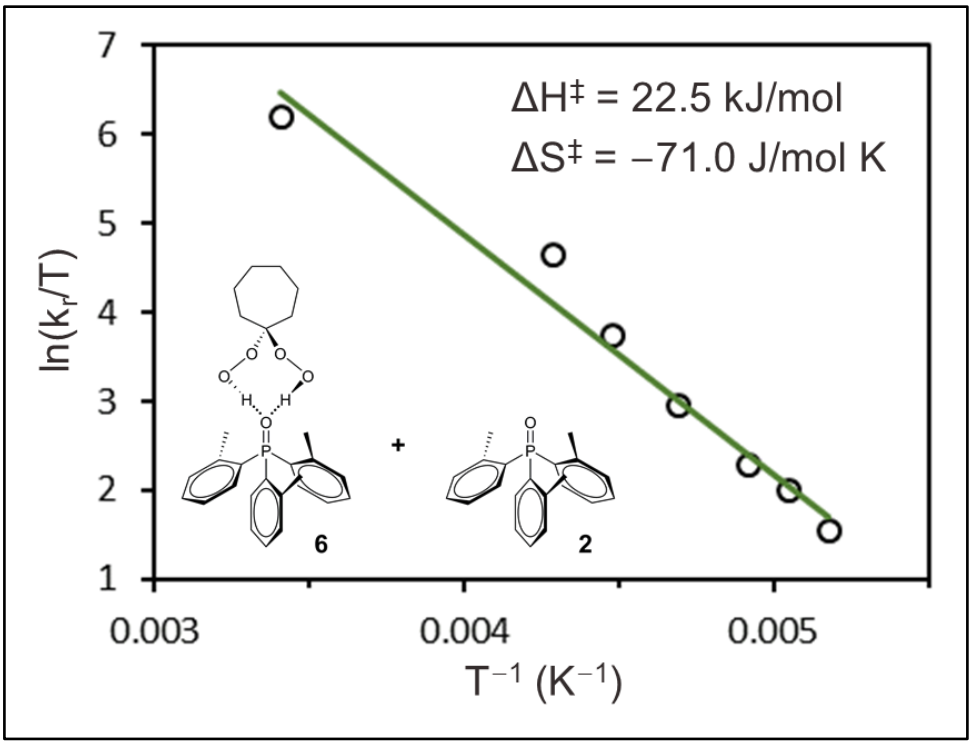

Figure S10. Temperature dependence of the exchange rate constant k_r depicted as $\ln(k_r/T)$ versus T^{-1} of a 1 : 1 mixture of *o*-Tol_3PO (**2**) and *o*-$Tol_3PO{\cdot}(HOO)_2C(CH_2)_6$ (**6**) in dichloromethane.